Porous Organic Frameworks in Catalysis

Bavykina, Anastasiya

DOI
10.4233/uuid:27802bfc-c459-4c71-acc8-7678ca3cc5d4

Publication date
2017

Document Version
Final published version

Citation (APA)
Bavykina, A. (2017). *Porous Organic Frameworks in Catalysis*. [Dissertation (TU Delft), Delft University of Technology]. https://doi.org/10.4233/uuid:27802bfc-c459-4c71-acc8-7678ca3cc5d4

POROUS ORGANIC FRAMEWORKS IN CATALYSIS

Author: Anastasiya V. Bavykina

PhD Thesis, Delft University of Technology

The Netherlands,

April, 2017

Cover design by Anastasiya Bavykina

Porous Organic Frameworks in Catalysis

Proefschrift

ter verkrijging van de graad van doctor
aan de Technische Universiteit Delft,
op gezag van de Rector Magnificus prof. ir. K.C.A. M. Luyben;
voorzitter van het College voor Promoties,
in het openbaar te verdedigen op
11 april 2017 om 12:30 uur

door

Anastasiya BAVYKINA
Master of Science in Environmental Protection Technology
Gdansk University of Technology
Geboren te Berdsk, Rusland

Dit proefschrift is goedgekeurd de promotor:
Prof. dr. F. Kapteijn, Prof. dr. ir. M. Makkee and Prof. dr. J. Gascon Sabate

Samenstelling promotiecommissie:
Rector Magnificus, voorzitter
Prof. dr. F. Kapteijn, Technische Universiteit Delft, promotor
Prof. dr. J. Gascon Sabate, Technische Universiteit Delft, promotor
Prof. dr. ir. M. Makkee, Technische Universiteit Delft, promotor

Onafhankelijke leden:
Prof. dr. F. Schüth, Max-Planck-Institut für Kohlenforschung
Prof. dr. P. Van Der Voort, Ghent University
Prof. dr. U. Hanefeld, Technische Universiteit Delft
Dr. G. Prieto, Max-Planck-Institut für Kohlenforshung
Prof. dr. ir. M.T. Kreutzer, Technische Universiteit Delft, reservelid

The research reported in this thesis was conducted in the Catalysis Engineering section of the Chemical Engineering Department, Faculty of Applied Sciences (TNW) of the Delft University of Technology and received funding from European project Eco^{2}CO$_2$, grant agreement number 309701.

Proefschrift, Technische Universiteit Delft

Met samenvatting in het Nederlands

Printed by: Ipskamp Printing, Enschede

ISBN/EAN: 978-94-028-0594-9

It is important to do everything with passion,
it embellishes life enormously.

Lev Landau.

CONTENTS

CHAPTER ONE

Introduction

Single site catalysis in Covalent Organic Frameworks and Porous Organic Polymers

This Chapter is based on the following publication:

S.M.J. Rogge, A. Bavykina, J. Hajek, H. Garcia, A. Olivos, A. Sepúlveda-Escribano, A. Vimont, G. Clet, P. Bazin, F. Kapteijn, M. Daturi, E. V. Ramos-Fernandez, F.X. Llabrés i Xamena, V. Van Speybroeck, and J. Gascon.

Chem. Soc. Rev, accepted.

The number of abbreviations in this section is large. The reader will find a section at the end of the chapter, which lists all abbreviations.

1.1. INTRODUCTION

This thesis focuses on the development of single site heterogeneous catalysts making use of Porous Organic Frameworks (POFs). Most POFs possess high chemical and physical stability, combined with tunability owing to the diversity of synthetic routes. Catalysts based on POFs are robust, heterogeneous, possess high surface area and high density of active sites. This makes their applications in heterogeneous catalysis very promising. In the this chapter, the main advances of using POFs in catalysis for relevant reactions is critically reviewed.

Here, we refer to POFs as a class of porous materials that are constructed from organic building blocks. Recently, POFs have been gaining increasing interest, since they are believed to be able to complement their inorganic counterparts – *e.g.* zeolites, mesoporous silicas or MOFs – in a number of applications.

The diversity of synthetic routes to obtain POFs is immense, allowing scientists to form different types of frameworks. POFs possess high surface area, tunable pore size, adjustable skeletons, which brings promise to a wide range of applications of POFs. In addition, POFs can be locally decorated with molecular catalysts that may acquire activities and selectivities comparable to homogeneous analogues. It is convenient to divide all POFs into two groups depending whether material is crystalline or not. Amorphous Porous Organic Polymers (POPs) hold enhanced chemical and physical stability due to their fully covalent nature; they can be safely exposed to a wide range of aggressive media. Covalent Organic Frameworks (COFs) have an advantage over POPs being crystalline materials from the perspective of structural characterization. However, reversible bonds within their structure bring limitations to the conditions under which they can be used. There exists a number of reviews on porous organic polymers, where their synthesis, properties, and possible applications are described.[1-4] In this overview, we solely focus on single catalytic sites development within these networks.

The vast majority of POFs is synthesised in a modular fashion, making straightforward incorporation of functional groups easy and, therefore, opening a promising playground for using POFs as catalysts. There is a reasonable number of potent ligands, that are active organocatalysts, and ligands that are prone to metal coordination (*e.g.* bipyridine, porphyrin

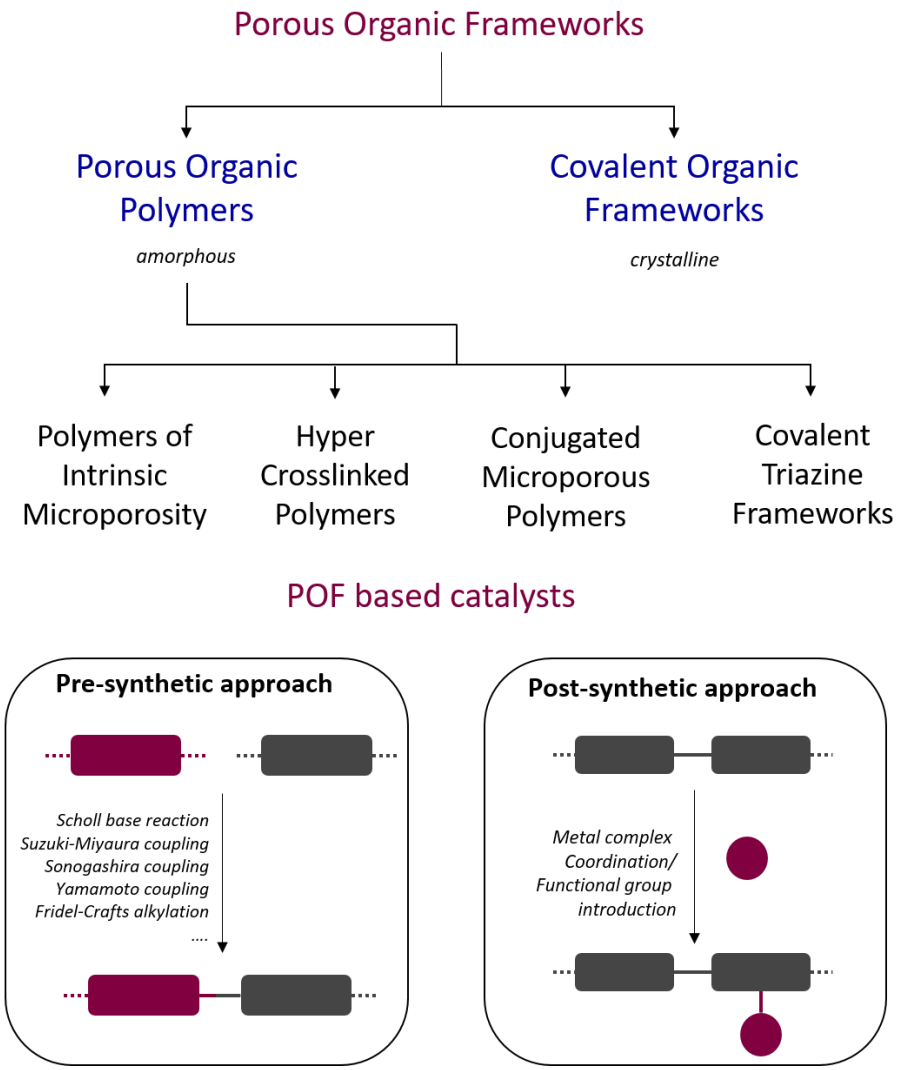

Scheme 1.1. Classification of POFs (*top*) and approaches towards POFs based catalysts (*bottom*)

or phthalocyanine); all can be used as building blocks to form a framework. Chemically different monomers can be bonded in a variety of different ways. Thus, employing building units that originally possess a required metal site or functional group can be a simple and direct bottom-up approach. This method can also be described as using homogeneous catalysts as a building block. Another approach is to employ POFs as a catalyst support – which is possible by means of the same modular chemistry, but using post-synthetic metalation or functionalisation of a framework (Scheme 1.1)

This chapter reviews single site catalysts based on Porous Organic Polymers and Covalent Organic Frameworks. It starts with a brief description on different types of POFs, their synthetic routes and properties. The next part elaborates on catalytic sites within POFs

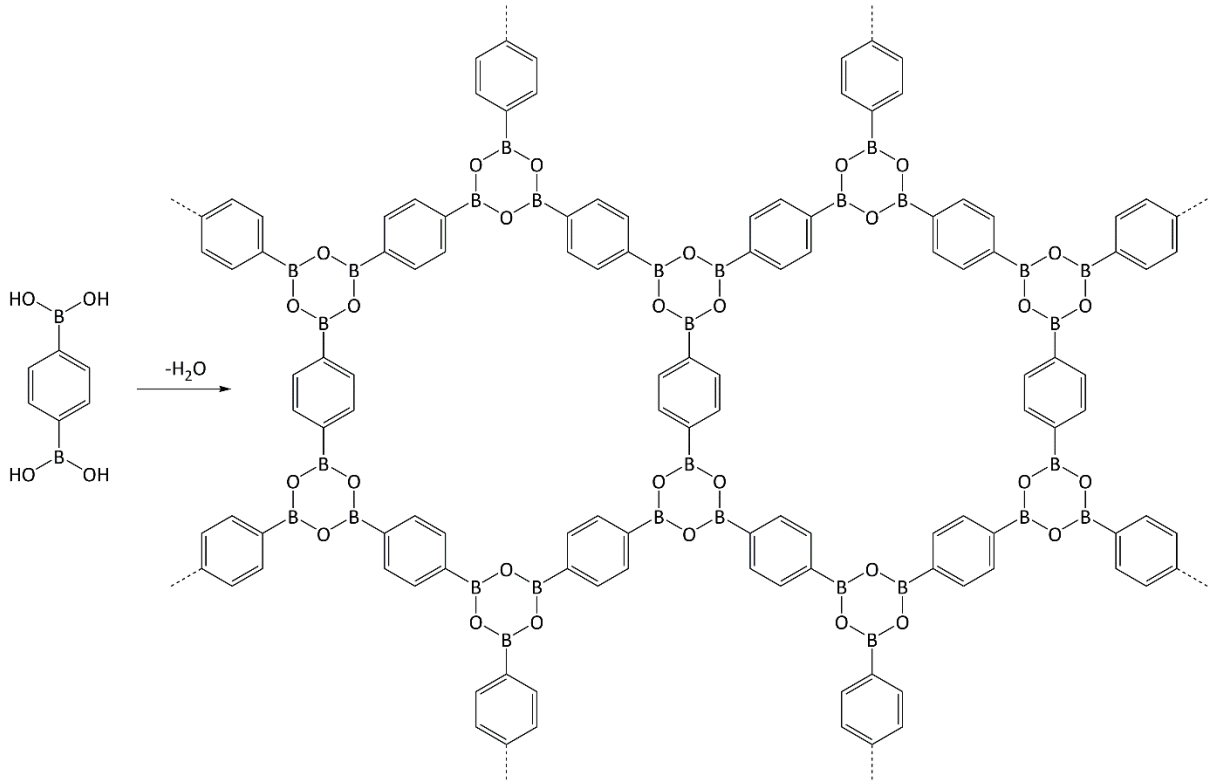

Figure 1.1. Structure of COF-1[5]

obtained from originally metal-containing building blocks (pre-synthetic strategy), followed by immobilisation of organometallic complexes on POFs (post-synthetic strategy). The strategies of employing metal free single-site catalysts are described.

1.2. POROUS ORGANIC FRAMEWORKS – TYPES OF NETWORKS

1.2.1. Covalent Organic Frameworks (COFs)

COFs were pioneered by the group of Yaghi. COFs are highly crystalline solids, synthesised via reversible formation of boroxine rings. The simplest example of this class of materials is COF-1 (Figure 1.1), obtained by self-condensation of benzene-1,4-diboronic acid.[5] It has a BET surface area of 711 m^2g^{-1} and an average pore size of 0.7 nm. COFs can also be constructed via co-condensation of two or more building blocks – multiple combinations of aromatic boronic acids and diols. This allows constructing COFs of different properties and functions. Boron-containing COFs are highly porous, crystalline materials with low density, which makes them promising functional materials. However, their application is often limited since COFs are not stable in water.[6]

It has to be noted that the term *COF* is currently being used not only for boroxine rings containing materials, but any *crystalline* porous organic framework. For instance, the vast

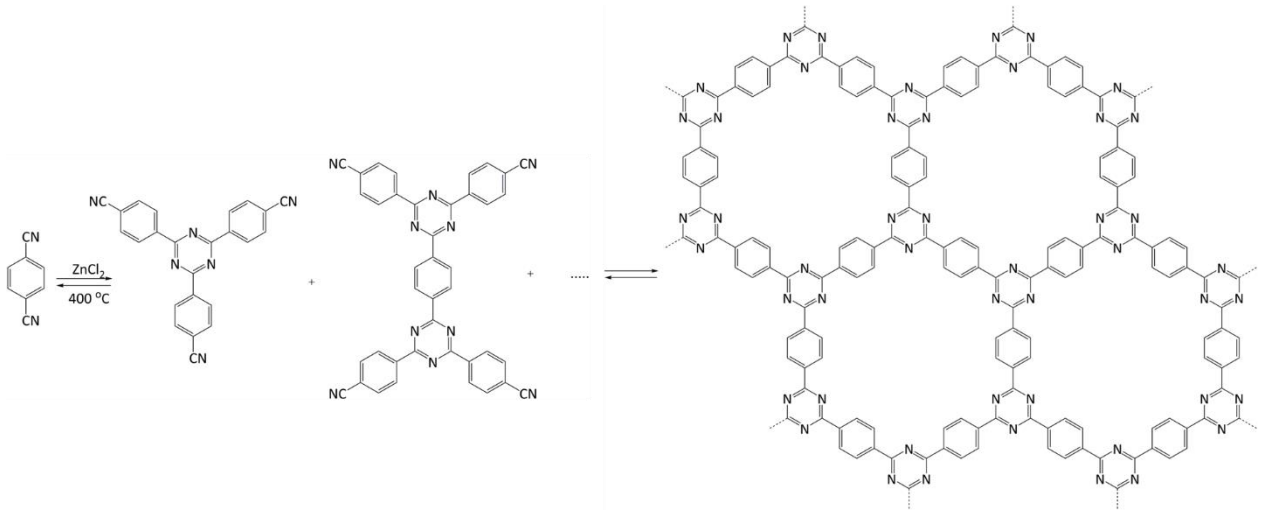

Figure 1.2. Structure of CTF-1[9]

majority of imine-linked polymers, prepared by co-condensation of aromatic aldehydes with amines, are amorphous networks. By varying the synthetic conditions, the crystalline form of the material can be obtained. Thus, group of Yaghi reported the COF-300, a crystalline imine-linked polymer prepared by condensation of the tetrahedral building block tetra-(4-anilyl)methane with the linear linking unit terephthaldehyde.[7] Group of Dichtel reported on the insight into the crystallisation of amorphous imine-linked polymer networks to 2D COFs.[8] It was shown that COF formation occurs through the initial rapid precipitation of an amorphous, low surface area imine-linked network, which crystallises into COF over days under conditions that facilitate imine exchange.

1.2.2. Covalent Triazine Frameworks (CTFs)

CTFs are porous aromatic frameworks that are made upon trimerisation of aromatic nitriles, first reported by Thomas *et al*. The first triazine framework, CTF-1 (Figure 1.2), was prepared from 1,4-dicyanobenzene, and the structure is isoelectronic to COF-1. However, CTF-1 outperforms COF-1 in terms of both thermal and chemical stability.[9] CTFs are prepared using excess of molten $ZnCl_2$ as both solvent and catalyst for polymerisation, however Cooper *et. al.* reported the alternative synthetic procedure using triflic acid as a catalyst via room-temperature and microwave assisted synthesis.[10]

Triazine ring containing networks can be synthesised by other methods as well. E.g. Schwab *et. al.* reported on synthesis of porous polymer through Schiff Base Chemistry by condensation of melamine with different di- and trialdehydes.[11] Another example is reported

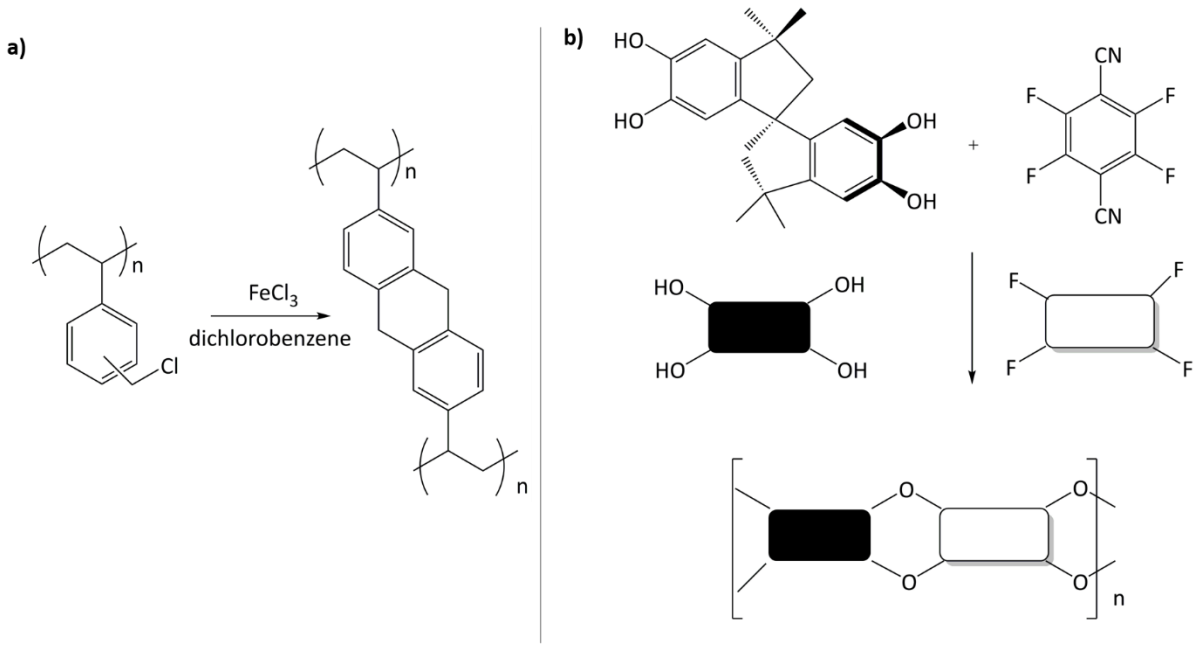

Figure 1.3. a) Preparation of hypercrosslinked styrenic polymer from poly-(vinylbenzyl) chloride gel-type resin precursor[15] b) Preparation of polymer PIM-1[26]

by Grate *et. al.* – conversion of cyanuric chloride to side-chain functionalised sequence-defined polymers.[12]

1.2.3. Hypercrosslinked polymers (HCPs) and analogous crosslinked frameworks

HCP is a big class of polymers introduced by Davankov in 1969.[13] HCPs are typically synthesized from linear or low crosslinked polyarylates or polysulfones using a post-crosslinking agent via the Friedel–Crafts reaction.[14] HCPs have also been produced by the direct polycondensation of small molecule monomers. One of the examples is depicted on Figure 1.3a. HCPs are rigid polymers that possess a low level of chain entanglement. They have a high free volume and ability to swell due to the loose chain packing. HCPs can be obtained with different porosities, varying synthetic parameters, *e.g.* synthesis temperature, the degree to which the used precursor is cross-linked or a catalyst for Friedel–Crafts reaction.[15]

1.2.4. Conjugated microporous polymers (CMPs)

CMPs are network that are built up by multiple carbon–carbon bonds and aromatic rings in a π-conjugated fashion. The conditions required for their synthesis are milder than in case of CMPs or CTFs, which allows the inclusion of big range of functionalities. CMPs are obtained via different types of carbon-carbon coupling – Sonogashira coupling[16], Yamamoto

coupling[17], Suzuki-Miyaura coupling[18], cobalt[19] or palladium[20] catalysed homocoupling of di- or tri-alkynes.

In 2007 the group of Cooper reported on the synthesis of several CMPs obtained via Sonogashira–Hagihara coupling. CMP-1 constructed from 1,3,5-triethynylbenzene and 1,4-diiodobenzene showed the highest surface area of 834 m^2g^{-1}.[20]

In 1994 Wuest *et. al.* presented three-dimensional organic networks with zeolitic properties replacing carbon atom within the framework by Si and Sn.[21] Later Kaskel *et. al.* introduced Elemental Organic Frameworks (EOFs) – a type of CMPs that contain Si[22], Sn, Sb, Bi[23] elements connected via organic linkers by element-carbon bonds.

2.1.5. Polymers of Intrinsic microporosity (PIMs)

PIMs were pioneered by McKeown and Budd.[24-25] PIMs are polymers that possess contorted structure with a rigid backbone, which does not allow any free rotation around it. They are made via non-reversible condensation, which results in ineffective packing of the polymer. Porosity in PIMs is coming from bent monomers possessing a so-called "site of contortion" – a tetrahedral carbon atom. In other words, PIMs do not require a network of covalent bonds to exhibit microporosity; appropriate free volume is trapped within the network due to an irregular, twisted backbone. PIM-1 (Figure 1.3b), synthesised from tetrafluoroterephthalonitrile and 5,5',6,6'-tetrahydroxy-3,3,3',3'-tetramethyl-1,1'-spirobisindane, has a BET area of 850 m^2g^{-1} and the total pore volume of 0.98 $cm^3\ g^{-1}$.[26]

1.3. POFs BASED CATALYSTS OBTAINED BY PRE-SYNTHETIC STRATEGY

The "bottom-up" strategy is often preferred since it allows distributing a high density of functional groups or catalytic sites more homogeneously within the network.

1.3.1. Metal containing POFs based catalysts obtained be pre-synthetic strategy

Chen *et. al.* described in 2010 a synthesis of CMPs using a Fe metalloporphyprin building block via Suzuki coupling.[27] The obtained FeP-CMP catalyst (Figure 1.4) was

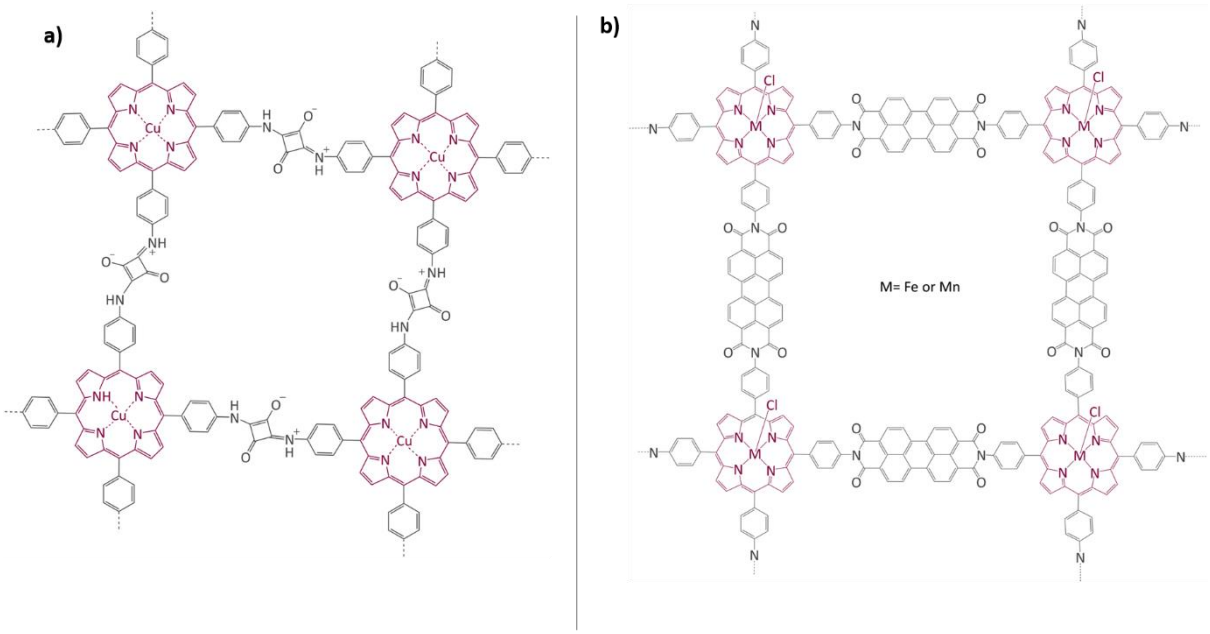

Figure 1.4. Structures of porphyrin containing COFs a) Nagai *et. al.*[28] b) Singh *et.al.* [30]

employed for the activation of molecular oxygen under ambient conditions to convert sulfide to sulfoxide. The catalyst showed activity with a broad range of substrates showing large *TON* (97320) and up to 99% conversion.[27] Three years later, the same group described a synthesis of CuP-SQ catalyst – a crystalline porous polymer obtained via condensation of squaric acid and copper(II)5,10,15,20-tetrakis(4-aminophenyl)porphyrin (Figure 1.4a). CuP-SQ COF was tested in oxygen evolution reaction as a photocatalyst. The extended π conjugation, due to the presence of squarine building blocks, improved the light harvesting capacity and lowered the bandgap, compared to its porphyrin monomer. CuP-SQ COF, that contains no noble metal, was able to generate the triplet excited state that triggers the activation of molecular oxygen upon the absorption of visible photons.[28]

Lin *et. al.* presented COF-366-Co and COF-367-Co as catalysts for electrochemical reduction of CO_2 to CO in water. The frameworks are built up by imine-condensation of 5,10,15,20-tetrakis(4-aminophenyl)porphinato cobalt and 1,4-benzenedicarboxaldehyde or 4,4'-biphenyldicarbaldehyde. The catalyst exhibited a high Faradaic efficiency (90%) and turnover numbers up to 290 000.[29] Singh et.al also recently described synthesis and application of a porphyrin containing network. They reported bis-imide linked iron and manganese porphyrin networks, prepared via condensation of of 5,10,15,20-tetrakis(4-aminophenyl) iron or manganese porphyrin with perylene-3,4,9,10-tetracarboxylic

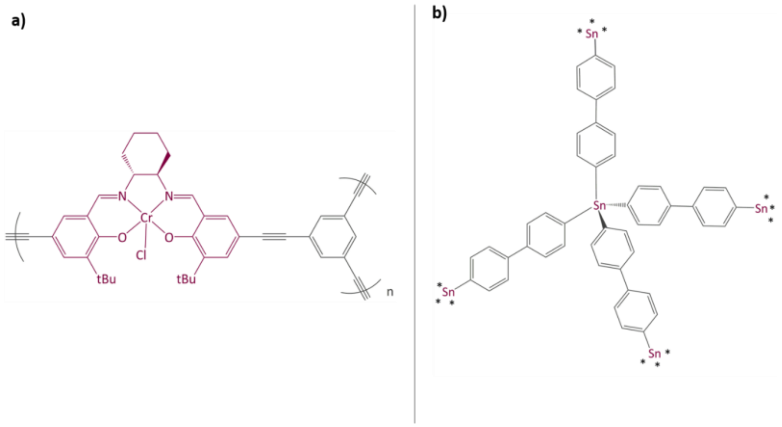

Figure 1.5. Structure of a) MsMOP-1[32] b) EOF-3[35]

dianhydride (Figure 1.4b). These materials were employed in selective oxidation of alkanes and alkenes with *tert*-butyl hydroperoxide; they showed very good recyclability.[30]

Jiang et al. employed CMP based catalyst, where bypiridine and phenylpyridine complexes of Re, Rh and Ir were incorporated into a framework via Sonogashira–Hagihara cross-coupling. Two different Metal–Organic Conjugated Microporous Polymers (abbreviated by the authors as MOP-CMPs) were synthesised from two different preformed metal–organic monomers – bi- and tetra-functional with respect to the Sonagashira–Hagihara reaction. In the latter case, the situation resembles bonding patterns in MOFs where the metal atoms are integral nodes in the network structure. In the same work, post-functionalisation of the framework with the same iridium complex was performed to obtain CMP-CpIr-3 catalyst. CMP-CpIr-3 was tested as a catalyst in a reductive amination of ketones. The catalyst displayed high catalytic with yields of isolated product higher than 90%, which are comparable with the results obtained for a related homogeneous Ir catalyst. [31]

Li *et. al.* described a synthesis of metallosalen microporous organic polymer (referred to as MsMOP-1) with salen-palladium building blocks (Figure 1.5a). The framework was employed as a catalyst for Suzuki-Miyaura coupling for a range of substrates; it showed high activity and good recyclability – the reaction was repeated five times without any significant loss of activity.[32] Another example of using salen complex as a building block was reported by the group of Deng.[33-34] They have prepared Co- and Al-coordinated CMP capable of capturing and conversing CO_2 to propylene carbonate at room temperature and atmospheric pressure.[33] When co-catalysed with a quaternary ammonium salt TBAB, Co-CMP and Al-CMP showed a superior catalytic activity to corresponding homogeneous catalyst – with a

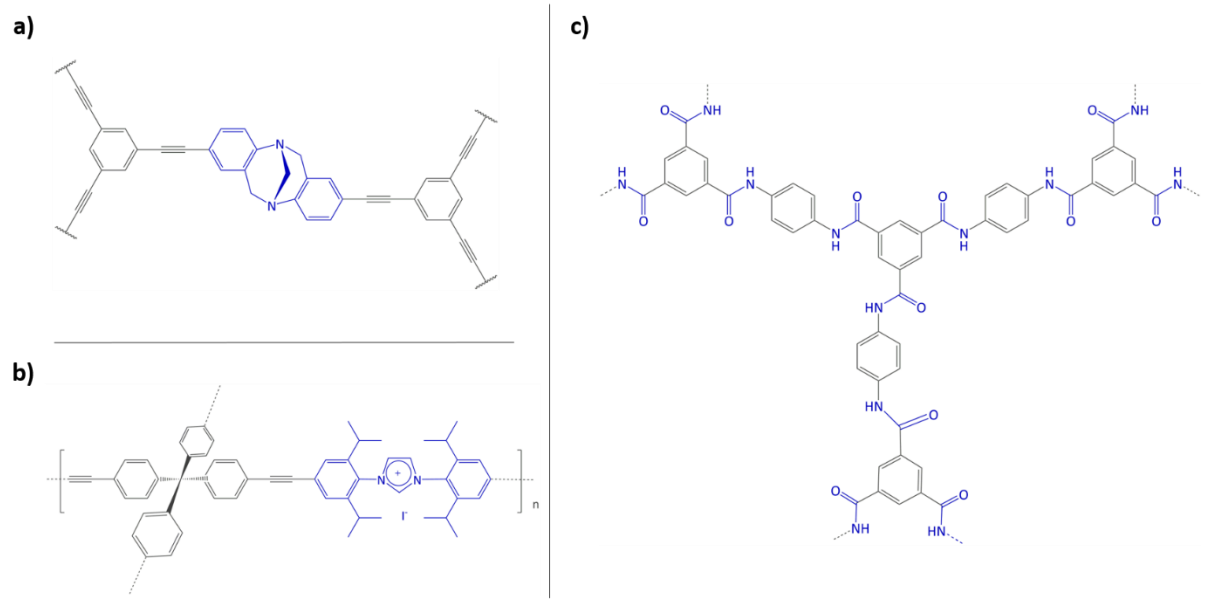

Figure 1.6. Structures of a) Tröger's base functionalised framework[37] b) T-IM[39] c) Am-MOP[41]

homogeneous salen-Co-OAc *TON*s of 158 were obtained, while Co- and Al-CMP showed *TON*s of 201 and 187 respectively. The higher activity of the heterogeneous system was explained by enriched CO_2 capture ability of Co(Al)-CMP and, therefore, the higher local concentration of CO_2 within the polymer. Co-CMP was recycled 22 times without the significant loss of activity, while with Al-CMP the reaction yields dropped from 78.2% to 51.3% after only three times. Trace water in the system may have formed inactive Al species due to the highly hygroscopic nature of salen-Al. Later, they synthesised a chromium implanted network Cr-CMP, which was used to capture CO_2 and subsequently catalyse its cycloaddition to epoxides forming cyclic carbonates. The catalyst showed a superior activity to its homogeneous counterpart and was reused more than ten times without significant loss in its activity.[34]

Wang *et. al.* reported a series of porous organic polymers prepared via Sonogashira chemistry from N-heterocyclic carbine gold(I) and alkynes of different chain length. Different linker size and allowed to control the porosity of the obtained framework. They reported however, that the surface area may be tuned not only varying linker size but also through concentration control during the synthesis. These frameworks were tested in alkyne hydration reaction for a range of substrates. The catalysts were reused at least five times without a significant loss of activity.[35]

Fritsch *et. al.* presented aforementioned EOFs based on Sn (EOF-3, Figure 1.5b), Sb (EOF-4) and Bi (EOF-5) as heterogeneous catalysts for cyanosylilation of benzaldehyde. All three networks showed good stability and catalytic activity. The heterogeneity of the reaction

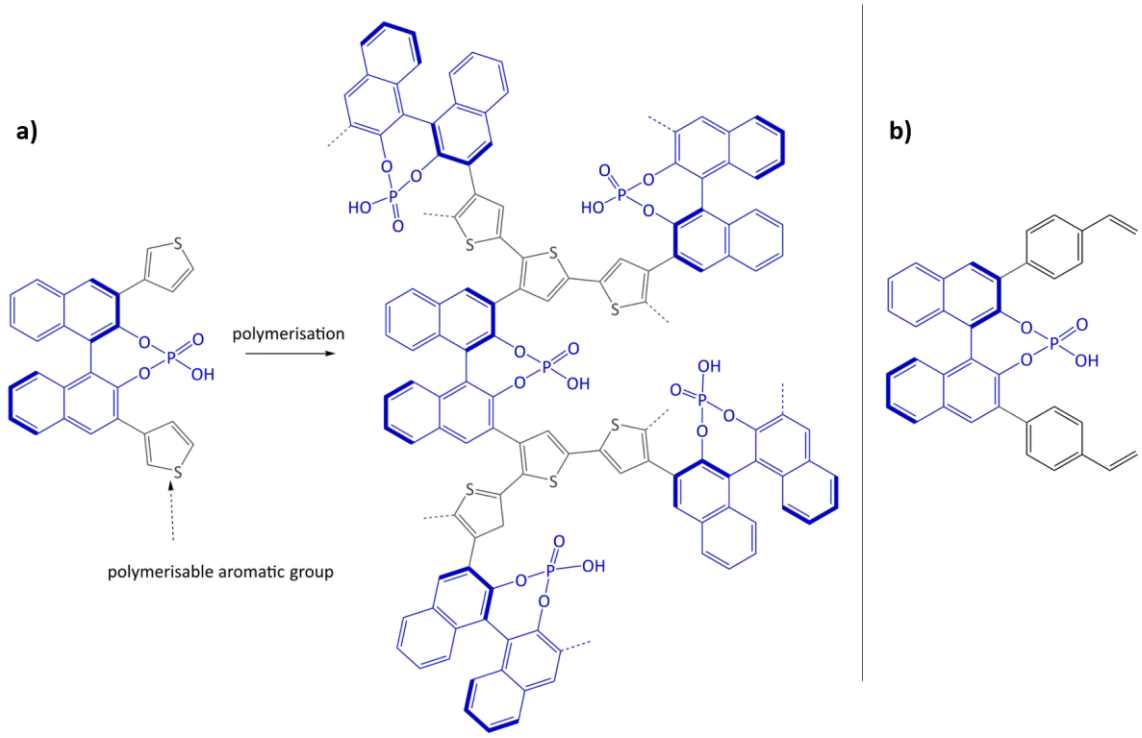

Figure 1.7. a) Concept of immobilisation of BINOL-derived phosphoric acid via oxidative coupling of thiophene[38] b) BINOL building block for copolymerisation with styrene and divinylbenzene[40]

was proven by filtration test.[36] Wee *et. al.* also used Sn-EOF, this time it was tested as a catalyst for esterification of oleic acid with glycerol. It outperformed several MOFs, which were also tested under the same conditions, in terms of stability and catalytic performance, achieving >98% selectivity towards monoglyceride at 40% conversion.[37]

1.3.2. Metal -free POFs based catalysts obtained be pre-synthetic strategy

Du *et.al.* described a synthesis of microporous polymer which contains bicovalently-bonded Tröger's base a functional moiety (Figure 1.6a). The network was constructed via Sonogashira-Hagihara coupling reaction and has a BET area of 750 m^2g^{-1}. Such network was for the first time tried as a catalyst – the addition reaction of diethylzinc to 4-chlorobenzaldehyde was performed. The catalyst showed a comparable activity to homogeneous Tröger's-base derivatives; it did not show appreciable decrease in catalytic activity after three runs. [38]

Bleschke *et. al.*, using the same bottom-up approach introduced chirality into a fully organic framework. Chiral 1,1'-bi-2-naphthol scaffold (BINOL) was used as a chiral tecton (the word "tecton" represents a molecule whose interactions are dominated by particular

associative forces that induce the self-assembly of an organised network with specific architectural or functional features), in order to introduce enantioselectivity into a desired catalyst. BINOL was chosen because of its structure-directing function, and on top of that, its corresponding phosphoric acid is well-known as an important organocatalyst. Substitution of BINOL's phenyl groups by bulkier aromatic groups increases the catalyst's enantioselectivity. In this work, the original idea to substitute phenyl groups by polymerisable aromatic groups was implemented. The porous network was constructed by oxidative coupling of thiophenes (Figure 1.7a). The catalyst was applied in transfer hydrogenation of dihydro-*2H*-benzoxazine. It showed increased enantioselectivity in comparison to the homogeneous reaction from 34% to 56% *ee*. Recycling of the catalyst showed no leaching.[39] In the follow-up work the same catalyst was tested in asymmetric hydrogenation of 3-phenyl-*2H*-1,4-benzoxaine, range of 2-aryl quinolones and asymmetric Friedel-Crafts alkylation of pyrrole, showing high activity and selectivity in all cases.[40] Rueping *et.al.* also employed BINOL building block to build up an organic network. However different approach was used, where the precursor (Figure 1.7b) was copolymerised with styrene and divinylbenzene. In contrast to most polysterene-based systems, this catalyst was not removed by filtration, but was designed in a form of a polymer-stick by tea-bag approach – the mixture was placed into a tube and allowed to solidify until it was possible to remove the stick shaped catalyst from the tube. The catalyst was tested in transfer hydrogenation reaction of benzoxazine in several solvents. The product was obtained with good isolated yields and excellent enantioselectivities. The polymer stick was recycled 12 times, and no deactivation was observed.[41]

Cho *et.al*. prepared a tube-shaped microporous organic network bearing imidazolium salt (T-IM) by Sonogashira coupling of tetrakis(4-ethylphenyl)methane with diiodoimidazolium salt (Figure 1.6b). T-IM was tested as a heterogeneous catalyst in conversion of CO_2 with epoxides into cyclic carbonates. It showed very promising activity with TOFs range 92-142 h^{-1}. [42] Rose *et.al.* used imidazolium linker as well, preparing a highly crosslinked EOF by Suzuki-Miyaura coupling. The carbon and silica based EOF were tested in conjugated umpolung of α,β-unsaturated cinnamaldehyde and coupling with trifluoroacetophenone. The catalysts showed similar results compared to molecular species in homogeneous catalysis.[22]

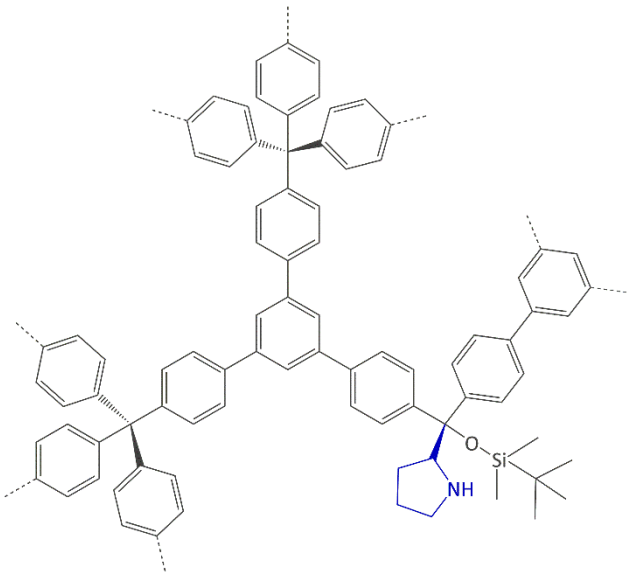

Figure 1.8. Structure of JH-CPP [44]

Suresh *et.al.* reported the synthesis of an amide functionalised microporous organic polymer (by the authors referred to as Am-MOP, Figure 2.6c). The framework is constructed trimesic acid and *p*-phenylenediamine using thiony chloride. The framework allows highly selective CO_2 uptake over other gases, since its pore surface is very polar. It also showed a catalytic activity in Knoevenagel condensation of aldehydes and methylene compounds.[43]

Group of Zhao recently described the synthesis of porous polymers bearing functional quaternary ammonium salts by copolymerisation of divinylbenzene and hydroxyl functionalised quaternary ammonium salts. This is a highly cross-linked material with BET area of 708 m^2g^{-1}. It showed excellent catalytic performance in synthesis of cyclic carbonates from epoxides and CO_2 in under metal-solvent-free conditions. High activity was explained by synergetic effect between Br^- active centres present within the network and functional -OH groups.[44]

Wang *et. al.* presented robust chiral porous polymer with an embedded Jørgensen-Hayashi catalyst, denoted JH-CPP (Figure 1.8). JH-CPP was synthesised by the $Co_2(CO)_8$-mediated trimerisation of tetrahedrally structured building blocks. There are both micro- and mesopores present with BET area 881 m^2g^{-1}. JH-CPP showed high activity in catalysing the asymmetric Michael addition of aldehydes to nitroalkenes, achieving good to excellent yield (67-99%), high enantioselectivity (93-99 % *ee*) and high diastereoselectivity (diastereomeric ratio of 74:26 to 97:3). The catalyst was reused four times without loss of selectivity.[45]

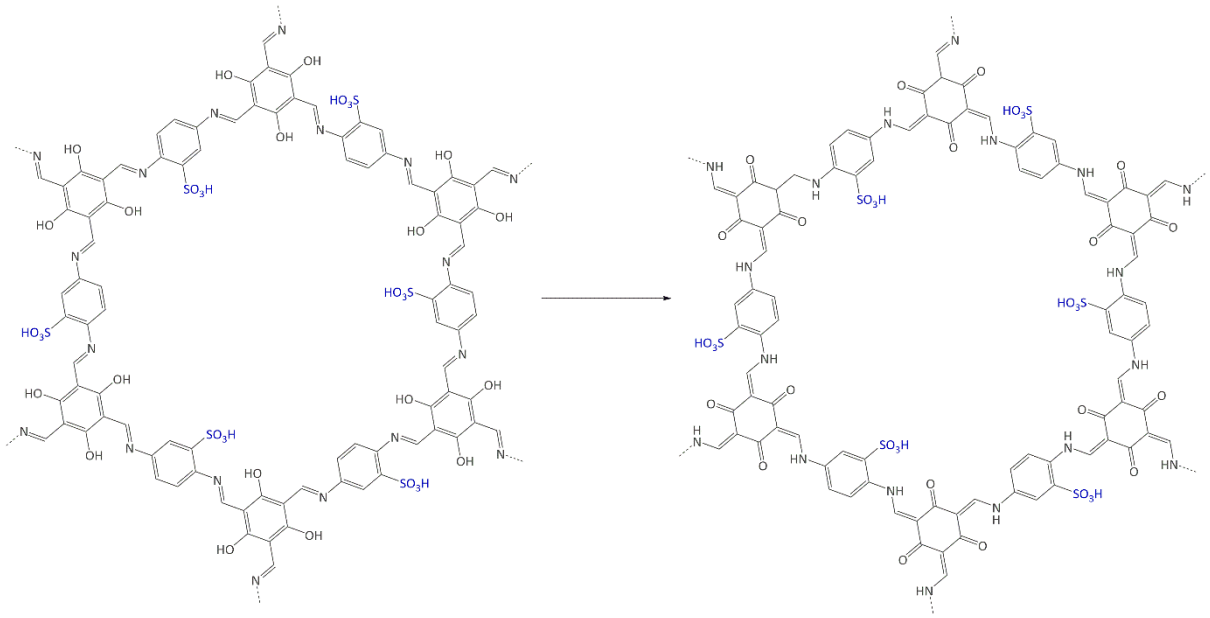

Figure 1.9. Enol-to-keto tautomerisation that followed Schiff base reaction in order to obtain TFP-DABA [45]

Sulfonated crystalline network, was reported by Peng *et.al.* The framework was prepared via Schiff base condensation of 1,3,5-triformylphloroglucinol and 2,5-diaminobenzenesulfonic acid, followed by irreversible enol-to-keto tautomerisation, which stabilised the framework, named TFP-DABA (Figure 1.9). TFP-DABA was studied as acid catalyst in fructose dehydration to 5-hydroxymethylfurfural (HMF) and, if KBr was employed a co-catalyst, to 2,5-diformylfuran (DFF). It exhibited 97% and 65% yield for HMF and DFF respectively, combined with good chemoselectivity. After recycling the catalyst three times, it lost its crystallinity; this was explained by possible partial exfoliation of the framework. The crystallinity was easily reconverted by subjecting the COF into the initial synthetic conditions.[46]

Saptal *et. al.* reported the synthesis of two catechol porphyrin COF catalysts for chemical fixation of carbon dioxide via cyclic carbonates and oxazolidinones. The COFs were synthesised via Schiff base reaction using 2,3-dihydroxyterephthalaldehyde (2,3-DhaTph) or 2,3-dimethoxyterephthalaldehyde (2,3-DmaTph) units. The 2,3-DhaTph framework is bearing hydrogen bond donor and it was found to be highly active, selective and recyclable catalyst for the chemical fixation of carbon dioxide under solvent-free conditions. The catalyst showed high turnover frequency and high regioselectivity for both synthesis of cyclic carbonates and oxazolidiones.[47]

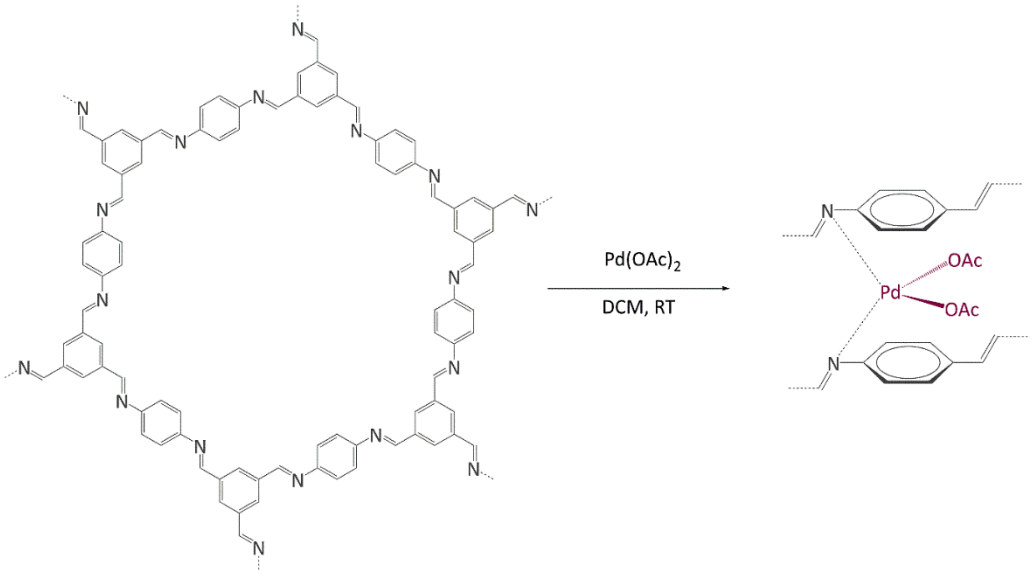

Figure 1.10. Proposed structure of COF-LZU1 and its post-treatment to obtain Pd/COF-LZU1[46]

1.4. POFs BASED CATALYSTS OBTAINED BY POST-SYNTHETIC STRATEGY

1.4.1. Pd based catalysts for Suzuki-Miyaura coupling and other reactions

In 2011 Ding *et.al.* described the application of imine-linked COF (COF-LZU1, named after Lanzhou University, China) as a support for Pd complex. Simple post-treatment of COF-LZU1 resulted in Pd/COF-LZU1 (Figure 1.10) catalyst with robustly incorporated $Pd(OAc)_2$. The crystallinity of the framework after the post-functionalisation was fully preserved, and coordination of Pd to N atoms was confirmed by XPS and ^{13}C CPMAS NMR. The catalyst showed a superior activity in Suzuki-Miyaura coupling of a broad range of reactants, showing excellent yields and high stability. The tolerance of COF-LZU1 in relatively harsh conditions was verified.[48]

Li *et.al.* prepared a high surface area microporous materials, referred to as Knitting Aryl Networks (KAP) via knitting of PPh_3 with benzene. Further binding PPh_3 groups with $PdCl_2$ produced KAPs(Ph-PPh_3)-Pd catalyst. The frameworks enabled efficient dispersion of Pd within its structure. The presence of PPh_3 functional groups and incorporation of Pd was confirmed by FTIR, SS ^{13}CPMAS and ^{31}P HPDEC NMR, and XPS techniques. KAPs(Ph-PPh_3)-Pd exhibited excellent activity and selectivity in Suzuki-Miyaura cross-coupling reaction of aryl chlorides.[49] Later the same group reported a cost-effective approach to prepare microporous organic polymers via Scholl reaction. The approach involves the elimination of two aryl-

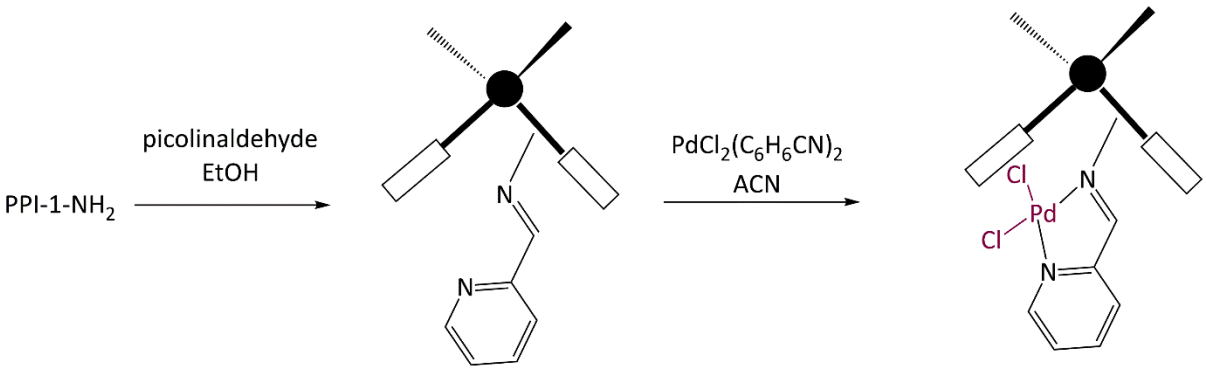

Figure 1.11. Synthesis of heterogenised Pd catalyst PPI-NPy-Pd[51]

bonded hydrogen atoms accompanied by the formation of a new aryl-aryl bond in the presence of Friedel-Crafts catalyst. A series of polymers was prepared varying the starting building blocks. Frameworks named SMP-8a and SMP-9a (Scholl-coupling Microporous Polymers), both prepared from *sym*-$PhPh_3$, and PPh_3 and bipyridine as a second building block, respectively, were analysed as catalyst supports. SMP-8b catalyst, obtained by treating SMP-8a framework with $PdCl_2$, showed high activity in Suzuki-Miyaura coupling reaction (*TOF*s up to 59 400 h^{-1}) using water-ethanol mixture as a solvent. It and was recycled four times without performance drop. The heterogeneous nature of the catalyst was confirmed by hot filtration test. SMP-9a framework was coordinated with Cu(NO3)2. The obtained catalyst, SMP-9b was employed in alcohol oxidation reaction.[50]

Li *et.al.* described a synthesis of two urea-based porous organic frameworks, named UOF-1 and UOF-2, synthesised via condensation of 1,3,5-benzenetriisocyanate with 1,4-diaminobenzene and benzidine, respectively. The palladium containing catalysts, Pd^{II}/UOF-1 and Pd^{II}/UOF-2 were obtained by treating the pristine polymers with $[Pd(OAc)_2]$. The coordination of Pd^{II} species was confirmed with ^{13}C CPMAS NMR and XPS. Both catalysts showed high catalytic activity in Suzuki-Miyaura coupling in water for a large range of substrates. Pd^{II}/UOF-1 showed a slight loss in catalytic activity in the fourth reaction run, whereas the reactivity of Pd^{II}/UOF-2 decreased after the third run. Both Pd^{II}/UOF-1 and Pd^{II}/UOF-2 were also tested in the reaction of reduction of nitroarenes. Pd^{II}/UOF-1 did not show any drop in catalytic activity through four reaction runs, but the selectivity had dropped. However, the activity and selectivity of Pd^{II}/UOF-2 dropped only in the fifth catalytic run. TEM and XPS analysis of the spent catalysts demonstrated that Pd^{II} was partially reduced to Pd^{o} and well dispersed metal nanoparticles were formed after the first run of a reaction.[51]

Group of Iglesias presented functionalised porous polyimides (dubbed PPI-*n*) prepared by condensation of aromatic amines with pyromellitic dianhydride. The frameworks were functionalised with amino groups (PPI-*n*-NH_2) – first, nitration was performed, followed by the reduction of nitro groups by $SnCl_2 \cdot 2H_2O$ in THF. The incorporation of Pd was performed in two steps. First, amino-functionalised frameworks reacted with picolinaldehyde to yield the imino pyridine ligands (PPI-*n*-NPy). After, these derivatives reacted with *bis*(benzonitrile)palladium(II) chloride (PPI-*n*-NPy-Pd, Figure 1.11). The catalysts were tried in Suzuki coupling in pure water. The catalyst showed high activity for a range of substrates and its heterogeneous nature was confirmed by hot filtration test. The catalyst also demonstrated good recyclability, while ICP analysis for one of the reused Pd functionalised frameworks demonstrated that 20% of Pd was lost after seven runs, probably due to the washing of the powder.[52]

Hou *et.al.* presented a nitrogen-rich COF built up from 5,10,15,20-tetra(*p*-amino-phenyl)porphyrin and 4,4'-biphenyldialdehyde. The periodically distributed N atoms allowed to uniformly disperse Pd ions. To prepare the catalyst, $Pd(OAc)_2$ was used, and its coordination was confirmed by XPS and ^{13}C CP/TOSS NMR. The catalyst showed high activity in Suzuki-Miyaura coupling reaction with good selectivity and yields. The hot filtration test indicated the heterogeneous nature of the catalyst. TEM analysis of a spent catalyst did not reveal any obvious aggregates or morphology change. Leaching of Pd was below the detection limit of ICP instrumentation.[53]

Haosoul *et.al.* developed 4,4'-biphenyl/phosphine based amorphous framework with high PAr_3 content. Palladium coordination to P atoms was achieved from $Pd(acac)_2$ precursor, while $Pd(dba)_2$ led to formation of Pd^o. The coordination was confirmed with ^{31}P NMR and DRIFTS spectroscopy. The catalyst was tested in telomerisation of 1,3-butadiene with phenol and glycerol. High activity and selectivity were obtained under solvent – and base-free conditions, and in the case of glycerol telomerisation, the catalyst outperformed its homogeneous analogue PPh_3. It was possible to increase selectivity by increasing ligand-to-metal ration, which also reduced the metal leaching.[54]

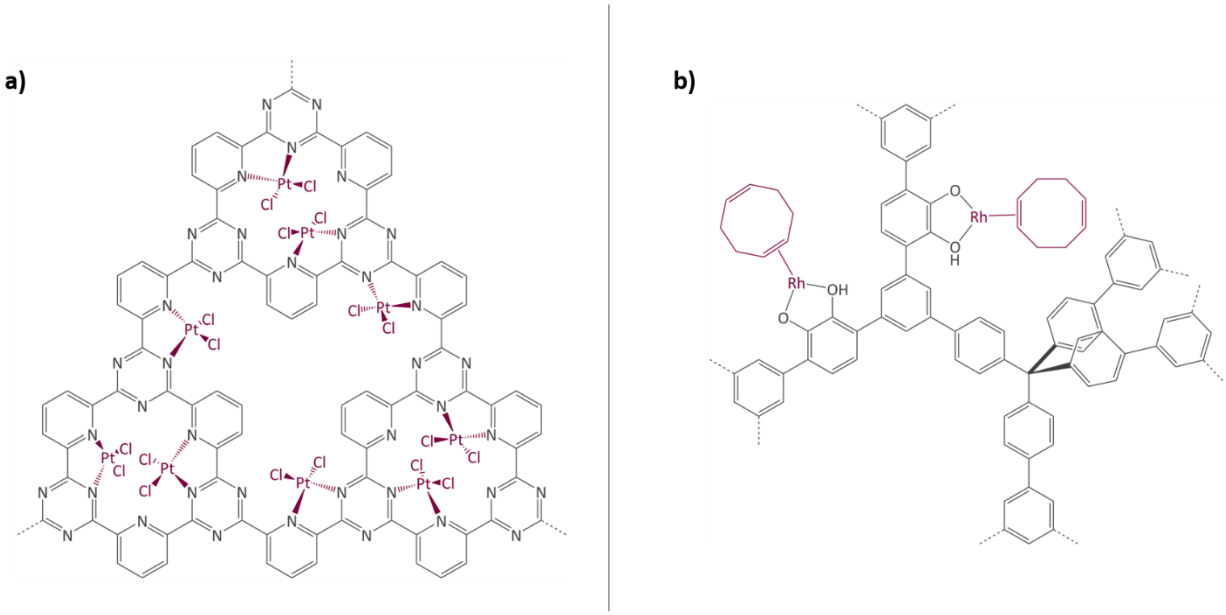

Figure 1.12. a) Periana catalyst immobilised on CTF[54] b) Rh(I) complex immobilised on Catecholate containing POP[57]

1.4.2. Other noble metal based catalysts

Palkovits *et.al*. presented an immobilised Periana catalyst on CTF support (Figure 1.12a). $K_2[PtCl_4]$ was chosen as platinum precursor and its successful coordination to bipyridine moieties within CTF was confirmed by XPS. Catalysed methane to methanol oxidation was conducted in oleum media at high temperature and pressure (215˚C and 40 bar). The catalyst showed remarkable stability in such harsh conditions. The first test showed *TONs* of only 26, but recycling the catalyst showed increased of activity (*TON*s above 250), which was preserved throughout several catalytic runs. Simple addition of CTF and $K_2[PtCl_4]$ in the catalytic reaction led to formation of the catalyst *in-situ* as well, which was confirmed by XPS of the spent powder. This catalyst also showed high catalytic activity (*TON*s of around 300 after five catalytic runs) and very little of deactivation.[55]

Kamiya *et.al.* also employed Pt and CTF to develop methanol-tolerant oxygen reduction electrocatalyst. To improve poor electrical conductivity of CTFs, carbon nanoparticles were introduced during its polymerisation process. Platinum from $K_2[PtCl_4]$ was successfully coordinated to the resulted material. The catalyst showed clear electrocatalytic activity for oxygen reduction in acidic media. Almost no activity for methanol oxidation was observed, in contrast to commercial carbon-supported Pt. This is an important aspect, since it allows to use the catalyst in direct methanol fuel cells.[56]

Rhodium complexes were also extensively employed to obtain porous heterogeneous catalysts. Fritsch *et.al.* employed already mentioned before phosphorus based framework EOF-17[36] to coordinate Wilkinson catalyst to P containing ligands. Only 5mol% of $RhCl(PPh)_3$ content was achieved and the complexation of Rh@EOF-17 was not investigated. Instead, complexation of palladium from $PdCl_2$ to EOF-17 was proven by ^{31}P NMR as an example. Rh@EOF-17 was tested in the transfer hydrogenation of cycloxenanone. The heterogeneous nature of this catalyst was proven by hot filtration test. After 6h of the reaction, the yield of 80% was observed. However it decreased to around 40% after three catalytic cycles.[23] In 2012 Weston *et.al.* reported a synthesis of catechol-containing POP using a cobalt catalysed acetylene trimerization strategy.[57] It was shown that post-metalation can be readily carried out with a wide range of metal precursors - Cu^{II}, Mg^{II}, and Mn^{II} salts and complexes. In 2014, together with Hock, the same catechol-containing POP was used to immobilise Rh(I) complex (Figure 1.12b). The coordination was confirmed by CP NMR, EXAFS and XANES. The obtained metalated POP was tested in vapour-phase plug-flow hydrogenation of propylene to propane, the catalyst showed a TOF of 22.5 h^{-1} at room temperature, while the oxidation state of rhodium remained unchanged. Rh(I) was proven to be the active catalytic site. When the catalyst was explored in toluene hydrogenation under the same conditions as propylene, it did not show any activity. A high temperature reduction of the Rh(I) metal centres to nanoparticles was performed; the obtained Rh(NP)(CAT-POP) converted toluene to methylcyclohexadiene (the ratio of H_2 to toluene was approximately 1:1) quantitatively at 25 °C (*TOF* of 9.3 × 10−3 mol g^{-1} h^{-1}).

Bavykina et.al. immobilised IrCp* complex employing bipyridine units of CTF. The employed framework was made by trimerisation of two building blocks – pyridine units introduced bipyridine moieties, while biphenyl units brought mesoporosity to CTF (Chapter 3 of this thesis). The successful coordination of Ir^{III} from $[IrCl_2Cp^*]_2$ was confirmed by XPS. Chlorine ions were removed by washing the solid in DMF. The catalyst was tested in hydrogen production from formic acid. The CTF framework worked not only as a support for the iridium complex, but behaved like a non-innocent ligand – pyridine units were able to deprotonate formic acid, launching the catalytic cycle, avoiding the use of an external base. The catalyst exhibited a record activity for this reaction for a heterogeneous catalyst (*TOF*s of 27000 h^{-1} were obtained).[58] The same group, in an attempt to bring the use of CTF-based molecular

catalysts a step closer to industrial reality, reported a one-step approach for the production of porous, mechanically rigid, and easy-to-handle CTF-based spheres prepared by a phase inversion method using the polyimide Matrimid® as a binder (Chapter 4 of this thesis). After obtaining the spheres, $Ir^{III}Cp^*$ was coordinated to the bipyridine moieties of CTF in a similar way as in previously mentioned works to obtain efficient catalyst. Both powder and shaped catalyst were tried in the hydrogenation of carbon dioxide to formic acid. Sphere shaped composites showed lower total activity than the powder, however, any iridium loss connected to handling, washing or filtering powder, was fully eliminated.[59] Park et.al employed the same approach, performing hydrogenation of carbon dioxide to formic acid.[60]The same $[IrCl_2Cp^*]_2$ complex was employed in order to coordinate Ir^{II} to a framework. CTF with bipyridine links was tested, the obtained catalyst showed high activity (*TOF*s of 5300 h^{-1}). A year later the same group tested a heptazine-based organic framework instead. This catalyst displayed good performance as well, *TON* value of 6400 was obtained, the highest reported value for a heterogeneous system for carbon dioxide reduction to formic acid.[61]

Porous polymer based catalyst for the same purpose of formic acid decomposition, but ruthenium based, was reported by Haosoul *et.al.* They employed phosphorous based polymer to coordinate the $[RuCl_2(p\text{-cymene})]$ complex. The catalyst showed high activity under base-free conditions, recycling tests revealed a low level of leaching and only a gradual decrease of activity after seven catalytic runs. The catalyst was proposed to be applied in the facile removal of formic acid, which is a by-product of conversion of cellulose to levulinic acid.[62] Salam *et.al.* described a facile *in-situ* radical polymerisation of 2,4,6-triallyloxy-1,3,5-triazine in aqueous medium in presence of an anionic surfactant (sodium dodecyl sulfate) as a template. Ruthenium chloride was successfully coordinated to the obtained network; by XPS analysis it was shown that oxidation state of Ru was 2+. The catalyst was tested in Suzuki-Miyaura coupling of aryl halides and transfer hydrogenation of carbonyl compounds. The catalyst showed high activity and was recycled several times without appreciable loss of activity.[63] Group of Xiao reported the preparation of chiral catalyst (Ru/PCP-BINAP) from copolymerisation of divinylbenzene and chiral 2,2'-bis(diphenylphosphino)-1,1'-binaphthyl] (BINAP) ligands. The obtained framework was coordinated with $[RuCl_2(benzene)]$; the coordination was confirmed by an obvious shift of UV-Vis spectra between PCP-BINAP and Ru/PCP-BINAP. To evaluate the catalyst efficiency, asymmetric hydrogenation of β-keto esters

was performed. With substrate/catalyst ratio of 2000, the highest reported enantioselectivity (for such ratio) was reported (94.6 % *ee*). Even with a ratio increased to 5000, methyl-3-hydroxybutyrate was completely converted with 90.1% *ee*. Such a high enantioselectivity was explained by not grafting of BINAP ligands into the framework, but its incorporation into the polymer backbone. Also the nature of Ru coordination to BINAP is quite similar to the homogeneous catalyst.[64]

1.4.3. Non-noble metal based catalysts

Zhang *et.al.* reported the synthesis of microporous polyisocyanurate (PICU), derived by cyclotrimerisation of diisocyanate using N-heterocyclic carbine as a catalyst. Fe/PICU was prepared by suspending PICU in hot solution of $FeCl_2$ in DMF. Oxidation of benzyl alcohol with hydrogen peroxide was over Fe/PICU was tested. It showed excellent activity, selectivity and recyclability. It was explained by concentration of benzyl alcohol in the micropores of PICU around active Fe sites, what further promotes the catalytic conversion.[65] Shultz *et.al.* synthesised a POP containing a free-base porphyrin subunit by condensation of bis(phtalic acid)porphyrin with tetra(4-aminophenyl)methane (named Fb-PPOP, Fb referring to the free-base porphyrin). Post-metalation was performed using $FeCl_2$ or $MnCl_2 \cdot 4H_2O$, achieving both Fe- and Mn-based PPOP respectively. Epoxidation of styrene was examined, where both catalysts showed better stability that homogeneous porphyrin analogues, *e.g.* Mn-PPOP was active for 2000 turnovers without displaying any sign of decomposition. However, during catalyst recycling, the activity loss observed. Fe-PPOP retained only 23% of conversion in the third catalytic run, while Mn-POP retained 60% in the second run. This loss was possibly attributed to the oxidation of individual pyrrolic rings, not destruction of the network.[66] Saha *et.al.* also employed a porphyrin unit based framework for Fe support. In this case, though, Fe^{III}-POP-1 was obtained via one-pot synthesis by reacting pyrrole with terephthaldehyde in the presence of $FeCl_3$. EPR analysis confirmed that Fe was in the oxidation state 3+ after the coordination and remained as such after several catalytic runs. Fe^{III}-POP-1 was tested in aerobic oxidation of 5-hydroxymethylfurfural to 2,5-furandicarboxylic acid. The catalyst showed high activity and its heterogeneity was proven by hot filtration test.[67] Kraft *et.al.* coordinated Fe to catecholate containing porous organic polymer, in a similar fashion to previously described for Pd[68]. $Fe[N(SiMe_3)_3]_2$ was chosen as iron source to obtain the catalyst Et_2OFe(CAT-POP). It was tried in hydrosilylation reaction of aldehydes and ketones with

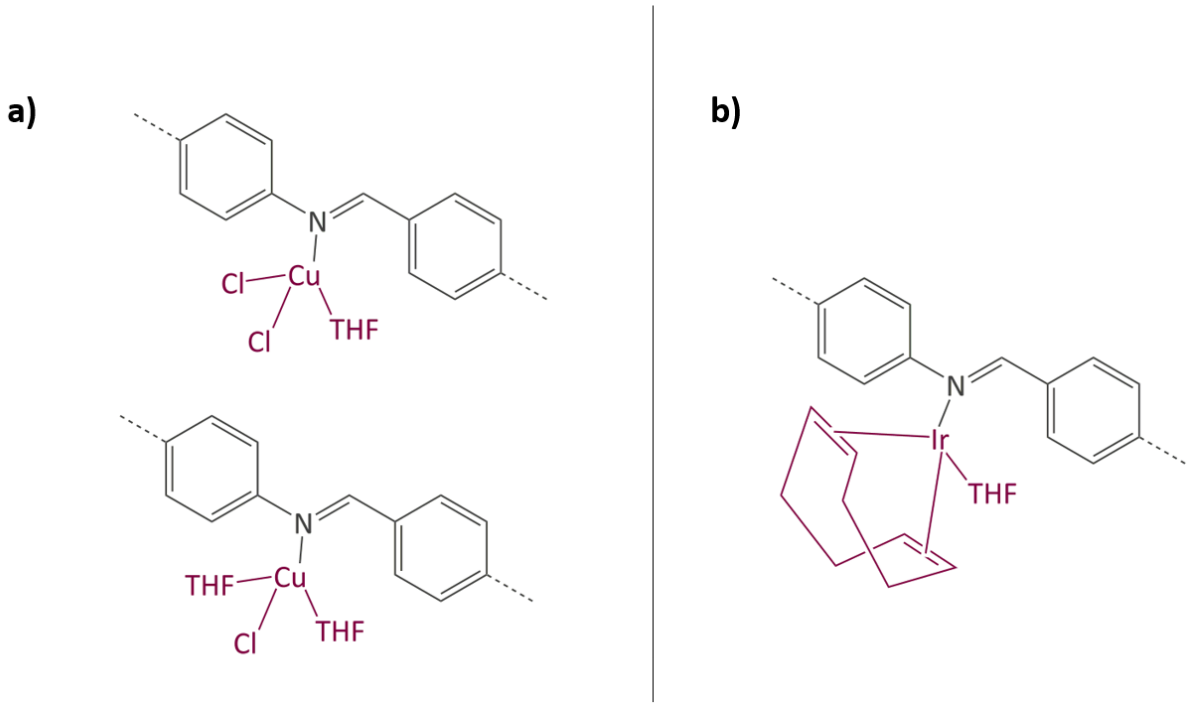

Fugure 1.13. Structures of a) Cu(I)- and Cu(II)-Th-POF b) Ir-Th-POF[73]

phenylsilane. The full conversion was rapidly achieved with average *TOF*s of 1.11s^{-1}. The catalyst is fully reusable, recyclable for three catalytic cycles and showed high thermal stability.[69] In a separate work by the same group, Et_2OFe(CAT-POP) was extensively characterised by *in-situ* XAS under variety of conditions. It was reported that as-prepared material to be three-coordinate Fe^{2+} that readily oxidises to Fe^{3+} upon exposure to air, but remains three-coordinate. Both Fe^{2+} and Fe^{3+} based catalysts were tested in olefin hydrogenation. The Fe^{3+} was active in this reaction, and did not reduce under hydrogen pressure. However, oxidised version of the catalyst did not show any activity in hydrosilylation.[70]

In the section 1.4.2, the use of carbon nanoparticles hybridised CTF (CTF/CPs) coordinated with Pt in electrocatalysis was discussed[56]. This approach was further extended to obtain non-noble metal oxygen reduction reaction (ORR) electrocatalyst. Copper version of the catalyst was prepared by coordination of CTF/CPs with $CuCl_2$. Cu-CTF/CPs was reported to be a very efficient electrocatalyst in ORR in neutral solutions. The ORR onset potential of the catalyst was 810 mV *vs.* RHE, the highest reported value at neutral pH for synthetic Cu based catalyst. Cu-CTF/CPs also displayed higher stability than Cu-based molecular complex, due to covalently cross-linked structure of CTF.[71] The same catalyst was found to be efficient in electrochemical reduction of nitrate to nitrous oxide. It exhibited an onset potential of -50 mV

vs. RHE. The Faradaic efficiency for N_2O formation reached 18% at -200mV *vs.* RHE while for copper metal it was negligible.[72]

Verde-Sesto *et.al.* described the synthesis of two imine-linked POFs with different geometries. C3v-POF and Th-POF were obtained via combining 1,4-benzenedicarbaldehyde with 1,3,5-tris(4-aminophenyl)benzene and tetra-(4-aminophenyl)methane respectively. Th-POF exhibited higher BET surface area and higher metal uptake during post-metalation of the framework. Therefore, only Th-POF was employed as catalyst support. For alkenes cyclopropanation reaction, Th-POF was coordinated with Cu(I) and Cu(II) from corresponding chlorides (Figure 1.13a). Cu(I) based solid showed higher activity. In cyclopropanation of cyclic olefins using EDA, the catalyst displayed remarkable diastereoselectivity. Its performance was unaltered during four catalytic runs and hot filtration experiment was performed to confirm its heterogeneity. On top of that, $[IrCl(COD)_2]$ was also coordinated to Th-POF (Figure 1.13b) and tested in hydrogenation of alkenes. The catalyst could be reused several times with a conversion range of 98%. Slight leaching of Ir to the solution was detected.[73]

Puthiaraj *et.al.* described the synthesis of a mesoporous covalent imine polymer (abbreviated MCIP-1) via Schiff-base condensation of 2,4,6-Tris(*p*-formylphenoxy)-1,3,5-triazine and mesitylene.[74] Post-metalation was performed by stirring the polymer with copper acetate in CH_2Cl_2. The obtained catalyst, Cu/MCIP-1, was used in Chan-Lam cross-coupling reaction N-arylation under mild conditions. The catalyst is highly stable; no metal leaching was observed. Roy *et.al.* anchored Cu^{II} to nitrogen-rich imine network to obtain Cu^{II}-CIN-1 catalyst for the synthesis of unsymmetrical organoselenides from aryl boronic acids. The coordination of copper species was confirmed by EPR, XPS and UV-vis DRS analyses. The catalyst showed high activity using green solvent (PEG-600), was recycled six times without significant loss of activity.[75]

Group of Nguyen has extensively studied metal catalysts supported on catecholate-based framework. In this review Fe[66] and Rh[68] containing catalysts were already discussed, while this approach was extended to other metals. Thus, La was successfully coordinated to the catecholate-functionalised POP. The catalyst was employed in solvolytic and hydrolytic degradation of the toxic organophosphate compound methyl paraoxon, a simulant for nerve agent.[76] Ta^{v} trialkyl was stabilised in the same framework and tested in hydrogenation of

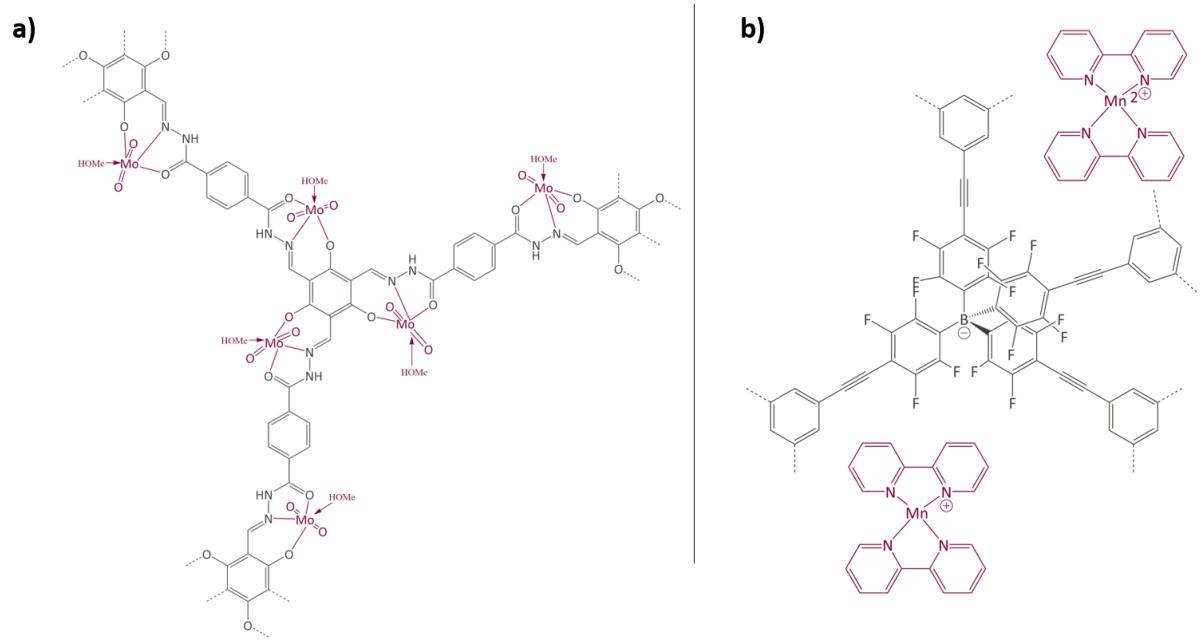

Figure 1.14. a) Mo supported on porous framework catalyst[83] b) Mn supported on anionic framework catalyst[84]

cyclohexene, showing enhanced activity compared to its homogeneous analogue.[77] In a separate work, five different species – V^{III}, Cr^{III}, Mn^{II}, Co^{II} and Ni^{II} – were incorporated into the catecholate-based framework. All the obtained catalysts were tested in alkyne hydrogenation, and all of them were found to be active and selective. For V^{III}, Cr^{III} and Mn^{II} it was the first report of their activity as single-site hydrogenation catalysts.[78] A similar approach to bind a metal via its coordination to hydroxyl groups was reported by Ma *et.al.* Five chiral cross-linked polymers (CCPs) based on 1,1'-binaphtyl were prepared via trimerisation of terminal alkyne groups by $Co_2(CO)_8$ catalyst. The CCPs were treated with $Ti(O^iPr)_4$ to generate chiral Lewis acid catalysts for the asymmetric diethylzinc addition to aldehydes. The catalysts were reused ten times without any loss of conversion or enentioselectivity which was from 55% to 81% *ee* for different frameworks.[79] An *et.al.* synthesised α,α,α',α'-tetraaryl-1,3-dioxolane-4,5-dimethanol (TADDOL) based chiral porous polymer, TADDOL-CPP. Using [$Ti(OiPr)_4$], TADDOL-CPP/Ti was also tested in asymmetric addition of diethylzinc to aldehydes, and presented excellent enantioselective control to variety of aldehydes.[80]

Aiyappa *et.al.* developed Co-TpBpy catalyst for water electrooxidation. Bipyridine-containing framework was used as a support for Co^{II} catalyst. The catalyst showed exceptional stability, even after 1000 cycles and 24 h of OER activity in phosphate buffer under neutral Ph

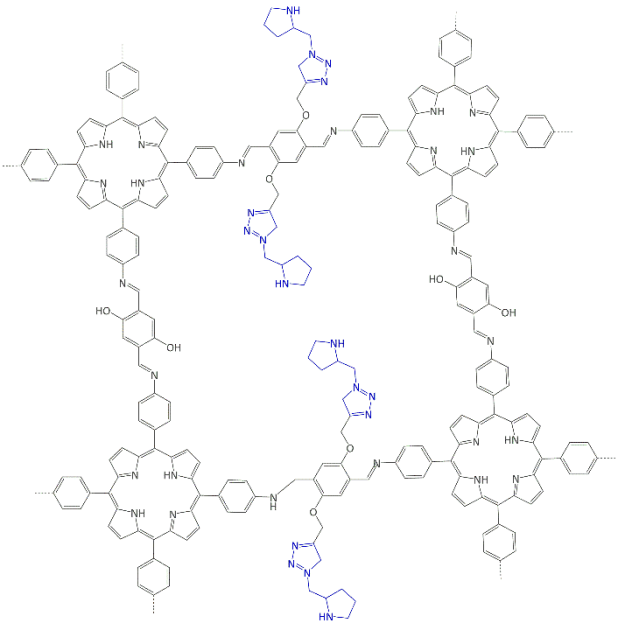

Figure 1.15. H_2P-COF[86]

conditions with an overpotential of 400mV at a current density of 1 mA cm^{-2}, 94% of its activity retained with *TOF* of 0.23 s^{-1} and Faradaic efficiency of 0.95.[81] Mackintosh *et. al.* presented the phthalocyanine and porphyrin based PIMs. Co was incorporated into the phthalocyanine framework and the obtained solid was tested in H_2O_2 decomposition, cyclohexene oxidation and hydroquinone oxidation. Similarly, Fe was introduced into the porphyrin based PIM, the iron catalyst showed the superior activity for hydroquinone oxidation.[82] Zhang *et.al.* synthesised a molybdenum-doped framework linked by a hydrazine linkage. Mo species were introduced into the framework from $MoO_2(acac)_2$ source to obtain a catalyst (Figure 1.14a) for alkenes epoxidation. The catalyst showed excellent performance for the range of different substrates.[83]

Fischer *et.al.* reported the synthesis of anionic microporous polymer network, prepared by the usinng lithium tetrakis(4-bromo-2,3,5,6-tetrafluorophenyl)borate as a tecton via Sonogashira coupling. The Li^+ cations were exchanged to Mn^{2+}, which was further coordinated with bipyridine to obtain a catalyst for the oxidation of styrene (Figure 2.14b). The catalyst is recyclable and stable during first three runs, hot filtration test confirmed the heterogeneity of the catalyst.[84]

1.4.4. Metal-free catalysts

Modak *et. al.* designed a cross-linked organic polymer COP-M from 2,4,6-tris(bromomethyl)mesitylene and 4,4'-bis(bromomethyl)-1,1'-biphenyl via Friedel–Crafts alkylation. COP-A, bearing highly acidic -CO_2H groups, was obtained from alkaline $KMnO_4$ oxidation of methyl functionalized COP-M. COP-A showed unprecedented catalytic activity in indole C – H activation at room temperature.[85]

Xu *et.al.* constructed a mesoporous imine-linked porphyrin COF as a scaffold in which the porphyrin units are located at the vertices and the phenyl groups occupy the edges of tetragonal polygon frameworks. In Figure 1.15a the final catalyst is shown, which was obtained via the click reaction of the ethynyl units with the azide compounds ([Pyr]x-H_2P-COF). The catalytic activitiy was investigated in a Michael addition reaction in aqueous solutions. The COF catalyst showed significantly higher catalytic activity than the monomeric catalyst while retaining the stereoselectivity. [86]

Goesten *et.al.* reported the synthesis, characterisation, sulfonation, and catalytic performance of two new porous aromatic frameworks obtained by the Suzuki–Miyaura cross-coupling of the commercially available precursors 1,3,5-tris(4-bromophenyl)benzene or tris(4-bromophenyl)-amine and benzene-1 4-diboronic acid. Post-synthetic treatment in sulfuric acid led to sulfonation approximately 65% of the benzene rings in the polymers. The sulfonated materials display an excellent catalytic performance in the acid-catalysed esterification of *n*-butanol and acetic acid and have a similar or even superior performance to that of state-of-the-art Amberlyst-15 over multiple catalytic cycles (Chapter 2 of this thesis).[18]

As outlined above the number of different POFs is massive, and rapidly increasing; there is bottomless and diverse chemistry that makes their synthesis possible. Depending on the catalytic application one aims for, different aspects might be considered, e.g. chemical stability, porosity, fashion of a catalytic site attachment, the overall cost.

In this thesis, several types of POFs were employed – (i) those obtained via Suzuki-Miyaura coupling frameworks (Chapter 1), (ii) Covalent Triazine Frameworks obtained from different building blocks (Chapters 2,3,4,5,6), (iii) Imine-linked Porous Organic Network (IL-PON, Chapter 6). The choice of these polymers was driven by the aim of obtaining highly stable and recyclable catalysts in a straightforward manner.

POFs from (i) possess excellent stability, witnessed by structural perseverance under very harsh conditions (highly acidic media). This valuable feature allowed for post-synthetic sulfonation to obtain a high content of supported acidic groups. CTFs (ii) are also characterised by outstanding physical and chemical stability. In addition, they contain quasi-bipyridine moieties and can therefore act as solid anchors towards organometallic complexes. This bonding is anticipated to be strong enough to prevent metal leaching under different reaction conditions. (iii) is referred to as IL-PON, comparably similar to CTFs, but instead of bipyridine it contains diiminopyridine units in its framework, allowing metal coordination in a similar manner as in CTF. IL-PON, differently from CTF, exists as a lamellar structure, which sparked to study the effect of differently structured POF supports for engineering a catalyst.

1.5. SCOPE AND OUTLINE OF THE THESIS

This thesis focuses on the development of Porous Organic Frameworks that contain molecular size catalytic sites along with their testing in various catalytic applications. In essence, these materials combine the virtues of homogeneous and heterogeneous catalysts; a well-defined molecular environment can be tuned towards optimal performance in catalysis, whilst its embedding in a polymer does not only render handling and recycling properties equal to common heterogeneous systems, but it some cases it also improves catalytic performance. The choice of the polymers was driven by the aim of obtaining highly stable and recyclable catalysts in a straightforward manner.

The thesis starts with this introduction Chapter 1, where different types of POFs are described, together with comprehensive overview of the state-of-the-art POF-based catalysts. Chapter 2 presents the synthesis, characterisation, sulfonation, and catalytic performance of two new porous aromatic frameworks obtained by the Suzuki–Miyaura cross-coupling. In Chapter 3, a heterogeneous molecular catalyst for formic acid dehydrogenation based on $Ir^{III}Cp^*$ attached to a Covalent Triazine Framework is reported. Chapter 4 describes the continuation of this work – it puts up an engineering approach to shape the CTF based catalyst into a sphere-composite via phase-inversion. Chapter 5 describes further engineering refinement of this catalyst, describing a methodology to create a CTF-coating on a cordierite monolith – a highly versatile catalyst support. Chapter 6 treats a range of new Ni based

catalysts on CTF and IL-PON supports, the influence of the support on reaction selectivity is extensively discussed.

Note that all the chapters have been written as individual publications and can be read independently. Because of this, some overlap may be present.

1.6. LIST OF ABBREVIATIONS

POF – Porous Organic Framework

COF – Covalent Organic Framework

CTF – Covalent Triazine Framework

CMP – Conjugated Microporous Polymer

HCP – Hypercrosslinked Polymer

PIM – Polymer of Intrinsic Microporosity

EOF- Element Organic Framework

FeP-CMP – Iron Porphyrin CMP[27]

CuP-SQ COF – Copper Porphyrin Squaraine COF[28]

MsMOP – Metallosalen-based microporous organic polymer[32]

T-IM - Tubular organic networks bearing imidazolium salts[42]

Am-MOP – Amide functionalised microporous organic[43]

JH-CPP – Jørgensen–Hayashi Chiral Porous Polymer[45]

TFP-DABA – framework prepared from 1,3,5-triformylphloroglucinol and 2,5-diaminobenzenesulfonic acid[46]

2,3-DhaTph – framework prepared from 2,3-dihydroxyterephthalaldehyde units[47]

2,3-DmaTph – framework prepared from 2,3-dimethoxyterephthalaldehyde units[47]

COF-LZU1 – COF named after Lanzhou University, China[48]

KAP – Knitting Aryl Networks[49]

SMP – Scholl-coupling Microporous Polymers[50]

UOF – Urea-Based Porous Organic Frameworks[51]

PPI-*n*-NPy – Porous Polyimides, imino pyridine functionalised[52]

PCP-BINAP – Porous Cross-linked Polymers with BINAP ligand[64]

PICU – Microporous Polyisocyanurate[65]

PPOP – Porphyrin Porous Organic Polymer[66]

Et_2OFe(CAT-POP) – Diethyl ether Iron Catechol Porous Organic Framework[69-70]

C3v-POF – Porous Organic Framework with 1,3,5-tris(4-aminophenyl)benzene unit[73]

Th-POF – Porous Organic Framework with tetra-(4-aminophenyl)methane unit[73]

MCIP-1 – Mesoporous Covalent Imine Polymer[74]

CIN-1 – Covalent Imine Network[75]

CCP – Chiral Crosslinked Polymer[79]

TADDOL-CPP – Chiral Crosslinked Polymer containing TADDOL unit[80]

Co-TpBpy – Co modified bipyridine-containing covalent organic framework[81]

COP-A – Cross-linked Organic Polymer bearing acidic groups[85]

[Pyr]x-H_2P-COF – Pyrrolidine derivatived Covalent Organic Framework[86]

1.7. REFERENCES

[1] A. I. Cooper, *Advanced Materials* **2009**, *21*, 1291-1295.

[2] R. Dawson, A. I. Cooper, D. J. Adams, *Progress in Polymer Science* **2012**, *37*, 530-563.

[3] A. Thomas, *Angewandte Chemie International Edition* **2010**, *49*, 8328-8344.

[4] J.-X. Jiang, A. I. Cooper, in *Functional Metal-Organic Frameworks: Gas Storage, Separation and Catalysis* (Ed.: M. Schröder), Springer Berlin Heidelberg, Berlin, Heidelberg, **2010**, pp. 1-33.

[5] A. P. Côté, A. I. Benin, N. W. Ockwig, M. Keeffe, A. J. Matzger, O. M. Yaghi, *Science* **2005**, *310*, 1166.

[6] L. M. Lanni, R. W. Tilford, M. Bharathy, J. J. Lavigne, *Journal of the American Chemical Society* **2011**, *133*, 13975-13983.

[7] F. J. Uribe-Romo, J. R. Hunt, H. Furukawa, C. Klöck, M. O'Keeffe, O. M. Yaghi, *Journal of the American Chemical Society* **2009**, *131*, 4570-4571.

[8] B. J. Smith, A. C. Overholts, N. Hwang, W. R. Dichtel, *Chemical Communications* **2016**, *52*, 3690-3693.

[9] P. Kuhn, M. Antonietti, A. Thomas, *Angewandte Chemie International Edition* **2008**, *47*, 3450-3453.

[10] S. Ren, M. J. Bojdys, R. Dawson, A. Laybourn, Y. Z. Khimyak, D. J. Adams, A. I. Cooper, *Advanced Materials* **2012**, *24*, 2357-2361.

[11] M. G. Schwab, B. Fassbender, H. W. Spiess, A. Thomas, X. Feng, K. Müllen, *Journal of the American Chemical Society* **2009**, *131*, 7216-7217.

[12] J. W. Grate, K.-F. Mo, M. D. Daily, *Angewandte Chemie International Edition* **2016**, *55*, 3925-3930.

[13] V. A. Davankov, M. P. Tsyurupa, *Reactive Polymers* **1990**, *13*, 27-42.

[14] M. P. Tsyurupa, V. A. Davankov, *Reactive and Functional Polymers* **2002**, *53*, 193-203.

[15] N. Fontanals, R. M. Marce, F. Borrull, P. A. G. Cormack, *Polymer Chemistry* **2015**, *6*, 7231-7244.

[16] M. Trunk, A. Herrmann, H. Bildirir, A. Yassin, J. Schmidt, A. Thomas, *Chemistry – A European Journal* **2016**, *22*, 7179-7183.

[17] J. Schmidt, M. Werner, A. Thomas, *Macromolecules* **2009**, *42*, 4426-4429.

[18] M. G. Goesten, À. Szécsényi, M. F. de Lange, A. V. Bavykina, K. B. Gupta, F. Kapteijn, J. Gascon, *ChemCatChem* **2016**, *8*, 961-967.

[19] S. Yuan, B. Dorney, D. White, S. Kirklin, P. Zapol, L. Yu, D.-J. Liu, *Chemical Communications* **2010**, *46*, 4547-4549.

[20] J.-X. Jiang, F. Su, H. Niu, C. D. Wood, N. L. Campbell, Y. Z. Khimyak, A. I. Cooper, *Chemical Communications* **2008**, 486-488.

[21] X. Wang, M. Simard, J. D. Wuest, *Journal of the American Chemical Society* **1994**, *116*, 12119-12120.

[22] M. Rose, A. Notzon, M. Heitbaum, G. Nickerl, S. Paasch, E. Brunner, F. Glorius, S. Kaskel, *Chemical Communications* **2011**, *47*, 4814-4816.

[23] J. Fritsch, F. Drache, G. Nickerl, W. Böhlmann, S. Kaskel, *Microporous and Mesoporous Materials* **2013**, *172*, 167-173.

[24] N. B. McKeown, S. Makhseed, P. M. Budd, *Chemical Communications* **2002**, 2780-2781.

[25] P. M. Budd, N. B. McKeown, D. Fritsch, *Macromolecular Symposia* **2006**, *245-246*, 403-405.

[26] P. M. Budd, B. S. Ghanem, S. Makhseed, N. B. McKeown, K. J. Msayib, C. E. Tattershall, *Chemical Communications* **2004**, 230-231.

[27] L. Chen, Y. Yang, D. Jiang, *Journal of the American Chemical Society* **2010**, *132*, 9138-9143.

[28] A. Nagai, X. Chen, X. Feng, X. Ding, Z. Guo, D. Jiang, *Angewandte Chemie International Edition* **2013**, *52*, 3770-3774.

[29] S. Lin, C. S. Diercks, Y.-B. Zhang, N. Kornienko, E. M. Nichols, Y. Zhao, A. R. Paris, D. Kim, P. Yang, O. M. Yaghi, C. J. Chang, *Science* **2015**, *349*, 1208.

[30] M. K. Singh, D. Bandyopadhyay, *Journal of Chemical Sciences* **2016**, *128*, 1-8.

[31] J.-X. Jiang, C. Wang, A. Laybourn, T. Hasell, R. Clowes, Y. Z. Khimyak, J. Xiao, S. J. Higgins, D. J. Adams, A. I. Cooper, *Angewandte Chemie International Edition* **2011**, *50*, 1072-1075.

[32] H. Li, B. Xu, X. Liu, S. A, C. He, H. Xia, Y. Mu, *Journal of Materials Chemistry A* **2013**, *1*, 14108-14114.

[33] Y. Xie, T.-T. Wang, X.-H. Liu, K. Zou, W.-Q. Deng, *Nature Communications* **2013**, *4*, 1960.

[34] Y. Xie, R.-X. Yang, N.-Y. Huang, H.-J. Luo, W.-Q. Deng, *Journal of Energy Chemistry* **2014**, *23*, 22-28.

[35] W. Wang, A. Zheng, P. Zhao, C. Xia, F. Li, *ACS Catalysis* **2014**, *4*, 321-327.

[36] J. Fritsch, M. Rose, P. Wollmann, W. Böhlmann, S. Kaskel, *Materials* **2010**, *3*.

[37] L. H. Wee, T. Lescouet, J. Fritsch, F. Bonino, M. Rose, Z. Sui, E. Garrier, D. Packet, S. Bordiga, S. Kaskel, M. Herskowitz, D. Farrusseng, J. A. Martens, *Catalysis Letters* **2013**, *143*, 356-363.

[38] X. Du, Y. Sun, B. Tan, Q. Teng, X. Yao, C. Su, W. Wang, *Chemical Communications* **2010**, *46*, 970-972.

[39] C. Bleschke, J. Schmidt, D. S. Kundu, S. Blechert, A. Thomas, *Advanced Synthesis & Catalysis* **2011**, *353*, 3101-3106.

[40] D. S. Kundu, J. Schmidt, C. Bleschke, A. Thomas, S. Blechert, *Angewandte Chemie International Edition* **2012**, *51*, 5456-5459.

[41] M. Rueping, E. Sugiono, A. Steck, T. Theissmann, *Advanced Synthesis & Catalysis* **2010**, *352*, 281-287.

[42] H. C. Cho, H. S. Lee, J. Chun, S. M. Lee, H. J. Kim, S. U. Son, *Chemical Communications* **2011**, *47*, 917-919.

[43] V. M. Suresh, S. Bonakala, H. S. Atreya, S. Balasubramanian, T. K. Maji, *ACS Applied Materials & Interfaces* **2014**, *6*, 4630-4637.

[44] S. Cai, D. Zhu, Y. Zou, J. Zhao, *Nanoscale Research Letters* **2016**, *11*, 1-9.

[45] C. A. Wang, Z. K. Zhang, T. Yue, Y. L. Sun, L. Wang, W. D. Wang, Y. Zhang, C. Liu, W. Wang, *Chemistry – A European Journal* **2012**, *18*, 6718-6723.

[46] Y. Peng, Z. Hu, Y. Gao, D. Yuan, Z. Kang, Y. Qian, N. Yan, D. Zhao, *ChemSusChem* **2015**, *8*, 3208-3212.

[47] V. Saptal, D. B. Shinde, R. Banerjee, B. M. Bhanage, *Catalysis Science & Technology* **2016**, *6*, 6152-6158.

[48] S.-Y. Ding, J. Gao, Q. Wang, Y. Zhang, W.-G. Song, C.-Y. Su, W. Wang, *Journal of the American Chemical Society* **2011**, *133*, 19816-19822.

[49] B. Li, Z. Guan, W. Wang, X. Yang, J. Hu, B. Tan, T. Li, *Advanced Materials* **2012**, *24*, 3390-3395.

[50] B. Li, Z. Guan, X. Yang, W. D. Wang, W. Wang, I. Hussain, K. Song, B. Tan, T. Li, *Journal of Materials Chemistry A* **2014**, *2*, 11930-11939.

[51] L. Li, Z. Chen, H. Zhong, R. Wang, *Chemistry – A European Journal* **2014**, *20*, 3050-3060.

[52] E. Rangel Rangel, E. M. Maya, F. Sanchez, J. G. de la Campa, M. Iglesias, *Green Chemistry* **2015**, *17*, 466-473.

[53] Y. Hou, X. Zhang, J. Sun, S. Lin, D. Qi, R. Hong, D. Li, X. Xiao, J. Jiang, *Microporous and Mesoporous Materials* **2015**, *214*, 108-114.

[54] P. J. C. Hausoul, T. M. Eggenhuisen, D. Nand, M. Baldus, B. M. Weckhuysen, R. J. M. Klein Gebbink, P. C. A. Bruijnincx, *Catalysis Science & Technology* **2013**, *3*, 2571-2579.

[55] R. Palkovits, M. Antonietti, P. Kuhn, A. Thomas, F. Schüth, *Angewandte Chemie International Edition* **2009**, *48*, 6909-6912.

[56] K. Kamiya, R. Kamai, K. Hashimoto, S. Nakanishi, *Nat Commun* **2014**, *5*.

[57] M. H. Weston, O. K. Farha, B. G. Hauser, J. T. Hupp, S. T. Nguyen, *Chemistry of Materials* **2012**, *24*, 1292-1296.

[58] A. Bavykina, M. Goesten, F. Kapteijn, M. Makkee, J. Gascon, *ChemSusChem* **2015**, *8*, 809-812.

[59] A. V. Bavykina, E. Rozhko, M. G. Goesten, T. Wezendonk, B. Seoane, F. Kapteijn, M. Makkee, J. Gascon, *ChemCatChem* **2016**, *8*, 2217–2221.

[60] K. Park, G. H. Gunasekar , N. Prakash, K.-D. Jung, S. Yoon, *ChemSusChem* **2015**, *8*, 3410-3413.

[61] G. Gunniya Hariyanandam, D. Hyun, P. Natarajan, K.-D. Jung, S. Yoon, *Catalysis Today* **2016**, *265*, 52-55.

[62] P. J. C. Hausoul, C. Broicher, R. Vegliante, C. Göb, R. Palkovits, *Angewandte Chemie International Edition* **2016**, *55*, 5597-5601.

[63] N. Salam, S. K. Kundu, A. S. Roy, P. Mondal, K. Ghosh, A. Bhaumik, S. M. Islam, *Dalton Transactions* **2014**, *43*, 7057-7068.

[64] Q. Sun, X. Meng, X. Liu, X. Zhang, Y. Yang, Q. Yang, F.-S. Xiao, *Chemical Communications* **2012**, *48*, 10505-10507.

[65] Y. Zhang, S. N. Riduan, J. Y. Ying, *Chemistry – A European Journal* **2009**, *15*, 1077-1081.

[66] A. M. Shultz, O. K. Farha, J. T. Hupp, S. T. Nguyen, *Chemical Science* **2011**, *2*, 686-689.

[67] B. Saha, D. Gupta, M. M. Abu-Omar, A. Modak, A. Bhaumik, *Journal of Catalysis* **2013**, *299*, 316-320.

[68] S. J. Kraft, G. Zhang, D. Childers, F. Dogan, J. T. Miller, S. T. Nguyen, A. S. Hock, *Organometallics* **2014**, *33*, 2517-2522.

[69] S. J. Kraft, R. H. Sánchez, A. S. Hock, *ACS Catalysis* **2013**, *3*, 826-830.

[70] S. J. Kraft, B. Hu, G. Zhang, J. T. Miller, A. S. Hock, *European Journal of Inorganic Chemistry* **2013**, *2013*, 3972-3977.

[71] K. Iwase, T. Yoshioka, S. Nakanishi, K. Hashimoto, K. Kamiya, *Angewandte Chemie International Edition* **2015**, *54*, 11068-11072.

[72] T. Yoshioka, K. Iwase, S. Nakanishi, K. Hashimoto, K. Kamiya, *The Journal of Physical Chemistry C* **2016**, *120*, 15729-15734.

[73] E. Verde-Sesto, E. M. Maya, A. E. Lozano, J. G. de la Campa, F. Sanchez, M. Iglesias, *Journal of Materials Chemistry* **2012**, *22*, 24637-24643.

[74] P. Puthiaraj, K. Pitchumani, *Chemistry – A European Journal* **2014**, *20*, 8761-8770.

[75] S. Roy, T. Chatterjee, B. Banerjee, N. Salam, A. Bhaumik, S. M. Islam, *RSC Advances* **2014**, *4*, 46075-46083.

[76] R. K. Totten, M. H. Weston, J. K. Park, O. K. Farha, J. T. Hupp, S. T. Nguyen, *ACS Catalysis* **2013**, *3*, 1454-1459.

[77] K. K. Tanabe, N. A. Siladke, E. M. Broderick, T. Kobayashi, J. F. Goldston, M. H. Weston, O. K. Farha, J. T. Hupp, M. Pruski, E. A. Mader, M. J. A. Johnson, S. T. Nguyen, *Chemical Science* **2013**, *4*, 2483-2489.

[78] K. K. Tanabe, M. S. Ferrandon, N. A. Siladke, S. J. Kraft, G. Zhang, J. Niklas, O. G. Poluektov, S. J. Lopykinski, E. E. Bunel, T. R. Krause, J. T. Miller, A. S. Hock, S. T. Nguyen, *Angewandte Chemie International Edition* **2014**, *53*, 12055-12058.

[79] L. Ma, M. M. Wanderley, W. Lin, *ACS Catalysis* **2011**, *1*, 691-697.

[80] W.-K. An, M.-Y. Han, C.-A. Wang, S.-M. Yu, Y. Zhang, S. Bai, W. Wang, *Chemistry – A European Journal* **2014**, *20*, 11019-11028.

[81] H. B. Aiyappa, J. Thote, D. B. Shinde, R. Banerjee, S. Kurungot, *Chemistry of Materials* **2016**, *28*, 4375-4379.

[82] H. J. Mackintosh, P. M. Budd, N. B. McKeown, *Journal of Materials Chemistry* **2008**, *18*, 573-578.

[83] W. Zhang, P. Jiang, Y. Wang, J. Zhang, Y. Gao, P. Zhang, *RSC Advances* **2014**, *4*, 51544-51547.

[84] S. Fischer, J. Schmidt, P. Strauch, A. Thomas, *Angewandte Chemie International Edition* **2013**, *52*, 12174-12178.

[85] A. Modak, J. Mondal, A. Bhaumik, *ChemCatChem* **2013**, *5*, 1749-1753.

[86] H. Xu, X. Chen, J. Gao, J. Lin, M. Addicoat, S. Irle, D. Jiang, *Chemical Communications* **2014**, *50*, 1292-1294.

CHAPTER TWO

Sulfonated Porous Aromatic Frameworks as Solid Acid Catalysts

The synthesis, characterisation, sulfonation, and catalytic performance of two new porous aromatic frameworks are presented. The polymers, which were obtained by the Suzuki–Miyaura cross-coupling of commercially available precursors display excellent thermal and chemical stability, and allow for post-synthetic functionalisation under very harsh reaction conditions. Upon post-synthetic treatment at 160 °C in 98 wt% sulfuric acid, approximately 65 % of the benzene rings in the polymers were sulfonated. The sulfonated materials display an excellent catalytic performance in the acid-catalysed esterification of *n*-butanol and acetic acid and have a similar or even superior performance to that of state-of-the-art Amberlyst-15® over multiple catalytic cycles.

This Chapter is based on the following publication:

M. G. Goesten, A. Szécsényi, M. F. de Lange, A. V. Bavykina, K. S. Gupta, F. Kapteijn, J. Gascon, *ChemCatChem* 8 (2016) 961-967

2.1. INTRODUCTION

The past few decades have seen considerable efforts made in the development of new porous materials, especially for applications in catalysis and gas separation[1]. Although classical inorganic materials based on silica and alumina are applied widely in industry, they possess a limited degree of chemical tunability. Activated carbon allows for certain post-synthetic modifications,[2–4] but remains an ill-defined structure from a chemistry point of view; it usually contains a large number of elements and moieties that may induce undesired properties or events for some applications.[5]

For the implementation of acid functionality, by far the most required functionality in catalysis, solid materials such as ion-exchange resins based on sulfonic acid groups or sulphated oxides based on Zr, Si, or Al have been proposed. Unfortunately, the application window of such materials is limited: some of them exhibit swelling in solvents (polymers), others suffer from strong leaching (sulfated oxides), and none of them contains a defined porosity. As a result, the development of new nanostructured superacid catalysts remains a challenge.

In recent years, the potential of metal–organic frameworks (MOFs) in acid catalysis was demonstrated.[6,7] These highly crystalline porous materials are essentially coordination compounds of infinite nuclearity that are chemically highly tunable, well defined, and have the option of targeted catalysis by either the inorganic node or the organic bridging ligand (linker).[8,9] Catalysis by MOFs has seen great progress in recent years, and successful attempts to use MOFs as heterogeneous catalysts in acid, base, asymmetric, and photochemical reactions have been reported.[6,10–12] Despite this development, there is a potential drawback of the use of MOFs as solid catalysts: MOFs are constructed by dative (coordinate) covalent bonds, which are usually only of moderate strength and result in a certain degree of instability that can be detrimental for catalytic applications. In this sense, the use of structured polymers in catalysis offers several advantages over MOFs. Structured polymers are a class of porous materials similar to MOFs that have highly covalent bonds between their building units that are much less polar in nature than coordination bonds between organic linkers and metals. Although rigid polymer networks have been known and described for many years,[13] awareness of the possibilities in the creation of porosity within these networks has only recently become the focus of significant attention. Particularly, after the introduction of the

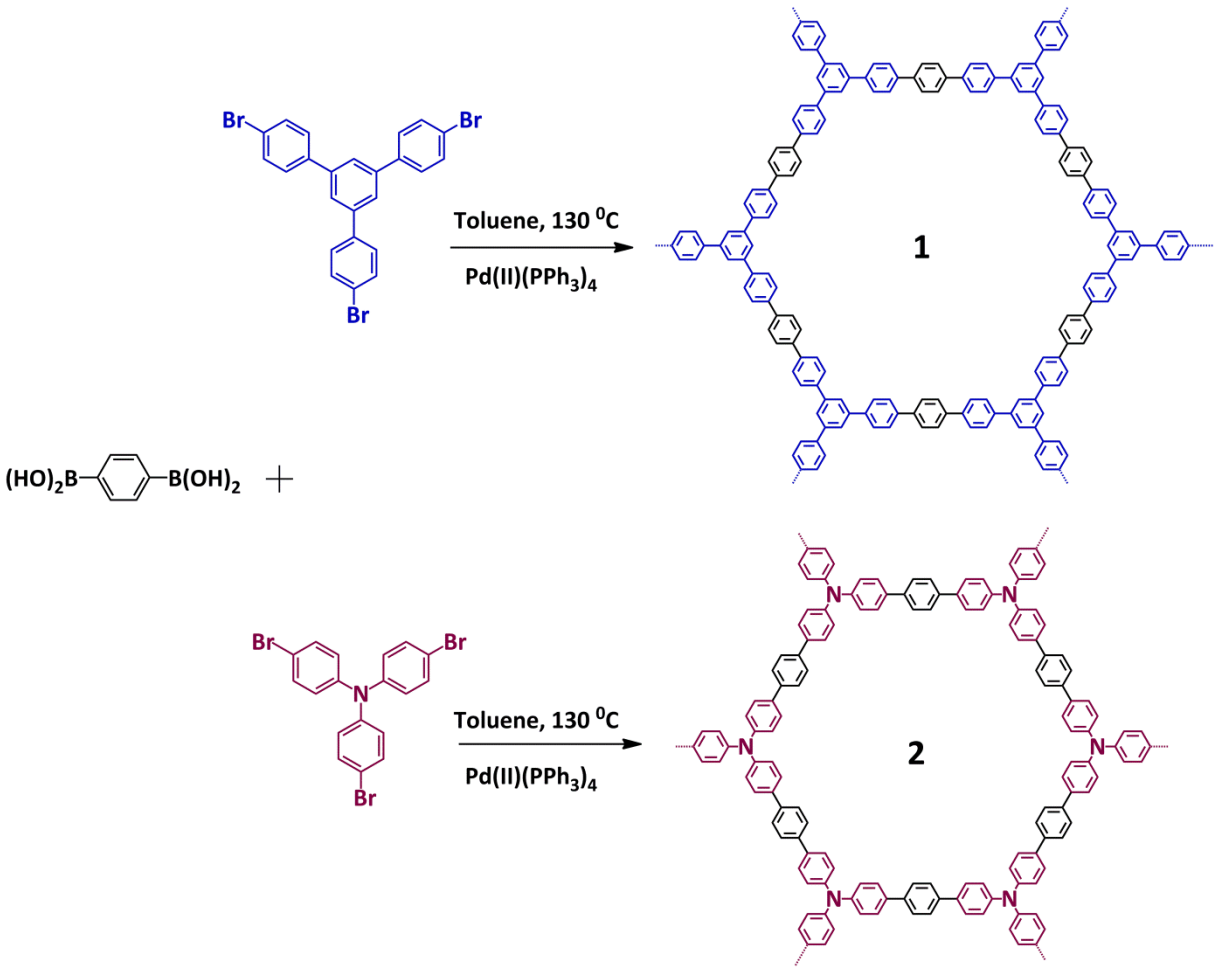

Figure 2.1. Synthesis and structure of both polymers

term "covalent organic frameworks" by Omar Yaghi in 2005,[14] intensive research effort has led to a variety of comparable materials, clustered in classes such as covalent triazine frameworks (CTFs),[15] conjugated microporous polymers (CMPs),[16] porous aromatic frameworks (PAFs),[17] element–organic frameworks (EOFs),[18] polymers of intrinsic microporosity (PIMs),[19] and hypercrosslinked polymers (HCPs).[20,21]In this work, we demonstrate that PAFs synthesized through the Pd-catalysed Suzuki–Miyaura coupling of appropriate building blocks (Figure 2.1, polymers 1 and 2) hold great promise for application as supports in heterogeneous catalysis. The synthesised polymers are fully microporous, extremely stable, and undergo post-synthetic sulfonation to yield solid Brønsted acid catalysts that have similar or even superior performances to state-of-the-art Amberlyst-15® over multiple cycles of the catalysed esterification of *n*-butanol and acetic acid.

2.2. EXPERIMENTAL SECTION

Materials

1,3,5-tris(4-Bromophenyl)benzene, acetic acid, aniline, benzene-1,4-diboronic acid, dichloromethane (DCM), ethanol, HCl, *n*-butanol (BuOH), KBr, Na_2CO_3, H_2SO_4, toluene, triphenylphosphine (PPh_3), tris(4-bromophenyl)amine, and tris(dibenzylideneacetone)dipalladium(0) ($Pd^0{}_2(dba)_3$) were purchased from Sigma–Aldrich and used without further purification.

Synthesis of 1

The preparation of the polymer was performed in a Teflon insert. $Pd^{II}(PPh_3)_4$ (0.5 mmol) was generated by the reaction of (air-stable) $Pd^0{}_2(dba)_3$ (0.229 g, 0.25 mmol) and PPh_3 (0.525 g, 2 mmol) in Ar degassed toluene (17.4 g, 20 mL) with a degassed 2M Na_2CO_3 (aq) solution (10 mL) and 1,3,5-tris(4-bromophenyl)benzene (3.258 g, 6 mmol). Then, benzene-1,4-diboronic acid (0.744 g, 6.1 mmol) and ethanol (5 mL) were added. The procedure was performed in a glovebox. Inside the glovebox, the insert was placed in an autoclave, which was closed and subsequently heated to 130 ^{0}C for 24 h in an oven or heated to 160 ^{0}C for 2 h in a microwave oven. The resulting, air-stable, yellow powder was collected, washed with HCl, aniline, toluene, and DCM, and activated under vacuum at 100 ^{0}C.

Synthesis of 2

The procedure is the same as described above, but the following amounts of reactants were used: 0.5 mmol $Pd^{II}(PPh_3)_4$, 0.25 mmol $Pd^0{}_2(dba)_3$ (0.229 g), 2 mmol PPh_3 (0.525 g), 20 mL Ar degassed toluene (17.4 g), 10 mL 2M Na_2CO_3 (aq) solution, 6 mmol tris(4-bromophenyl)amine (3.258 g), 6.1 mmol (0.744 g) benzene-1,4-diboronic acid, and 5 mL ethanol. This synthesis was performed inside a glovebox with the subsequent heat treatment as for **1**. The resulting powder was orange.

Sulfonation of 1 and 2

Polymers **1** and **2** were sulfonated with concentrated sulfuric acid (98 wt%) at 160 ^{0}C in an autoclave with a Teflon insert for 12 h. After sulfonation, the reaction mixture was diluted in ultrapure water and filtered. The black powder was washed with dichloromethane

(DCM) at ambient temperature and pressure overnight. Before analysis and catalytic testing, the sulfonated polymers were activated under vacuum at 180 ^{0}C for 24 h.

Characterization

The structure of the samples was confirmed by solid-state ^{13}C NMR spectroscopy by using a Bruker AV-750 spectrometer with a 17.6 T magnetic field, in which the ^{1}H and ^{13}C nuclei resonate at 750.13 and 188.64 MHz, respectively. A triple resonance H/X/Y 4 mm MAS probe-head with a standard ZrO_2 rotor were used to spin the sample at different spinning speeds. All the samples were spun at 13 kHz. Spinning sidebands were confirmed by spinning the samples at different speeds. The ^{13}C NMR spectra were obtained using the CPMAS technique with two-pulse phase-modulated (TPPM) decoupling. The ^{1}H and ^{13}C nuclei were irradiated with 80.6 and 62.5 kHz radiofrequency pulses, respectively, and a contact time of 2 ms was used to achieve the CPMAS (Hartman–Hahn) condition. The recycle delay was 1 s, and 256 scans were acquired. The line broadening function of 60 Hz was applied in the processing of the spectra. All the ^{13}C NMR spectra were referenced externally to the methyl resonance of tetramethylsilane (TMS).

XPS analysis was performed by using a *K*-alpha Thermo Fisher Scientific spectrometer using a monochromatic Al$K\alpha$ X-ray source. The measurements were performed using a line scan of three points, each of which had a spot size of 300 mm at ambient temperature and chamber pressure of ≈10^{-7} mbar. A flood gun is used for charge compensation. All the spectra measured were corrected by setting the reference binding energy of carbon (1*s*) at (285±0.025) eV. The electron energy analyser was operated with a pass energy of 50 eV, and each high-resolution spectrum was scanned 10 times. The spectra were analysed and processed using Thermo Avantage v5.52 software (Thermo Fisher Scientific). The peaks were fitted using a Lorentzian–Gaussian (L/G) ratio of 0.3. The binding energies reported are within ±0.1 eV.

Diffuse reflectance infrared Fourier transform (DRIFT) spectra were recorded by using a Nicolet model 8700 spectrometer equipped with a high-temperature DRIFT cell (KBr windows), a DTGS–TEC detector, and a 633 nm laser. The spectra were recorded in the range of σ =4000–600 cm^{-1} after the accumulation of 128 scans at a resolution of 4 cm^{-1}. A flow of He at 20 mL min^{-1} was maintained during the measurements. KBr was used to perform

background experiments. The sulfonated samples were pretreated under vacuum overnight at 180 ^{0}C to remove weakly adsorbed water.

Back-titration was utilised to calculate the degree of sulfonation of the studied catalysts: the sulfonated polymer was dispersed in an excess of KOH. After overnight stirring, HCl was used as the backtitration reagent. The amount of sulfonic acid groups was calculated from the molar amount of OH^- added minus the molar amount of H^+ added by titration until pH of the solution was 7.

CO_2 adsorption isotherms were measured by using a Micromeritics TriStar II 3020 at 0 ^{0}C. Vapour adsorption isotherms (*n*-butanol and methanol) were measured by using a Micromeritics 3Flex setup at 25 ^{0}C. Before the measurements of the isotherms and after loading the sample in the sample tube, the samples were degassed at 120 ^{0}C for 12 h in a N_2 flow for **1** and **2** or under vacuum at 180 ^{0}C for 12 h for sulfo-**1** and sulfo-**2**.

TGA was performed by using a Mettler Toledo TGA/SDTA851e type device under a flow of air (60 mL min^{-1}) at a heating rate of 5 ^{0}C min^{-1} up to 800 ^{0}C.

Catalytic performance

The esterification of acetic acid and *n*-butanol was performed without solvent with a molar ratio of acetic acid to *n*-butanol of 1:1 (60 mL) using 3 g catalyst per mol acetic acid. The reaction mixture was introduced into a round-bottomed flask before the temperature was increased to 80 ^{0}C, and the catalyst was added. Samples of 0.5 mL were taken at specific intervals. After reaction, the catalyst was recovered, filtered, and washed with water. The catalyst was then suspended in DCM and washed at ambient temperature overnight. The washing procedure was followed by filtration and activation of the polymer in a vacuum oven at 180 ^{0}C. The samples were analysed by GC by using a Chrompack CP 9001 and a CP-SIL 8 column (length: 50 m, diameter: 0.32 mm, thickness of the film: 5.0 µm). Turn-over frequencies (*TOF*s) – the number of molecular reactions or catalytic cycles per unit time and per sulfonic acid group– were calculated by fitting the obtained kinetic curves to a first-order rate equation, the slope of which at t = 0 was taken to obtain initial TOF values.

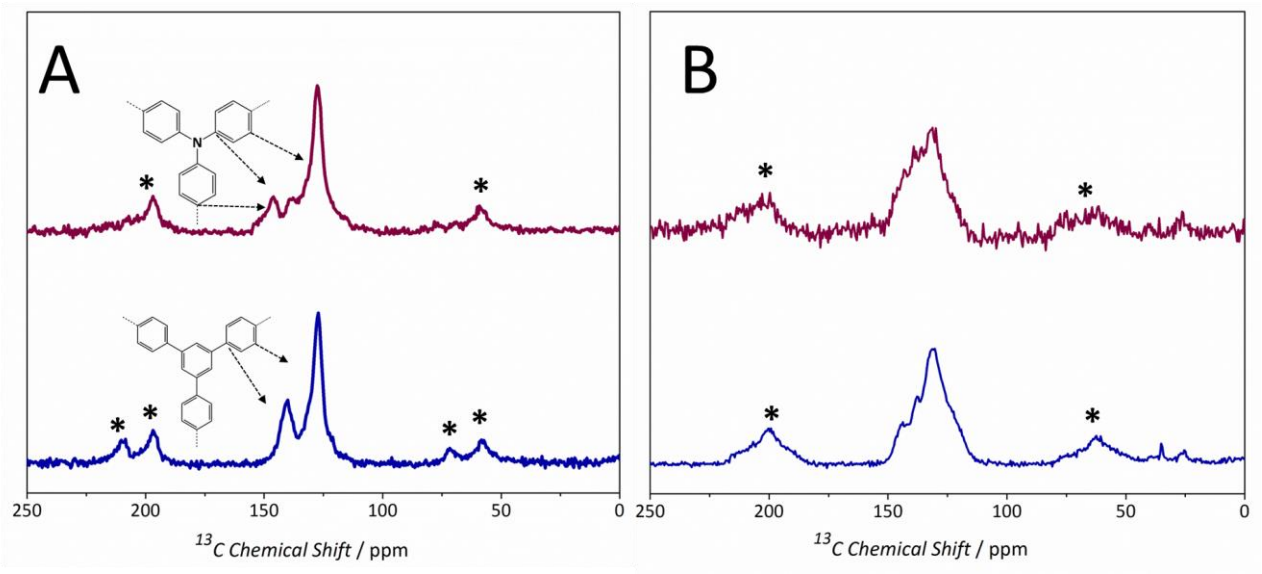

Figure 2.2. ^{13}C CPMAS NMR spectra of A) 1 (*bottom*) and 2 (*top*) and B) sulfo-1 (*bottom*) and sulfo-2 (*top*). The peaks marked with an asterisk are spinning sidebands.

2.3. RESULTS

The ^{13}C cross-polarisation magic-angle spinning (CPMAS) NMR spectra of 1 and 2 are shown in Figure 2.2A. Spectrum **1** in Figure 2A reveals two peaks at δ=127.4 and 140 ppm. The peak at δ= 127.4 ppm is assigned to the aromatic carbon atoms of the benzene rings, and the resonances at δ= 140 ppm are assigned to the quaternary carbon atoms that connect two benzene rings. In Spectrum **2** in Figure 2.2A, three resonances are observed at δ= 127.1, 138.1, and 145.7 ppm. The peak at δ= 127.1 ppm is assigned to the carbon atoms of the aromatic benzene rings, and the peak at δ= 138.1 ppm is assigned to the quaternary carbon atoms that connect two benzene rings. The peak at δ= 145.7 ppm is assigned to the quaternary carbon bound to N as the N atom is electronegative, which influences the downfield shift (left; increase in ppm) of the carbon chemical shifts. To conclude, the spectra confirm the expected chemical environment for both polymers. ^{11}B and ^{79}Br MAS NMR were used to confirm the absence of precursor species after polymerisation and thorough washing.

^{13}C CPMAS NMR spectra of the corresponding sulfonated polymers, sulfo-1 and sulfo-2, are shown in Figure 2.2B. Here, resonances do not contain a high enough resolution for clear peak assignment. If we compare spectrum sulfo-**1** in Figure 2.2B with spectrum **1** in Figure 2A, the appearance of three resonances suggests an additional resonance that we

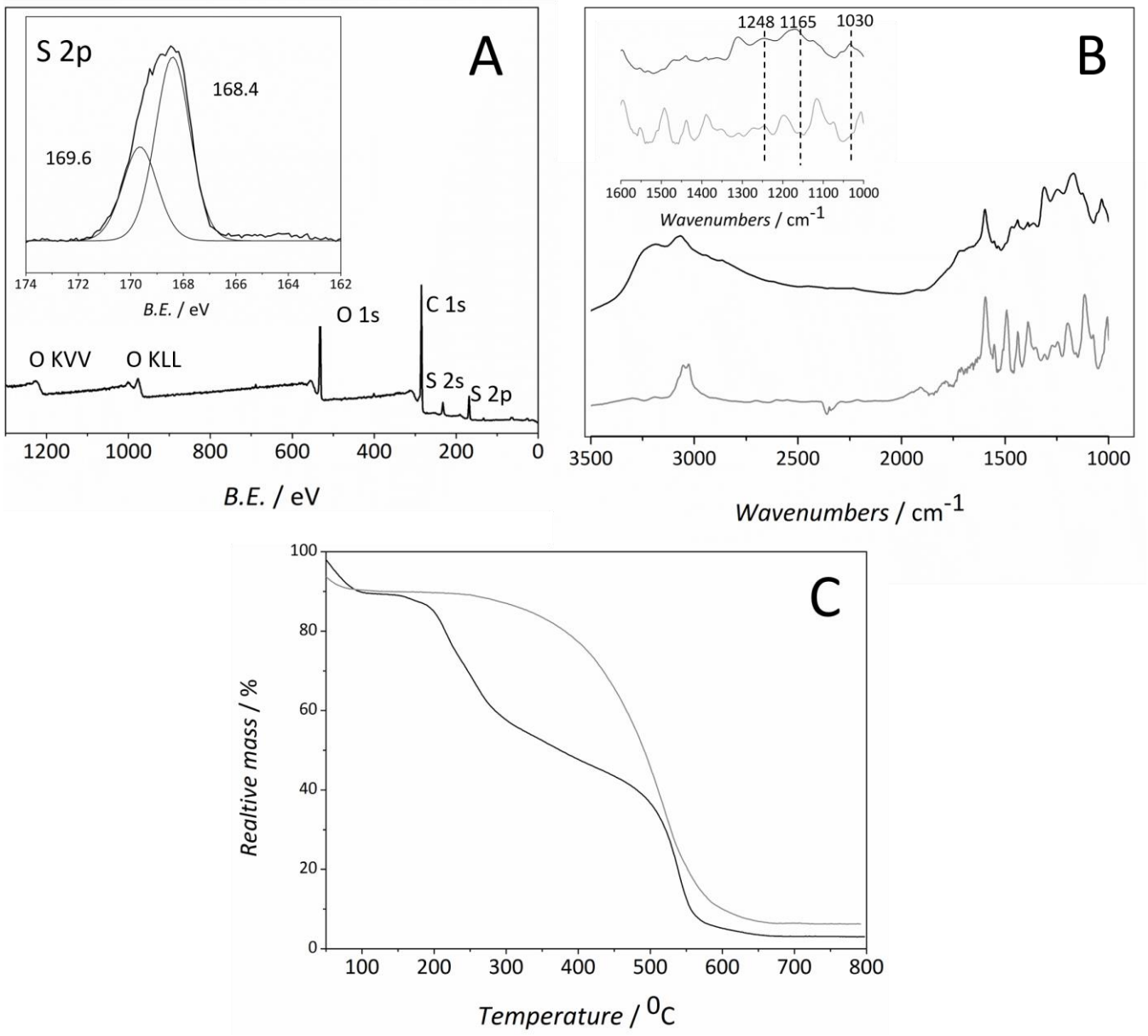

Figure 2.3. A) XPS survey spectrum of sulfo-1 with the S*2p* core level spectra inset. B) FTIR spectra of sulfo-1 (*black*) and 1 (*grey*). C) TGA in air of 1 (*grey*) and sulfo-1 (*black*).

assign to sulfur-bound carbon atoms. Back-titration indicated that around 65% of the aromatic rings of **1** and **2** were sulfonated successfully. This corresponds to a sulfonic acid weight content of ≈ 40 wt% or to an acidity of 5 mmol g^{-1} for both sulfo-**1** and sulfo-**2**. This content, on a weight basis, is higher than that of the acid resin Amberlyst-15® (4.2 mmol g^{-1}).

The thermogravimetric analysis (TGA) of **1** and sulfo-**1** is shown in Figure 2.3C. In spite of their fully carbonaceous nature, the synthesised PAFs display outstanding thermal stability even under oxidative conditions as the decomposition of the framework starts at

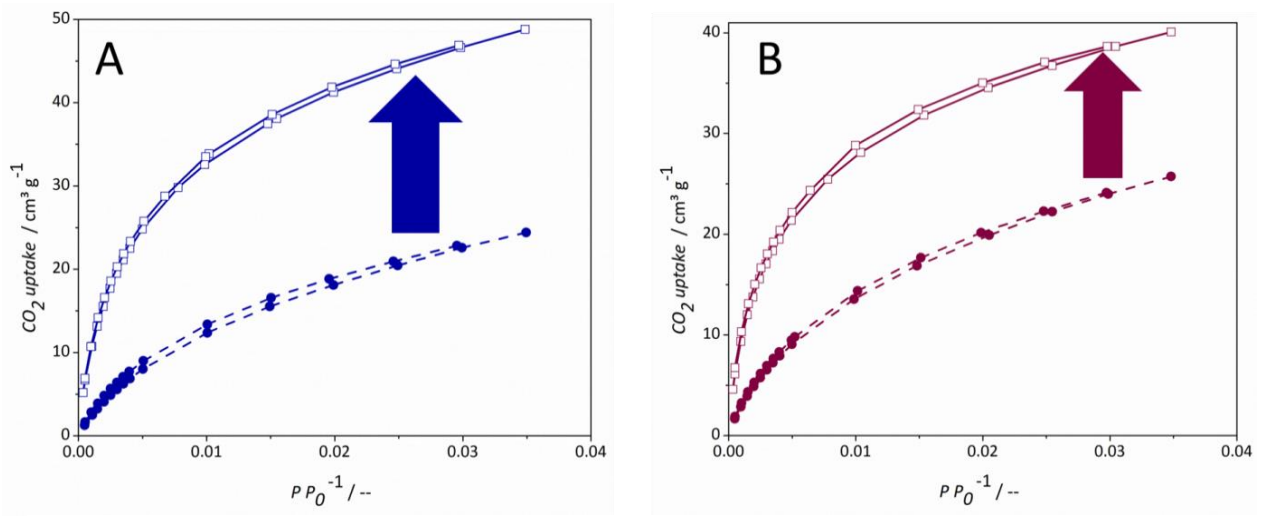

Figure 2.4. CO_2 adsorption isotherms measured at 0 ^{0}C of A) 1 (*dashed line*) and sulfo-1 (*solid line*), B) 2 (*dashed line*) and sulfo-2 (*solid line*)

temperatures higher than 350 ^{0}C. Once sulfonated, the desorption of a larger amount of water is observed at temperatures below 150 ^{0}C. The second step in the isotherm corresponds to the decomposition of the sulfonic acid groups (200–300 ^{0}C). The amount of sulfonic acid groups (≈ 40 wt%) as calculated from this TGA analysis in terms of weight loss observed between 200 and 300 ^{0}C, is in very good agreement with back-titration experiments.

The XPS analysis of the sulfonated polymers is shown in Figure 2.3B. The *2p* level is split upon ionisation into $2p_{1/2}$ and $2p_{3/2}$. This leads to a doublet with an area ratio of 1:2. The split in binding energy was found to be 1.2 eV, and the binding energies for sulphur are 168.4 eV for the $2p_{3/2}$ level and 169.6 eV for the $2p_{1/2}$ level.

The shift in the binding energy of the S *2p* core level and the calculated binding energies demonstrate the presence of a single sulfur species associated with the sulfonic acid groups[22] and the complete removal of sulfuric acid during the workup procedure, in good agreement with IR characterisation (Figure 2.3B): clear differences between the bare and sulfonated polymer are revealed if we observe the whole spectrum (σ= 4000–1000 cm^{-1}). The σ (OH) region (σ= 4000–3000 cm^{-1}) exhibits a broad band centered at σ = 3400 cm^{-1} in the spectrum of the sulfonated material, which is absent in that of the bare sample. This vibration corresponds to water molecules retained in the pores by strong hydrogen bonding with the sulfonic acid, even after *in situ* treatment at 150 ^{0}C for 1 h. Specific sulfonic acid stretchings can be observed in the fingerprint region (σ =1800–1000 cm^{-1}). New bands

Table 2.1. Surface areas of **1**, **2**, sulfo-**1**, sulfo-**2** calculated by Dubinin-Radushkevich formalism based on CO_2 adsorption at 273 K

Material	Specific Surface area[a, b] S_{CO2} [m^2g^{-1}]
1	150
2	180
Sulfo-**1**	270 (425[c])
Sulfo-**2**	210 (310[c])

[a] The specific surface area was calculated by converting the micropore volume by using the CO_2 cross-sectional area (0.187 nm^2). [b] Values are given per gram of material (including sulfonic acid). [c] S_{CO2} expressed per gram of carbon

appear at σ = 1190 and 1240 cm^{-1} attributed to the O=S=O symmetric and asymmetric stretching modes. The peak at σ = 1080 cm^{-1} corresponds to the S—O stretching vibration, and there is a slight shift of the band at σ = 1020–1030 cm^{-1}, possibly attributed to the influence of the HSO_3-substituted aromatic ring.[6,7]

Adsorptive characterisation of the synthesised and sulfonated polymers was performed using CO_2 at 273 K (Figure 2.4). N_2 sorption at 77 K suffered from diffusion-limitation problems, which is observed frequently for microporous materials. Analysis of the CO_2 adsorption isotherms with the Dubinin–Radushkevich formalism leads to specific surface areas of 150, 180, 270, and 210 m^2g^{-1} for **1**, **2**, sulfo-**1**, and sulfo-**2**, respectively (Table 2.1). Sulfonation apparently leads to a considerable increase in the specific surface area. After correcting for the sulfonic groups the areas are 425 and 310 $m^2\,g^{-1}$ expressed per gram of carbon. Pore size distribution analysis using a slit-pore CO_2-DFT model with a regularization factor of 0.03160 is shown in Figure 2.5 for all four polymers. For the original materials **1** and **2**, two main groups of pores are observed with sizes in the order of 0.6 and 0.85 nm, respectively.

Both pore types are slightly decreased in size upon sulfonation, and the contribution of the small pores becomes much more important, in line with the inclusion of relatively bulky sulfonic groups within the porosity.

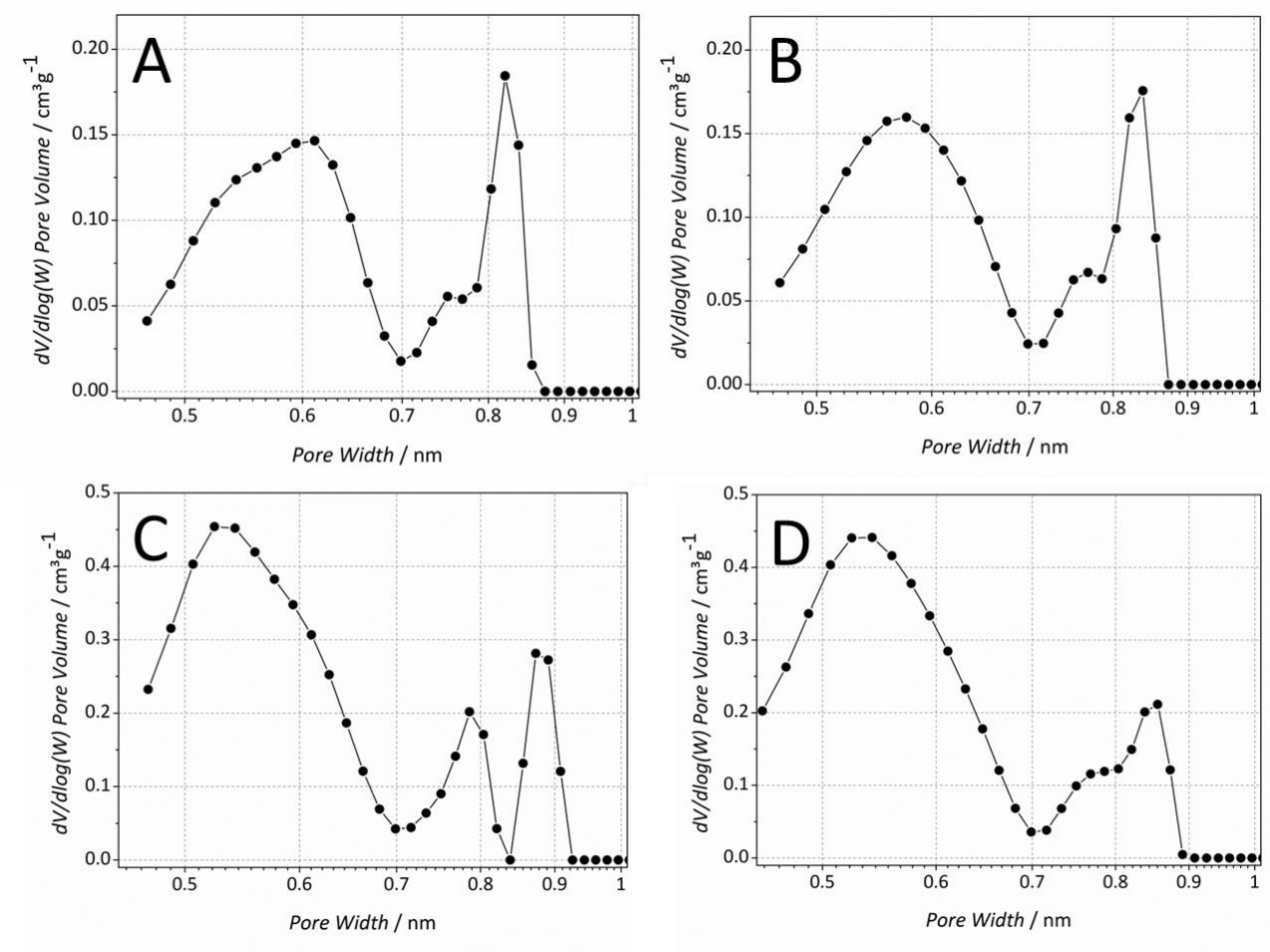

Figure 2.5. Pore size distribution of A) 1, B) 2, C) sulfo-1, and D) sulfo-2.

The performance in the Brønsted acid catalysis was compared to that of Amberlyst-15 for both sulfo-**1** and sulfo-**2** in the acid-catalysed esterification reaction between *n*-butanol and acetic acid at 80 ^{0}C (Figure 2.6). For both sulfo-**1** and sulfo-**2**, a decrease in the catalytic activity occurs after the first run, after which the performance stabilises at a comparable level, which is superior to that of Amberlyst-15 in the case of sulfo-**1**.

The initial turnover frequencies (*TOFs*) obtained for sulfo-**1** and sulfo-**2** over several catalytic cycles are summarised in Table 2.2. A similar loss of activity after the first catalytic run was also observed for Amberlyst-15 and is attributed to small amounts of adsorbed sulfuric acid that, despite washing, is still present after sulfonation and to the partial deactivation of the catalysts because of the formation of sulfate esters.[6] After the first catalytic run, the catalytic performance seems to be stable over several recycles, and sulfo-**1** displays an activity superior to that of Amberlyst-15. Hot-filtration experiments demonstrate the heterogeneous nature of the sulfonated polymers and the absence of leaching under the reaction conditions.

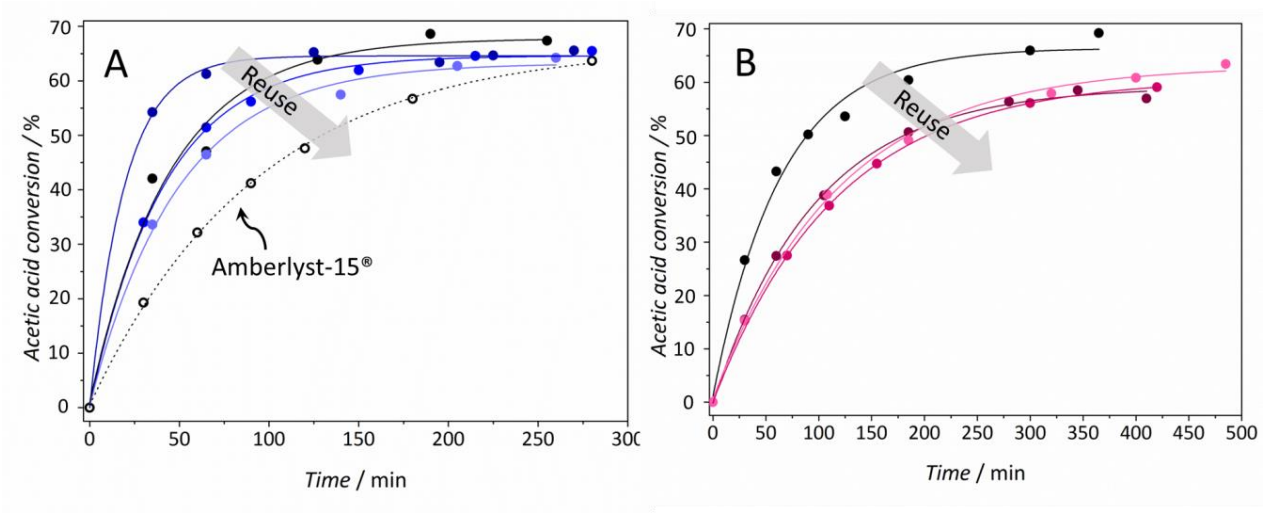

Figure 2.6. Esterification of *n*-butanol and acetic acid (1:1 molar ratio, solvent-free conditions) using 3 g catalyst A) sulfo-1, and B) sulfo-2 per mol reactant at 80 ^{0}C. The performance of Amberlyst-15 under similar reaction conditions is also given as a benchmark (the first run).

2.4. DISCUSSION

Two new microporous aromatic frameworks were prepared by Suzuki–Miyaura cross-coupling using appropriate building blocks. Similar strong-bond PAFs have been reported before using Sonogashira and Yamamoto couplings.[23–25] Herein, we present a straightforward methodology towards PAFs that are only structured by aromatic sp^2 C—C and C—N bonds from commercially available precursors to target high stability and excellent suitability for chemical functionalization. Typically, most porous organic and organic–inorganic networks are held together by bonds weak enough to be broken readily under the conditions of self-assembly, which allows the rapid correction of errors and permits the growth of fully crystalline structures at the cost of stability.[26,27] In this case, we aimed for high network stability at the cost of network crystallinity and we chose a synthesis method based on Pd-catalysed, irreversible C—C bond formation. Indeed, **1** and **2** are chemically analogous to porous organic polymers reported previously but consist of simple building blocks of a planar character and are not constructed from chemically unstable building blocks such as boroxine.[28]

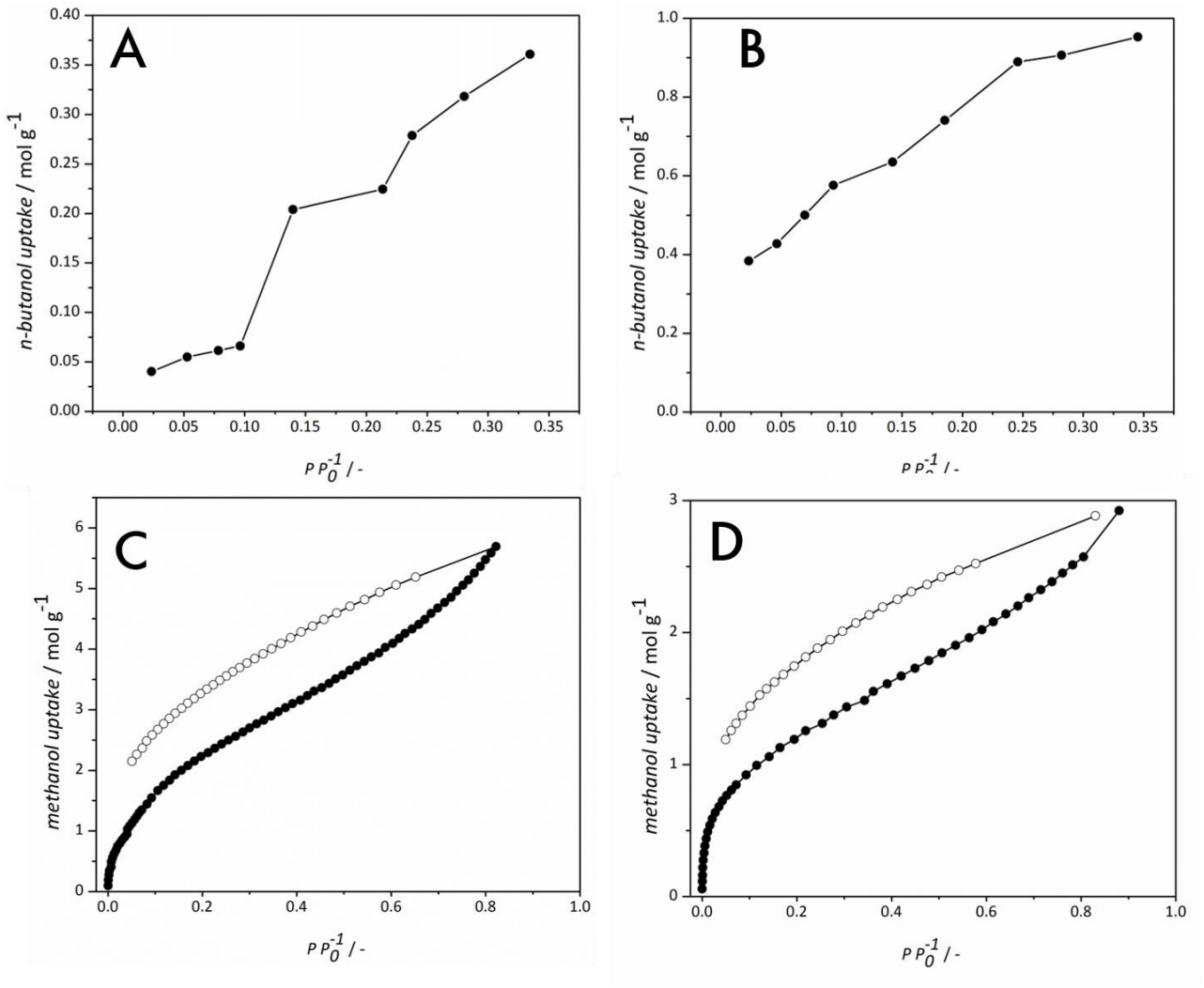

Figure 2.7. *n*-Butanol (A, B) and methanol (C, D) adsorption isotherms measured at 25 ^{0}C of sulfo-1 (A, C) and sulfo-2 (B, D).

NMR spectroscopy indicates that **1** and **2** can be synthesised in high purity. Both polymers possess a good thermal stability (up to 350 ^{0}C under oxidising conditions) and outstanding chemical stability. The latter is exemplified by the observation that the polymers do not break down upon sulfonation (@160 ^{0}C in pure sulfuric acid) and/or washing in HCl at 100 ^{0}C. Overall, more than 60% of the aromatic rings could be sulfonated. The CO_2 sorption analysis suggests that the porous scaffolds contain a large degree of planarity, directed by the building blocks. The fact that we could not observe the adsorption of N_2 at 77 K infers that intercatenation or random stacking of the polymer sheets occurs during synthesis and that this cannot be corrected upon activation because of the strength of the created C—C bonds. As a result, polymers that should, *a priori*, contain a certain degree of mesoporosity turned out to be completely microporous. Fortunately, the sulfonation leads to a significant increase in porosity. In the case of 1, if we consider that a 40% increase in mass is added to the

Table 2.2. *TOF*s [min $^{-1}$] for the esterification of *n*-butanol and acetic acid (1:1 molar ratio) using 3g of catalyst per mol of reactant at 80 ^{0}C. The *TOF*s were obtained for several catalytic runs by recycling the sample.

Catalyst	Acidity [mmol g^{-1}]	*TOF* [min^{-1}]			
		1st run	2nd run	3rd run	4th run
Amberlyst-15®	4.2	0.7	0.61	0.45	0.4
Sulfo-**1**	5.0	1.06	0.83	0.71	0.69
Sulfo-**2**	4.6	0.65	0.28	0.32	0.34

framework in the form of sulfonic groups, a 250% increase in specific surface area is observed upon sulfonation per initial polymer weight. We attribute this effect to the bulkiness of the sulfonic acid group, which leads to swelling similar to that described frequently for intercalation in structured graphite and graphene sheets and to an increase in the polarity of the framework, which is in line with the calculated pore size distributions. Similar swelling is expected to occur upon the incorporation of other types of functional groups as well, in particular, those that involve bulky groups.

In view of the differences observed in the catalytic performance of both polymers and to investigate whether the reactants and products of the studied reaction are able to penetrate the narrow polymer pores and to investigate the affinity of polar compounds for the catalysts, we measured the adsorption isotherms of *n*-butanol and methanol in both sulfo-1 and sulfo-2 (Figure 2.7).

Both sulfonated polymers adsorb considerable amounts of the bulkiest reactant, *n*-butanol, which demonstrates that the internal porosity of the polymers is accessible. In spite of the large differences in the total uptake of *n*-butanol, the methanol isotherms demonstrate that the total pore volume of both catalysts is quite similar and suggest a stronger affinity of sulfo-2 for polar compounds (see the higher uptake at lower partial pressures). These results infer that the differences in activity are related to the stronger adsorption of reactants and products on sulfo-**2** than sulfo-**1**.

In summary, we have reported the facile synthesis of two new structured polymers and their use as supports for acidic functionalities. Compared to state-of-the-art Amberlyst-15, sulfo-**1** displays a higher activity per sulfonic acid moiety. The catalytic performance of

sulfo-**2**, although still very good, is slightly lower than that of sulfo-**1** and Amberlyst-15. We attribute this lower activity to the interplay between diffusion and polarity in sulfo-**2** that may lead to slower kinetics caused by product (water) inhibition. Finally, the polymers presented here show also a higher stability than Amberlyst-15: the commercial catalyst can be only used at temperatures below 120 ^{0}C, the sulfonic acid groups in the sulfonated PAFs presented here do not decompose up to ~240 ^{0}C. Our results show that these PAFs combine the tunability of MOFs with the chemical stability of zeolites. With regard to the work that has been performed using triazination, trimerisation, and transition-metal catalysed Suzuki–Miyaura, Sonogashira, and Yamamoto coupling for the synthesis of new porous materials,[15,28,29] we are confident that the results presented in this work can be extended to a wide range of organic materials.

2.5. CONCLUSIONS

Porous aromatic frameworks synthesized through the Pd^{II}-catalyzed Suzuki–Miyaura coupling of appropriate building blocks hold great promise for application as supports in heterogeneous catalysis. In this work, two new, fully microporous polymers of outstanding stability were sulfonated post-synthetically to yield solid Brønsted acid catalysts with a similar or superior performance to that of Amberlyst-15 over multiple catalytic cycles. Although the resulting polymers are not crystalline, they are highly stable and chemically tunable.

2.6. REFERENCES

[1] F. Schüth, W. Schmidt, *Adv. Mater.* **2002**, *14*, 629–638.

[2] Y.-J. Xu, G. Weinberg, X. Liu, O. Timpe, R. Schlögl, D. S. Su, *Adv. Funct. Mater.* **2008**, *18*, 3613–3619.

[3] C. Moreno-Castilla, M. A. Ferro-Garcia, J. P. Joly, I. Bautista-Toledo, F. Carrasco-Marin, J. Rivera-Utrilla, *Langmuir* **1995**, *11*, 4386–4392.

[4] P. Vinke, M. van der Eijk, M. Verbree, A. F. Voskamp, H. van Bekkum, *Carbon N. Y.* **1994**, *32*, 675–686.

[5] J. L. Figueiredo, M. F. R. Pereira, in *Carbon Mater. Catal.*, John Wiley & Sons, Inc., **2008**, pp. 177–217.

[6] M. G. Goesten, J. Juan-Alcañiz, E. V Ramos-Fernandez, K. B. Sai Sankar Gupta, E. Stavitski, H. van Bekkum, J. Gascon, F. Kapteijn, *J. Catal.* **2011**, *281*, 177–187.

[7] J. Juan-Alcaniz, R. Gielisse, A. B. Lago, E. V Ramos-Fernandez, P. Serra-Crespo, T. Devic, N. Guillou, C. Serre, F. Kapteijn, J. Gascon, *Catal. Sci. Technol.* **2013**, *3*, 2311–2318.

[8] A. Corma, H. García, F. X. Llabrés i Xamena, *Chem. Rev.* **2010**, *110*, 4606–4655.

[9] J. Gascon, A. Corma, F. Kapteijn, F. X. Llabrés i Xamena, *ACS Catal.* **2014**, *4*, 361–378.

[10] J. Gascon, U. Aktay, M. D. Hernandez-Alonso, G. P. M. van Klink, F. Kapteijn, *J. Catal.* **2009**, *261*, 75–87.

[11] W. Lin, *Top. Catal.* **2010**, *53*, 869–875.

[12] M. A. Nasalevich, M. G. Goesten, T. J. Savenije, F. Kapteijn, J. Gascon, *Chem. Commun.* **2013**, *49*, 10575–10577.

[13] S. M. Aharoni, S. F. Edwards, *Adv. Polym. Sci.* **1994**, *118*, X–231.

[14] A. P. Côté, A. I. Benin, N. W. Ockwig, M. O'Keeffe, A. J. Matzger, O. M. Yaghi, *Science.* **2005**, *310*, 1166–1170.

[15] P. Kuhn, M. Antonietti, A. Thomas, *Angew. Chemie Int. Ed.* **2008**, *47*, 3450–3453.

[16] Y. Xu, S. Jin, H. Xu, A. Nagai, D. Jiang, *Chem. Soc. Rev.* **2013**, *42*, 8012–8031.

[17] T. Ben, S. Qiu, *CrystEngComm* **2013**, *15*, 17–26.

[18] M. Rose, W. Bohlmann, M. Sabo, S. Kaskel, *Chem. Commun.* **2008**, 2462–2464.

[19] P. M. Budd, B. S. Ghanem, S. Makhseed, N. B. McKeown, K. J. Msayib, C. E. Tattershall, *Chem. Commun.* **2004**, 230–231.

[20] C. F. Martin, E. Stockel, R. Clowes, D. J. Adams, A. I. Cooper, J. J. Pis, F. Rubiera, C. Pevida, *J. Mater. Chem.* **2011**, *21*, 5475–5483.

[21] R. Dawson, A. I. Cooper, D. J. Adams, *Prog. Polym. Sci.* **2012**, *37*, 530–563.

[22] M. M. Nasef, H. Saidi, *Appl. Surf. Sci.* **2006**, *252*, 3073–3084.

[23] H. Ren, T. Ben, E. Wang, X. Jing, M. Xue, B. Liu, Y. Cui, S. Qiu, G. Zhu, *Chem. Commun.* **2010**, *46*, 291–293.

[24] T. Ben, H. Ren, S. Ma, D. Cao, J. Lan, X. Jing, W. Wang, J. Xu, F. Deng, J. M. Simmons, et al., *Angew. Chemie Int. Ed.* **2009**, *48*, 9457–9460.

[25] D. Yuan, W. Lu, D. Zhao, H.-C. Zhou, *Adv. Mater.* **2011**, *23*, 3723–3725.

[26] D. Beaudoin, T. Maris, J. D. Wuest, *Nat Chem* **2013**, *5*, 830–834.

[27] J. D. Wuest, *Chem. Commun.* **2005**, 5830–5837.

[28] X. Feng, X. Ding, D. Jiang, *Chem. Soc. Rev.* **2012**, *41*, 6010–6022.

[29] A. I. Cooper, *Angew. Chemie* **2012**, *124*, 8014–8016.

CHAPTER THREE

Efficient Production of Hydrogen from Formic Acid Using a Covalent Triazine Framework Supported Molecular Catalyst

A heterogeneous molecular catalyst based on IrIIICp* (Cp*=pentamethylcyclopentadienyl) attached to a covalent triazine framework (CTF) is reported. It catalyses the production of hydrogen from formic acid with initial turnover frequencies (*TOF*) up to 27000 h^{-1} and turnover numbers (*TON*) of more than one million in continuous operation. The CTF support, with a Brunauer–Emmett–Teller (BET) area of 1800 m^2 g^{-1}, was constructed from an optimal 2:1 ratio of biphenyl and pyridine carbonitrile building blocks. Biphenyl building blocks induce mesoporosity and, therefore, facilitate diffusion of reactants and products whereas free pyridinic sites activate formic acid through β-hydride elimination at the metal, rendering unprecedented rates in hydrogen production. The catalyst is air stable, produces CO-free hydrogen, and is fully recyclable. Hydrogen production rates of over 60 mol $L^{-1}h^{-1}$ were obtained at high catalyst loadings of 16 wt% Ir, making it attractive towards process intensification.

This Chapter is based on the following publication:

A. V. Bavykina, M. G. Goesten, F. Kapteijn, M. Makkee, J. Gascon, *ChemSusChem* 8 (2015) 809-812

3.1. INTRODUCTION

The use of formic acid as a convenient material for hydrogen storage is increasingly gaining attention in the development of a hydrogen economy.[1,2] The main advantages of formic acid over proposed alternatives include easy handling, refuelling and transportation,[3] price (600–1250 $ per tonne), as well as the possibility of synthesising it through electrochemical reduction of CO_2 using water as hydrogen donor.[4]

Although the decomposition of formic acid to yield hydrogen and CO_2 is thermodynamically favourable ($HCO_2H \rightarrow H_2 + CO_2$, $\Delta G^o = -32.8$ kJmol^{-1}), efficient H_2 release is only obtained with the use of a catalyst. The most active catalysts are homogeneous and transition-metal based for which impressive turnover frequencies (*TOFs*) have been documented[5,6] even for a base metal such as iron.[7–9] The recent reports on base metals as catalysts, iron in particular, should be encouraged. However, these involve tailored ligands, most containing increasingly scarce phosphorus, which are more costly than the metal itself even when iridium is used.[10] The relatively low cost of the CTF support, and the truly heterogeneous nature of the catalyst in this work must be emphasized from this perspective.

The requirement of a heterogeneous catalytic system has been questioned,[11] yet the aim of developing an air-stable, solid catalyst that produces hydrogen seems justified as it would certainly present advantages in handling and recycling, two important parameters in device-based applications (for example, fuel cells). To date, the task of developing a heterogeneous catalyst that performs well in hydrogen production from formic acid has proven challenging. In comparison with homogeneous catalytic systems, suppression of the undesired dehydration reaction ($HCOOH \rightarrow H_2O + CO$) remains an obstacle (CO can poison the catalyst and high CO contents make an extra separation step a requirement). Moreover, *TOFs* and corresponding rates per unit reactor volume are often low. Whereas the majority of these attempts focus on the use of nanoparticles,[12–16] promising reports involve the use of heterogenised molecular catalysts.[17,18] Here, particular progress has come from the group of Laurenczy, who immobilised their homogeneous Ru-mTPPTS catalyst on various supports to develop a heterogeneous molecular catalyst.[19] As support, mesoporous silica worked best,

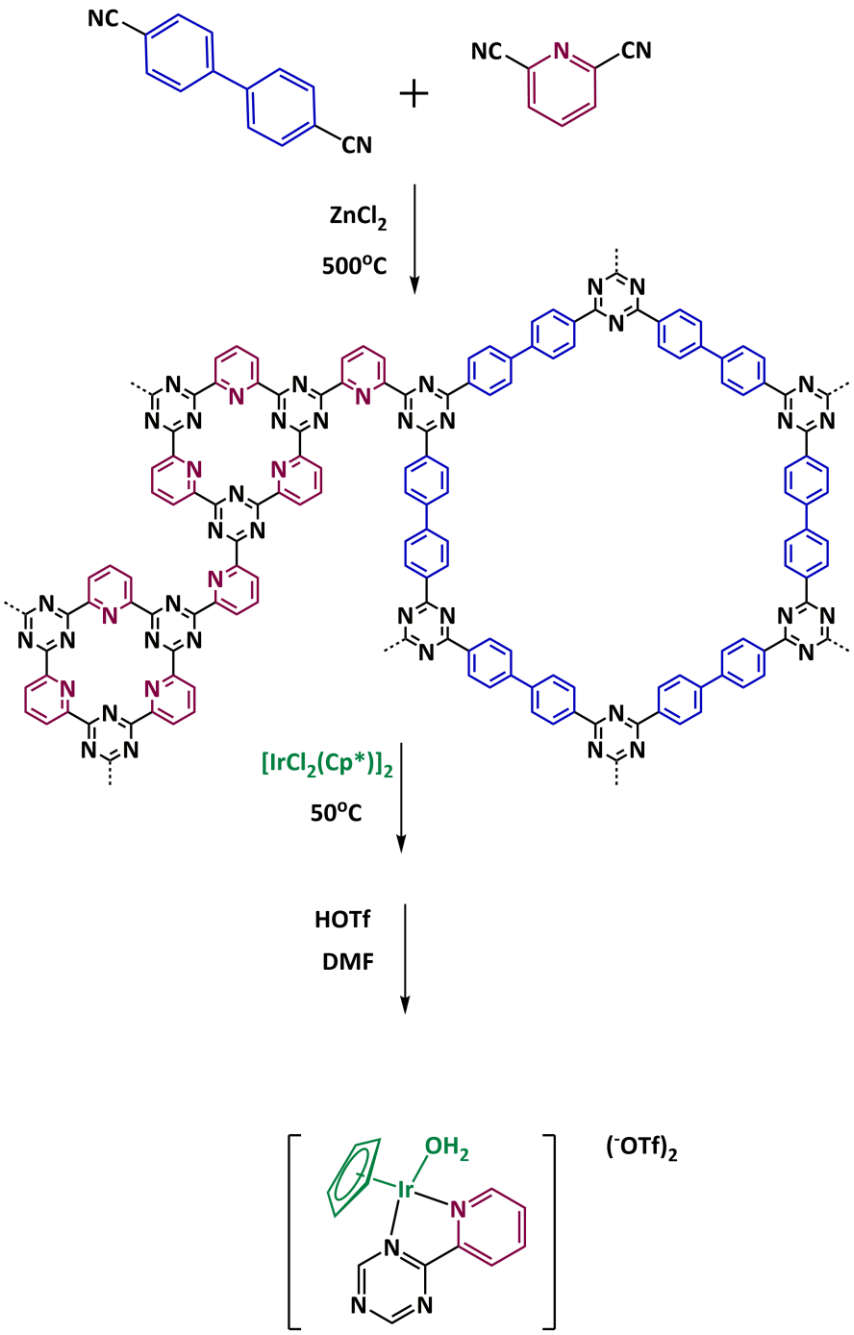

Figure 3.1. Synthesis of the CTF through triazination, with corresponding attachment of IrCp*(H_2O) and counterion exchange. The methyl groups of Cp* are omitted for the sake of clarity. The CTFs are depicted schematically, and no long-range order was observed using X-ray diffraction (XRD)

with a maximum TOF of 2780 h^{-1} at 110˚C.[20] This work demonstrates the potential of heterogenised molecular systems in catalysis.

Herein, we report a highly active, selective and air-stable molecular heterogeneous catalyst based on a Covalent Triazine Framework (CTF),[21–23] a porous type of organic polymer synthesised from inexpensive feedstocks that had earlier been successfully applied to

immobilise the molecular Periana catalyst for methane-to-methanol oxidation.[24] Here, $Ir^{III}Cp^*$ (Cp*=pentamethylcyclopentadienyl) is coordinated to a mesoporous CTF having a Brunauer–Emmett–Teller (BET) surface area of 1800 m^2g^{-1}, and which was constructed using a 1:2 ratio of 2,6-pyridinedicarbonitrile and 4,4'-biphenyldicarbonitrile. The coordination was confirmed by X-ray photoelectron spectroscopy (XPS).[25–27] In a subsequent step, the counterion Cl^{-1} was replaced by triflate, OTf^{-1}, a weakly coordinating anion. This was performed in DMF, a solvent known for binding H-Cl [28] instead of the conventional method using AgCl, which would result in precipitation within the CTF pores. The obtained heterogeneous catalyst Ir@CTF (Figure 3.1), is highly active for the production of hydrogen whilst being air stable and fully recyclable.

3.2. EXPERIMENTAL SECTION

Materials

$[IrCp^*Cl_2]_2$ was purchased from Strem Chemicals. All other chemicals were obtained from Sigma Aldrich and used without further purification.

Equipment

^1H NMR spectra were recorded in a Bruker Avance-400 NMR spectrometer, using 5 mm sample tubes, with 128 scans per sample. In all experiments, the gas phase was analysed with a Compact GC from Interscience equipped with a TCD detector possessing two columns (Porabond Q, 0.32 mm, 2 m; Carboxen 1010, 0.32 mm, 20 m). XPS measurements were performed by using a K-alpha Thermo Fisher Scientific spectrometer using a monochromatic Al$K\alpha$ X-ray source. The measurements were performed using a line scan of three points, each of which had a spot size of 300 mm at ambient temperature and chamber pressure of ≈ 10^{-7} mbar. A flood gun is used for charge compensation. All the spectra measured were corrected by setting the reference binding energy of carbon (*1s*) at (285±0.025) eV. The electron energy analyser was operated with a pass energy of 50 eV, and each high-resolution spectrum was scanned 10 times. The spectra were analysed and processed using Thermo Avantage v5.52 software (Thermo Fisher Scientific). The peaks were fitted using a Lorentzian–Gaussian (L/G)

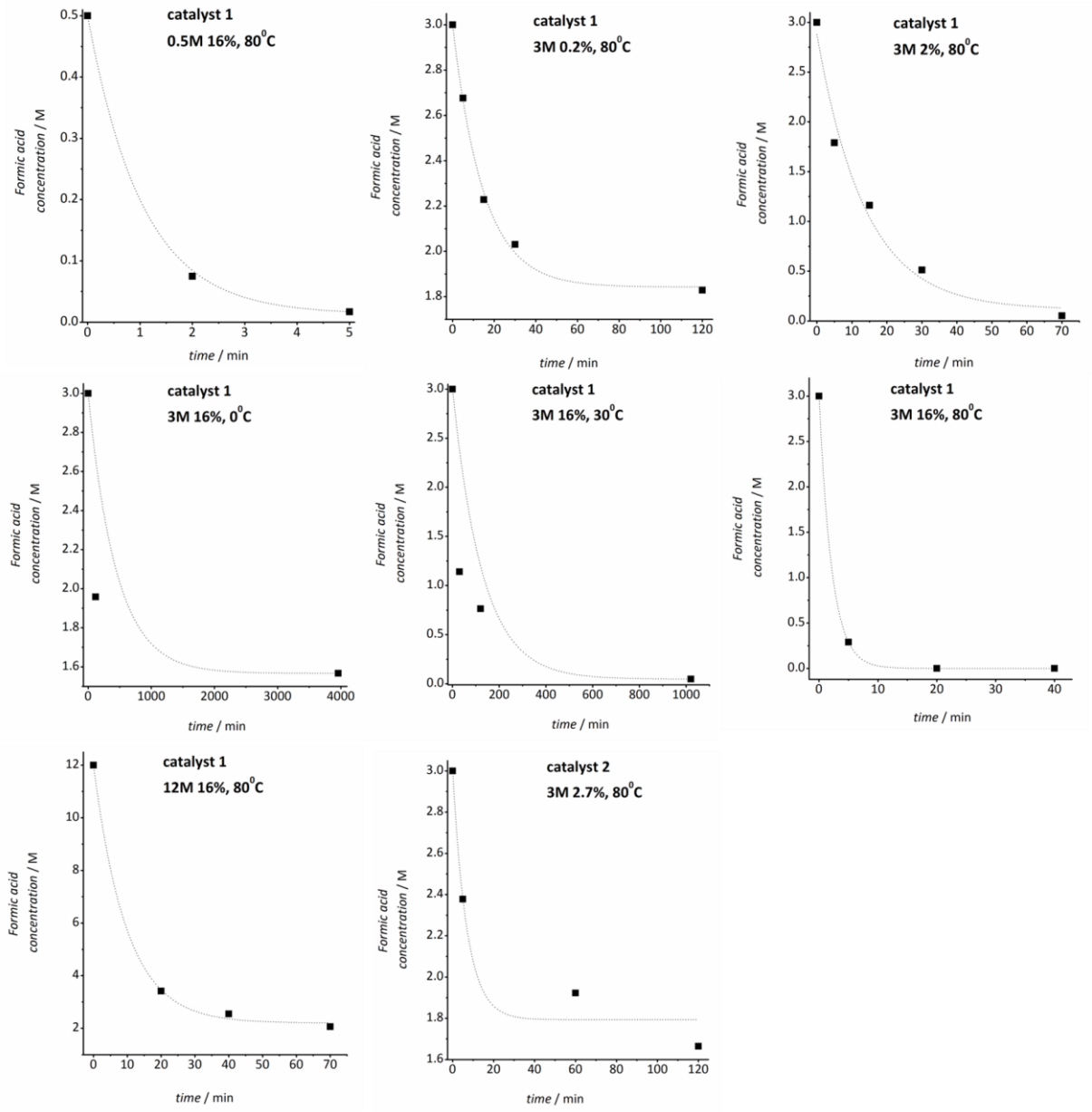

Figure 3.2. Formic acid concentrations in time for the different conditions.

ratio of 0.3. Nitrogen adsorption measurements were done using a Tristar II 3020 Micromeritics instrument employing N_2 gas (99.999 %). Argon adsorption was performed on a Micromeritics ASAP 2010 gas adsorption analyser (stainless steel version) at -185.15˚C. For the DFT calculations on the pore size distribution, the MicroActive v. 3.00 (Micromeritics) software package was used using a Cylindrical Pores NLDFT (Non Local Density Functional Theory) model, using a non-negative regularisation method with a factor of 0.03160, Standard Deviation of Fit: 0.85175 $cm^3\ g^{-1}$ STP. Continuous flow measurements were done by a flowmeter from Bioprocess Control. DRIFT spectra were recorded in a Bruker model IFS66 spectrometer, equipped with a high temperature cell with CaF_2 windows and a 633 nm laser.

The spectra were registered after accumulation of 128 scans and a resolution of 4 cm^{-1}. A flow of helium at 10 mL min^{-1} was maintained during the measurements. Before collecting the spectra, the different samples were pretreated in a helium flow at 119.85˚C for 30 min. KBr was used for background spectra. In-situ Mass Spectroscopy was carried out by a T100 Gas Analyser from Leiden Probe Measurements B.V, Leiden, the Netherlands.

For elemental analysis, samples were analysed by Mikroanalytisches Laboratorium KOLBE, (Mülheim an der Ruhr, Germany).

Synthesis of the meso-porous Covalent Triazine Framework

The following procedure is carried out for the preparation of the polymer: a glass ampoule was charged with 2,6-pyridinedicarbomitrile (0.041 g, 320 µmol), 4,4'-biphenyldicarbonitrile (0.131 g, 640 µmol) and anhydrous $ZnCl_2$ (0.664 g, 4.80 mmol), in a glovebox. The ampoule was flame sealed and subjected to the following temperature program: temperature is brought to 500 ^0C via a heating rate of 60 ^0C h^{-1}. It is kept at this temperature for 48 hours and then cooled to room temperature at a rate of 10 ^0C h^{-1}. To obtain the product, the ampoule was broken and the product was crushed in a mortar, then refluxed in 5M HCl (150 mL) overnight at 100 ^0C, filtered and washed with H_2O. It is then washed overnight at 60 ^0C in 6M NH_4OH, washed at 100 ^0C with H_2O, then washed with THF at 60 ^0C overnight, before activating the material in vacuum at 200 ^0C overnight. After all required filtrations, the fully amorphous powder was obtained with a final yield of at least 90%. The washing steps might seem excessive and are more severe than those described in literature,[29] but were, as we found, required to remove $ZnCl_2$ (as determined by XPS and elemental analysis).

Coordination of $IrCp^*(H_2O)[OTf]_2$

A mixture of 250 mg of CTF polymer and 375 mg of $[Cp^*Ir(Cl)_2]_2$ was placed in a Schlenk flask in a glovebox. Outside the glovebox, degassed water (40 mL) was added with a syringe to the flask under continuous Ar flow. The flask was closed and the mixture is stirred overnight and filtered. Afterwards, to remove the chloride ions, the powder is washed in a mixture of HOTf (283 mg) and a 1:1 DMF/water mixture (50 mL). The mixture is stirred in water at 50 ^0C

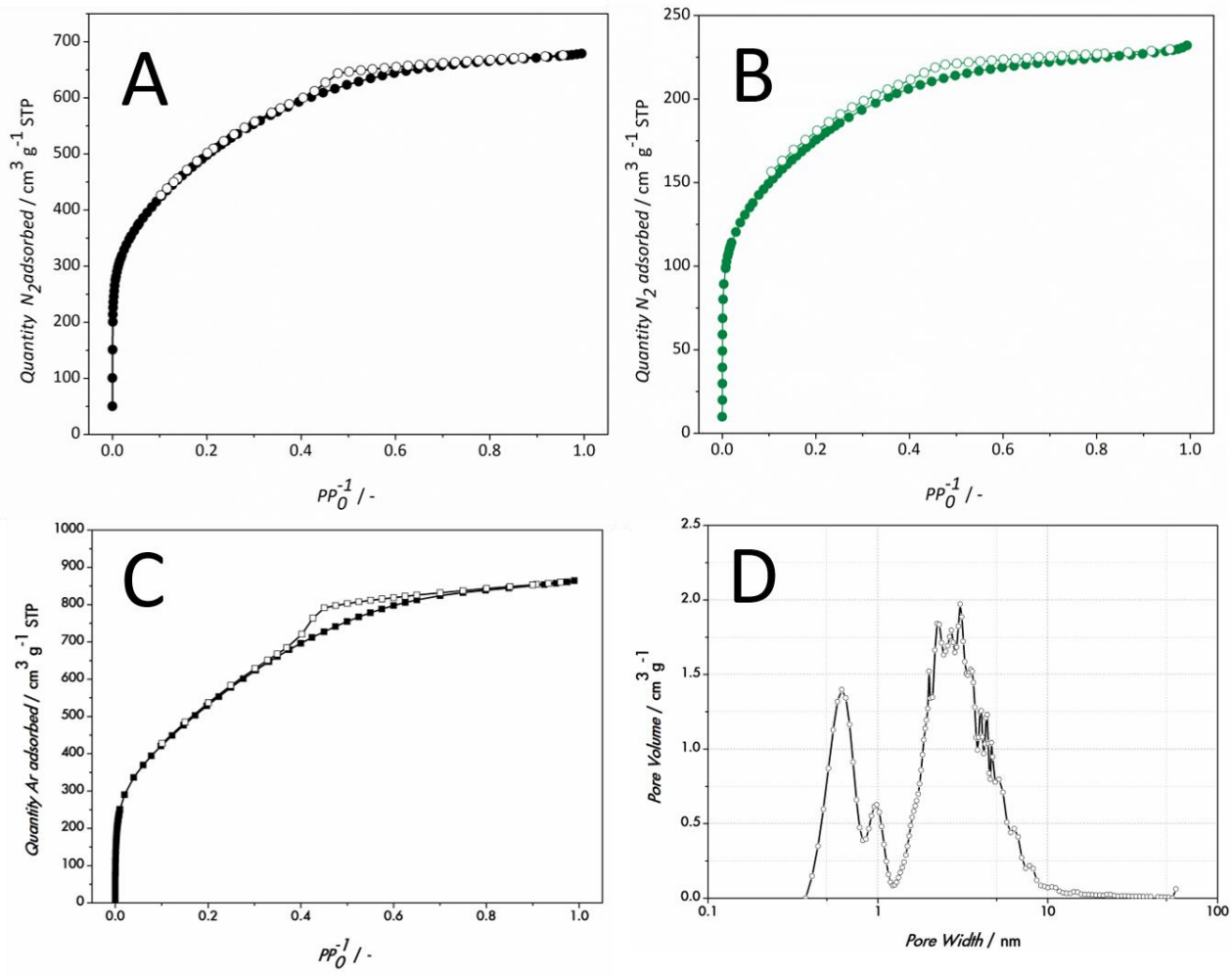

Figure 3.3. Nitrogen adsorption isotherms for A) mesoporous CTF support and B) Ir@CTFir@ctf catalyst with Ir loading of 16 wt%. C) Argon adsorption isotherm of CTF D) DFT calculated Pore size distribution of CTF.

for another 12 h, before being filtered and dried at vacuum at 50 ^{0}C. To prepare the Ru based catalyst the exact the same procedure was followed using $[C_6H_6Ru(Cl)_2]_2$ instead.

Catalyst Performance

Formic acid reactant stock solutions were prepared by dilution of 2.17/13.00/52.00 mL of 88% formic acid with H_2O to 100 mL to yield solutions with a concentration of 0.5/3/12M, respectively. The pH is adjusted to 1.5 by addition of HBF_4 (aq) or NaOH (aq). Test reactions were carried out in a 100 mL round bottom flask equipped with septum caps. 300 mg Ir@CTF (or Ru) catalyst is dispersed in 30 mL of 3/0.5/12 M aqueous formic acid solution. The flask with the reaction mixture is submerged in an oil bath and heated to desired temperature with continuous stirring. The reaction path was followed by ^{1}H NMR experiments, and the collected

gas phase was analysed by GC. For recycling the catalyst, the following procedure was carried out: The catalyst was filtered, washed vigorously with water and consequently dried at 50 ˚C under vacuum. For the continuous hydrogen production test, the following procedure is carried out. The reaction is performed in a 100 mL round bottom flask connected to a pump for continuous supply of formic acid. The level inside of the reaction vessel is kept constant with a secondary pump. The production of gaseous H_2 and CO_2 is measured using a continuous volumetric flowmeter (µFlow, Bioprocess Control). 300 mg Ir@CTF catalyst with 2 wt% iridium loading was dispersed in the 3M formic acid solution (see above). The reaction mixture is submerged in an oil bath and heated to 80 ^{0}C under continuous stirring.

Turnover frequency and total number of turnovers

The calculation of the *TOFs* and productions in the batch experiments were based on the integration of the formic acid signal in ^{1}H NMR spectra measured from the liquid phase samples taken at regular time intervals. An inert internal standard, dimethyl sulfone, was used. The kinetic curve obtained by this sampling was fit to a first order rate equation, of which the slope at t = 0 was taken to obtain initial *TOF*. The concentration of Ir that was used in experiments was determined using elemental analysis on the powder (*vide infra*, note that the elemental analysis provides a quantitative ratio between iridium and the (solid) powder, whereas the Ir concentration used in the calculations matters the total molar amount of iridium per mol of solution. In the continuous experiment, the net H_2 gas flow in mL(STP)/min was converted to a molar gas flow using the STP value of 22.4 mol/l. The turnover number *TON* was calculated as the molar ratio of the total hydrogen produced and the amount of Ir used in the experiment.

3.3. RESULTS AND DISCUSSION

Nitrogen adsorption @ -196,15˚C was performed before and after coordination of the Ir-Cp* moiety. The BET area changed from 1800 m^2g^{-1} to 630 m^2g^{-1} after coordination of 16 wt% Ir. This decrease is larger than expected for the increase in weight due to attachment of $IrCp^*(H_2O)(OTf^-)_2$, suggesting some pore mouths are (partially) blocked by the moiety. The decrease in magnitude and position of the hysteresis moving to somewhat lower partial pressures suggests that mainly some mesopores are less accessible. Nevertheless,

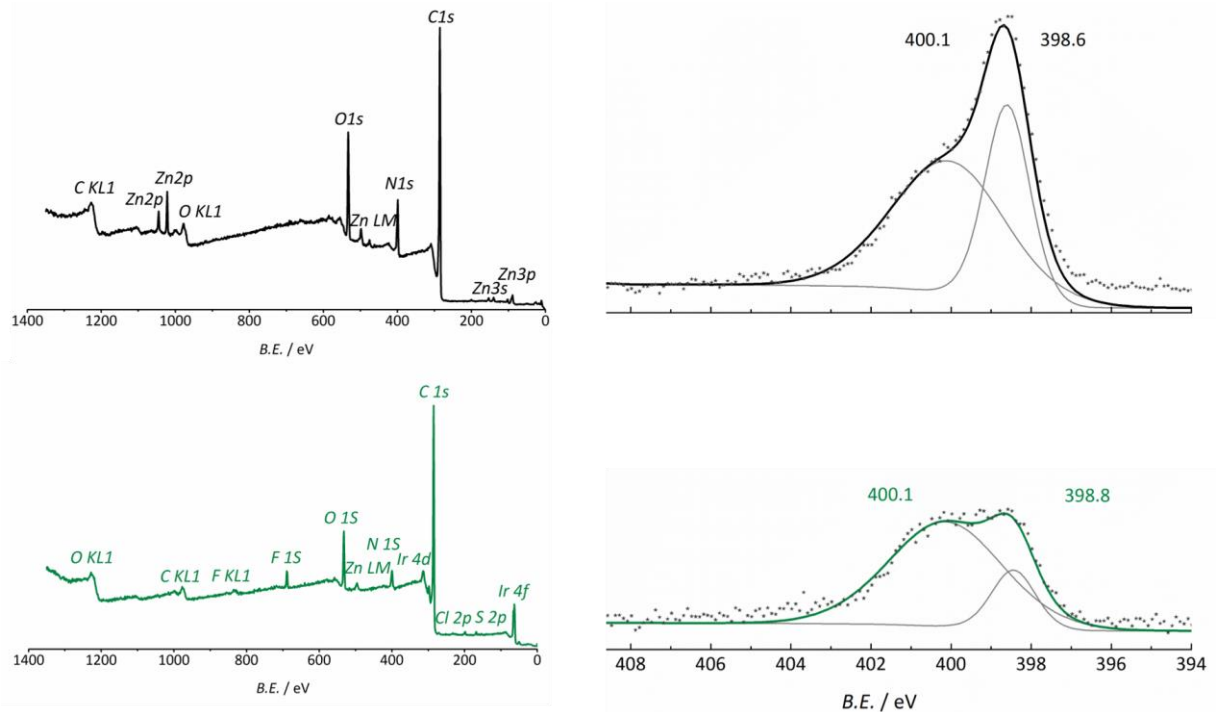

Figure 3.4. *Left*: Survey XPS spectrum of CTF (*black*) and Ir@CTF catalyst (*green*); *Right*: Nitrogen 1s XPS spectra of CTF (*black*) and of Ir@CTF with 16 wt% loading catalyst (*green*).

mesoporosity is still present even after the coordination of a large amount of Ir (16 wt%), which means the remaining surface area is sufficiently accessible for catalysis.

The as-synthesized CTF, despite being thoroughly washed, contains small concentrations of Zn, which is found to coordinate to some bipyridinic sites, resulting in two nitrogen peaks in XPS. The peak centered at 398.6 eV in the bare polymer is assigned to nitrogen within an aromatic ring (Figure 3.4), whilst the band centered at at 400.1 eV corresponds to metal-binding nitrogen species (Zn in case of the pristine CTF as can be seen in Figure 3.4). Upon coordination with Ir, practically all Zn was removed from the CTF as found by XPS. N*1s* XPS of this sample shows a much higher fraction of metal coordinated N moieties (400.1 eV) along with some uncoordinated N (398.4 eV). The total nitrogen content in pure polymer and in the catalyst is 12.2 and 6.4 atomic %, respectively. The catalyst tested contains 16% of Iridium, whilst the maximum theoretical amount of Iridium to be coordinated to bipyridinic sites is 19%. This explains that the peak corresponding to non metal-coordinated nitrogen species is smaller than the one of higher binding energy, since nearly all possible bipiyridinic sites are used for coordination. The overall drop in intensity can be explained by the shielding effect of Ir, which has a low binding energy.

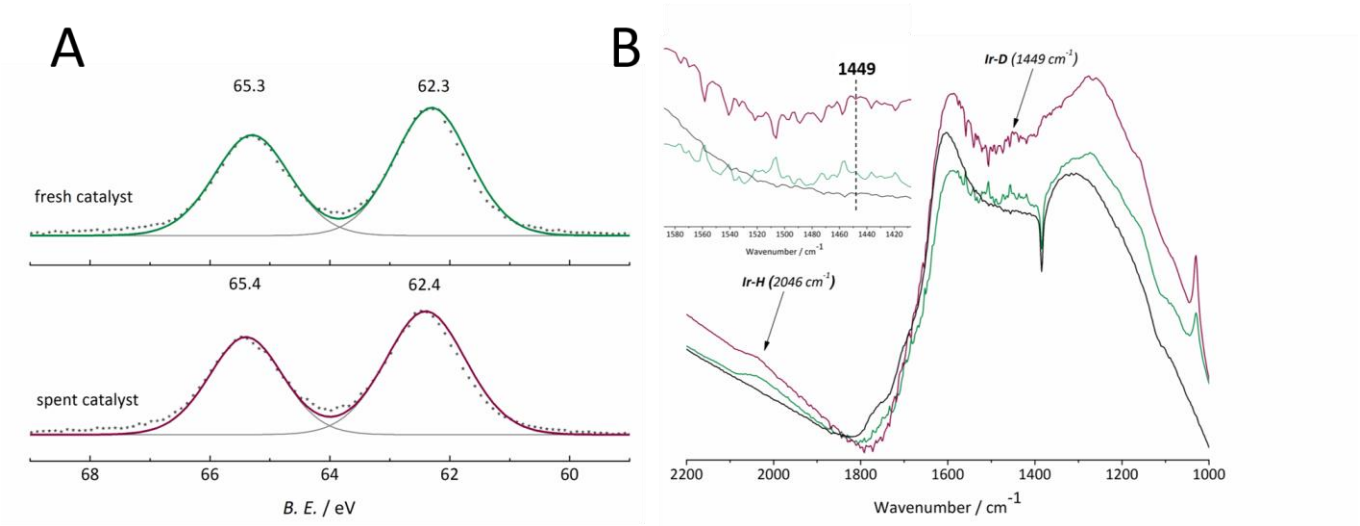

Figure 3.5. A) Iridium *4f* XPS spectra of the 16 wt% loaded catalyst, before (*green, top*) and after (*red, bottom*) use B) DRIFT spectra of the pure CTF (*black*) 16 wt.% Ir loaded (*green*), and 16 wt.% in the experiment with deuterated formic acid (*red*).

When dispersed in a 3M formic acid solution of pH 1.5 at 80 ^{0}C, Ir@CTF instantaneously produces a large flow of gas, which was determined by GC analysis to be a CO_2/H_2 (1:1) mixture with a CO concentration below the detection limit. The catalyst could be recycled for at least four times under standard reaction conditions (80 ^{0}C) without any observed loss of catalytic activity. The elemental analysis indicated that Ir leaching was negligible. During recycling, the catalyst was filtered and stored under ambient conditions, only requiring an oxygen-free environment during its synthesis. XPS (Figure 3.5A) indicates that the oxidation state of Ir remained +3 between runs. Crucially, Ir oxide species, instantaneously recognised for their *4f* symmetric peak pattern, separated 2.5-3 eV[26] are not formed. The binding energies correspond to similar organometallic Ir(III) species reported in literature and confirm the formation of the envisaged $Ir^{III}Cp^*$ catalyst within the pores of the CTF.[27]

At a loading of 0.2 wt % and at 80 ^{0}C, the catalyst reached an initial *TOF* of 27000 h^{-1}, by far the highest reported for any heterogeneous catalytic system to date for this reaction (Table 3.1). At 30^0 C and a loading of 16 wt%, the catalyst remained active at an initial *TOF* of 1350 $h^{-1}$and even at 0 ^{0}C the catalyst still displayed an initial *TOF* of 70 h^{-1}. Traces of methanol (< 0.08 mmol) were found to be present in the liquid phase after full conversion, a product from the formic acid disproportionation reaction (transfer hydrogenation of formic acid using formic acid as hydrogen donor), a reaction recently also reported for [$Ir^{III}Cp^*(H_2O)$ (bpy)] (bpy = 2,2'- bipyridine).[30] When an experiment with fully deuterated formic acid, DCOOD, was

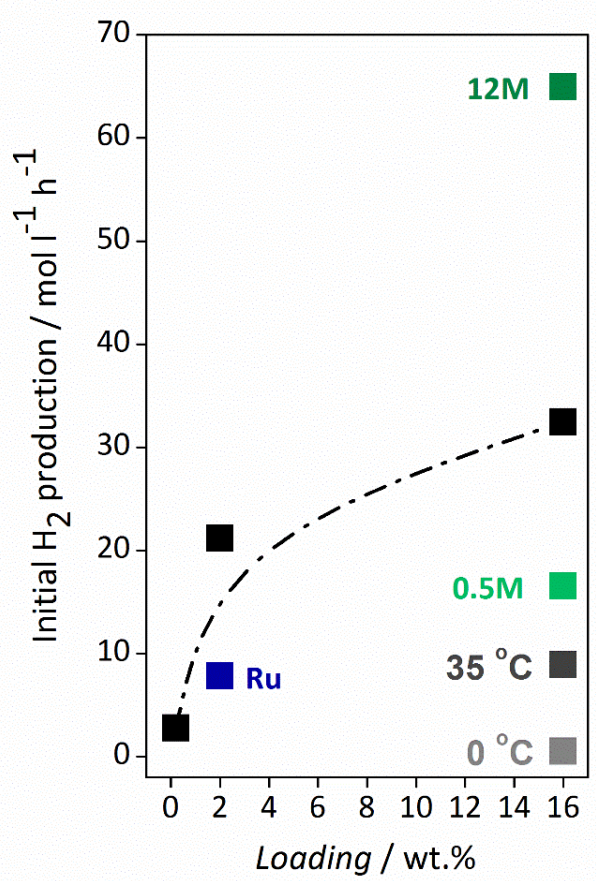

Figure 3.6. Performance of 1 at various metal loadings in the initial net production rate of H_2 per unit liquid volume. Standard conditions, unless differently specified: 3M formic acid solution, 80 ˚C, pH 1.5. [$Ru^{II}(\mu_6\text{-}C_6H_6)$] = Ru@CTF (see text). In all experiments, reactions were carried out in a 30 mL glass flask with 300 mg of solid catalyst.

followed *in situ* by means of mass spectroscopy, the molar flow ratios H_2/HD/D_2 were found to be 195:46:1. The surprisingly large value for H_2 suggests a protonic hydride and very efficient exchange of the type Ir—D ⇄ Ir—H, which had been observed by Ogo *et al*. before for [Ir^{III}Cp*(bpy)H] at low pH values.[31] It is possible to identify CTF-coordinated Ir-H species after reaction, as was earlier done for homogeneous Ir catalysts by Ogo *et al*. After reaction, a typical broad Ir—H stretching at 2050 cm^{-1} was identified performing diffuse reflectance infrared spectroscopy (DRIFTS) on the spent catalyst.[32] The stretchings are observed after catalysis, both when formic acid was used, and when deuterated formic acid was used. This is in line with the *in-situ* MS data (*vide supra*). Only in the case of Ir-D, a tooth looking stretching appears shown by Ogo *et al*. in a similar experiment with a homogeneous catalyst to be an Ir-D stretching, of which the position relative to the Ir-H stretching is in accordance with Hooke's law.[32]It is reasonable to assume that for loadings lower than 0.2 wt% even higher *TOFs* can

Table 3.1. Catalyst performance of in production of H_2 from formic acid. [a]

Catalyst	Conditions Loading [wt%]	T [˚C]	$C_{formic\ acid}$ [mol L^{-1}]	Time to 99% conversion [min]	Initial *TOF* [h^{-1}]
Ir@CTF	16	0	3	3600 [b]	70
Ir@CTF	16	30	3	1100	1350
Ir@CTF [c]	16	80	3	<20	3960
Ir@CTF	16	80	0.5	<5	2000
Ir@CTF	16	80	12	160	7900
Ir@CTF	2	80	3	70	21300
Ir@CTF	0.2	80	3	120 [d]	27000
Ru@CTF[e]	2.7	80	3	120 [d]	4020

[a] Standard conditions, unless specified differently: 30 mL 3m formic acid solution, 300 mg catalyst, 80˚C, pH 1.5; wt% refers to the metal loading on the CTF. [b] Max. conversion 65%. [c] The initial *TOF* on the fourth recycle was 3930 h^{-1}. [d] Max. conversion 65%. [e] Ru@CTF is the ruthenium(II)-based equivalent of Ir@CTF, using the benzene (η_6-C_6H_6) ligand instead of Cp*.

be obtained, but this goes at the cost of net productivity per unit reactor volume (or per mass of catalyst). Although the *TOF* value as parameter for catalytic efficiency should certainly not

be underestimated, the highest *TOFs* are usually obtained for very low concentrations of active sites per unit mass of catalyst, which translates to very large reactor dimensions to obtain reasonable total production rates. Since intensification of hydrogen production is clearly vital for device-based applications, we investigated the effect of catalyst metal loading, formic acid concentration and reactor temperature on (molar) hydrogen production rate pe runit volume. The results are shown in Figure 3.6. Although the *TOF* decreases for high loadings (Table 3.1), the trend in Figure 3.6 indicates that intensifying the hydrogen production through higher metal loadings and formic acid concentrations can be an attractive option. Using 16wt% Ir@CTF catalyst it is possible to produce enough hydrogen to charge iPhone6 (150 ml) within half of minute using a commercially available fuel cell "Horizon Edustak Junior 10 Cell"[33]. The hydrogen production rate is an important asset, for homogeneous systems frequently suffer from dramatic drops in performance and/or catalyst deactivation upon increased catalyst concentration.[34]

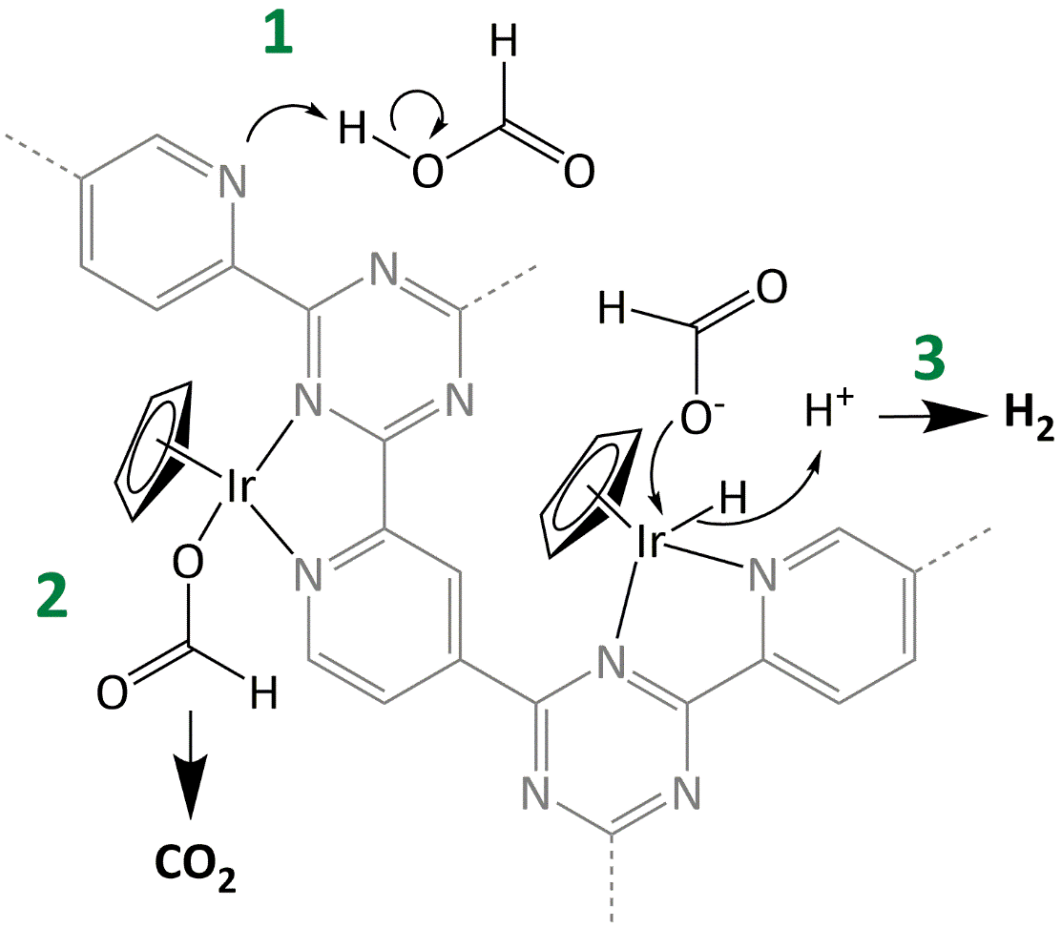

Figure 3.7. Simplified scheme displaying the catalytic cycle within the CTF polymer backbone (sketched grey). Methyl groups of the Cp* ligand and coordination of the labile aqua ligand are not depicted. 1) formic acid activation, 2) β-hydride elimination, 3) hydrogen release.

As indicated in Table 3.1, a less expensive catalytic system can be obtained by attaching $Ru^{II}(\eta_6\text{-}C_6H_6)$, **2**, to CTF instead of $Ir^{III}Cp^*$, but the corresponding catalytic activity is lower (Figure 3.6).

To test its suitability for device-based application, the Ir catalyst's durability was tested in continuous mode, in which a highly concentrated formic acid solution (88 wt%) was fed to a glass reactor initially containing a 30 mL 3M formic acid solution at 80 ˚C. The H_2/CO_2 production was measured by a volumetric flowmeter in a fashion similar to the experimental procedure reported by Beller *et al*. At termination of this experiment, a turnover number (*TON*) of 1 060 000 (mol FA/mol Ir) was obtained, which demonstrates the durability of the catalyst.

Figure 3.7 displays a plausible reaction mechanism, which consists of the three steps that have been shown to govern this particular type of catalysis: 1) formic acid deprotonation, 2) β-hydride elimination under decarboxylation and 3) hydrogen evolution. Of these three steps, (2) has been shown to be rate limiting for a very similar system ($[Rh^{III}Cp^*(bpy)(H_2O)][SO_4]$),[35] but also for an iron phosphine system $[P(CH_2CH_2PPh_2)_3FeH]^+$.[36] Evidence for step 2 to proceed starting from coordinated formato was proposed for similar systems,[32] which is herein further supported by elemental analysis indicating that weakly coordinating OTf^- is washed out during the recycling of the catalyst, pointing at formate/formato replacing triflate as charge-balancing anion within the scaffold. For step 2 to occur, formic acid must be deprotonated, which only occurs under relatively basic conditions ($pK_{a\ (HCOOH)}$ = 3.77) in which Ir hydride species are too stable for efficient hydrogen production and thus impede step 3.[35] It is for this reason that many catalysts for hydrogen production operate in tandem with an additional base.[3] The catalyst in this study operates efficiently without any auxiliary base, which we link to the presence of the free pyridinic sites that provide inherent basicity within the CTF matrix (see step 1 in Figure 3.7).[37] Indeed, formic acid is well known to have strong hydrogen-bonding interactions with pyridine, which facilitates the abstraction of protons.[38] It is noteworthy that this CTF is a co-polymer and that the ratio between the building blocks in Figure 3.7 can be tailored to yield an optimum between inherent basicity (by 2,6-pyridinedicarbonitrile) and reactant diffusion (by mesopore-inducing 4,4'-biphenyldicarbonitrile building blocks).

3.4. CONCLUSIONS

Mesoporous CTF was employed as a catalyst support. The respective 1:2 ratio between the building blocks reported in this work provides an ideal match between basic functionality and mesoporosity. The CTF based obtained molecular heterogeneous catalyst has an outstanding performance in hydrogen production from formic acid. The framework itself works as a non-innocent ligand providing basicity needed for formic acid activation. For now, this CTF supported $Ir^{III}Cp^*$ catalyst sets a new standard for hydrogen production from formic acid using heterogeneous catalysts. The catalyst provides flexibility for process intensification in a broad temperature range. Being a molecular catalyst, Ir@CTF is a fully heterogeneous

system in a powder form which allows easy handling and recycling. The Chapter 4 describes the catalyst shaping in a form of a sphere, which makes the catalyst recovery yet more straightforward and easier.

3.5. REFERENCES

[1] C. Fellay, P. J. Dyson, G. Laurenczy, *Angew. Chemie Int. Ed.* **2008**, *47*, 3966–3968.

[2] A. Boddien, F. Gärtner, C. Federsel, P. Sponholz, D. Mellmann, R. Jackstell, H. Junge, M. Beller, *Angew. Chemie Int. Ed.* **2011**, *50*, 6411–6414.

[3] S. Enthaler, J. von Langermann, T. Schmidt, *Energy Environ. Sci.* **2010**, *3*, 1207–1217.

[4] P. Kang, T. J. Meyer, M. Brookhart, *Chem. Sci.* **2013**, *4*, 3497–3502.

[5] J. F. Hull, Y. Himeda, W.-H. Wang, B. Hashiguchi, R. Periana, D. J. Szalda, J. T. Muckerman, E. Fujita, *Nat Chem* **2012**, *4*, 383–388.

[6] R. E. Rodríguez-Lugo, M. Trincado, M. Vogt, F. Tewes, G. Santiso-Quinones, H. Grützmacher, *Nat Chem* **2013**, *5*, 342–347.

[7] T. Zell, B. Butschke, Y. Ben-David, D. Milstein, *Chem. – A Eur. J.* **2013**, *19*, 8068–8072.

[8] A. Boddien, D. Mellmann, F. Gärtner, R. Jackstell, H. Junge, P. J. Dyson, G. Laurenczy, R. Ludwig, M. Beller, *Science (80-.).* **2011**, *333*, 1733–1736.

[9] A. Boddien, B. Loges, F. Gärtner, C. Torborg, K. Fumino, H. Junge, R. Ludwig, M. Beller, *J. Am. Chem. Soc.* **2010**, *132*, 8924–8934.

[10] A. Behr, P. Neubert, *Applied Homogeneous Catalysis*, Wiley-VCH, Weinheim, Bergstr, **2011**.

[11] M. Grasemann, G. Laurenczy, *Energy Environ. Sci.* **2012**, *5*, 8171–8181.

[12] S. Zhang, Ö. Metin, D. Su, S. Sun, *Angew. Chemie Int. Ed.* **2013**, *52*, 3681–3684.

[13] Y.-Y. Cai, X.-H. Li, Y.-N. Zhang, X. Wei, K.-X. Wang, J.-S. Chen, *Angew. Chemie Int. Ed.* **2013**, *52*, 11822–11825.

[14] Z.-L. Wang, J.-M. Yan, Y. Ping, H.-L. Wang, W.-T. Zheng, Q. Jiang, *Angew. Chemie Int. Ed.* **2013**, *52*, 4406–4409.

[15] J. H. Lee, J. Ryu, J. Y. Kim, S.-W. Nam, J. H. Han, T.-H. Lim, S. Gautam, K. H. Chae, C. W. Yoon, *J. Mater. Chem. A* **2014**, *2*, 9490–9495.

[16] W. Zhang, H. Huang, F. Li, K. Deng, X. Wang, *J. Mater. Chem. A* **2014**, *2*, 19084–19094.

[17] K. Maeda, K. Sekizawa, O. Ishitani, *Chem. Commun.* **2013**, *49*, 10127–10129.

[18] M. Trincado, D. Banerjee, H. Grutzmacher, *Energy Environ. Sci.* **2014**, *7*, 2464–2503.

[19] W. Gan, P. J. Dyson, G. Laurenczy, *React. Kinet. Catal. Lett.* **2009**, *98*, 205–213.

[20] W. Gan, P. J. Dyson, G. Laurenczy, *ChemCatChem* **2013**, *5*, 3124–3130.

[21] P. Kuhn, A. Thomas, M. Antonietti, *Macromolecules* **2009**, *42*, 319–326.

[22] P. Kuhn, A. Forget, D. Su, A. Thomas, M. Antonietti, *J. Am. Chem. Soc.* **2008**, *130*, 13333–13337.

[23] P. Kuhn, M. Antonietti, A. Thomas, *Angew. Chemie Int. Ed.* **2008**, *47*, 3450–3453.

[24] R. Palkovits, M. Antonietti, P. Kuhn, A. Thomas, F. Schüth, *Angew. Chemie Int. Ed.* **2009**, *48*, 6909–6912.

[25] J. R. Pels, F. Kapteijn, J. A. Moulijn, Q. Zhu, K. M. Thomas, *Carbon N. Y.* **1995**, *33*, 1641–1653.

[26] S. Kato, J. Jung, T. Suenobu, S. Fukuzumi, *Energy Environ. Sci.* **2013**, *6*, 3756–3764.

[27] F. Angersbach-Bludau, C. Schulz, J. Schoffel, P. Burger, *Chem. Commun.* **2014**, *50*, 8735–8738.

[28] M. G. Goesten, P. C. M. M. Magusin, E. A. Pidko, B. Mezari, E. J. M. Hensen, F. Kapteijn, J. Gascon, *Inorg. Chem.* **2014**, *53*, 882–887.

[29] S. Hug, M. E. Tauchert, S. Li, U. E. Pachmayr, B. V Lotsch, *J. Mater. Chem.* **2012**, *22*, 13956–13964.

[30] A. J. M. Miller, D. M. Heinekey, J. M. Mayer, K. I. Goldberg, *Angew. Chemie Int. Ed.* **2013**, *52*, 3981–3984.

[31] T. Abura, S. Ogo, Y. Watanabe, S. Fukuzumi, *J. Am. Chem. Soc.* **2003**, *125*, 4149–4154.

[32] S. Ogo, R. Kabe, H. Hayashi, R. Harada, S. Fukuzumi, *Dalt. Trans.* **2006**, 4657–4663.

[33] "Edustak Junior 10 Cell," can be found under http://fuelcellstore.com/fuel-cell-stacks/low-power-fuel-cell-stack/edustack-junior-fcsu-32

[34] T. Van Gerven, A. Stankiewicz, *Ind. Eng. Chem. Res.* **2009**, *48*, 2465–2474.

[35] S. Fukuzumi, T. Kobayashi, T. Suenobu, *ChemSusChem* **2008**, *1*, 827–834.

[36] X. Yang, *Dalt. Trans.* **2013**, *42*, 11987–11991.

[37] J. Roeser, K. Kailasam, A. Thomas, *ChemSusChem* **2012**, *5*, 1793–1799.

[38] M. J. Fernandez-Berridi, J. J. Iruin, L. Irusta, J. M. Mercero, J. M. Ugalde, *J. Phys. Chem. A* **2002**, *106*, 4187–4191.

CHAPTER FOUR

Shaping Covalent Triazine Frameworks for the Hydrogenation of Carbon Dioxide to Formic Acid

A facile one-step method is reported to shape covalent triazine framework (CTF) powders into spherical particles for catalytic applications. Phase inversion of the CTF powder by using a polyimide as a binder in a microfluidic device results in the formation of composite spheres with accessible CTF porosity and a high mechanical and thermal stability. The fabricated spheres can be used to host organometallic complexes. The obtained shaped catalyst, Ir@CTF spheres, is active and fully recyclable in the direct hydrogenation of carbon dioxide to formic acid under mild reaction conditions (20 bar and 50–90 ˚C), and in the dehydrogenation of formic acid.

This Chapter is based on the following publication:

A.V. Bavykina, E. Rozhko, M. G. Goesten, T. Wezendonk, B. Seoane, F. Kapteijn, M. Makkee, J. Gascon, *ChemCatChem* 13 (2016)

4.1 INTRODUCTION

Covalent triazine frameworks, CTFs, are a class of solid, porous organic polymers, formed by the trimerization of aromatic nitriles. Within materials chemistry, CTFs have recently attracted considerable attention as they provide a unique combination of high porosity, high thermal and chemical stability, and a high degree of chemical tunability.[1–7] Most interestingly, tuning of their solid-state properties is possible by varying their starting building blocks.[8,9] For instance, the use of pyridinic precursors leads to an inherently basic material, highly suitable for the activation of small molecules. Recently, we reported the application of such a CTF as a non-innocent support for $Ir^{III}Cp^*$ (Cp*=pentamethylcyclopentadienyl) and the use of the resulting catalyst in the dehydrogenation of formic acid, demonstrating that the CTF framework does not only immobilize the metal complex, but itself promotes the catalytic cycle by deprotonating formic acid under acidic conditions.[10]

In the frame of reversible hydrogen storage, essential in a hydrogen economy, the reversibility of the abovementioned reaction — the hydrogenation of CO_2 to yield formic acid — is particularly important. Progress in realizing this challenge has, to a large extent, relied on homogeneous catalysts, often based on Ir,[11–13] Rh,[14,15] and Ru.[16–19] Although the performance of such catalysts is generally outstanding from the perspective of turnover frequencies (*TOF*s), they usually operate under very low concentrations, making them unsuitable for intensified process operation. It is, therefore, logical that there exists a surging quest for efficient heterogeneous systems capable of catalysing this reaction.[20] Some promising steps forward have already been presented, mainly in the form of molecular heterogeneous catalysts; for example, a Ru-based catalyst by Zhang *et al*.[21] and most interestingly, a CTF-supported Ir-based system by Park *et al*. of great similarity to the one employed by us in the dehydrogenation of formic acid.[22] Although this clearly shows that CTF-based catalysts hold great promise as solid molecular catalysts, laboratory practice still relies on using the catalyst in a slurry operation as a powder. Notably, the use of powder invokes a number of problems in prospective applications, most particularly the partial loss upon sampling or recovery in catalyst recycling, yet the all-important aspect and potential of

CTFs in catalyst formulation, shaping, or embedding in applied reactor conditions has remained unexplored.

In an attempt to bring the use of CTF-based molecular catalysts one step closer to industrial reality, we herein report a one-step method for the production of porous, mechanically rigid, and easy-to-handle CTF-based spheres prepared by a phase inversion method using the polyimide Matrimid® as a binder. After obtaining the spheres, $Ir^{III}Cp^*$ was coordinated to the bipyridine moieties of CTF to obtain efficient catalytic functionality. This sphere-based catalyst was shown to be a highly and easily recyclable catalyst in the hydrogenation of CO_2.

4.2. EXPERIMENTAL

Materials

$[IrCp^*Cl_2]_2$ was purchased from Strem Chemicals. All other chemicals were obtained from Sigma Aldrich and used without further purification.

Meso-CTF synthesis

The following procedure was carried out for the preparation of the polymer: a quartz ampoule was loaded with 2,6-pyridinedicarbonitrile (0.41 g, 3.2 mmol), 4,4'-biphenyldicarbonitrile (1.31 g, 6.40 mmol), and anhydrous $ZnCl_2$ (6.64 g, 0.048 mol), in a glovebox. The ampoule was flame sealed and subjected to the following temperature programme: temperature is brought to 500 ˚C with a heating rate of 60 ˚C h^{-1}, kept at this temperature for 48 h, then cooled to room temperature at a rate of 10 ˚C h^{-1}. The product was crushed in a mortar, then subsequently heated at reflux in 5M HCl (150 mL) at 100 ˚C, 6M NH_4OH at 60 ˚C, H_2O (150 mL) at 100 ˚C, and THF (150 mL) at 60 ˚C. Every washing step was performed overnight. Activation of the material was performed by drying it under vacuum at 200 ˚C for 24 h. After all required filtrations, a fully amorphous powder was obtained with a final yield of at least 90% on a molar basis. The washing steps might seem excessive and are more severe than those described in the literature, but were required, as we found, to remove $ZnCl_2$.

Sphere production

A Matrimid 5218 solution was prepared by dissolving the polymer (0.4 g) in a mixture of THF (3.6 mL) and N-methylpyrrolidone (1.8 mL). Subsequently, 0.6 g meso-CTF was added aiming at a loading of 60 wt%, and the mixture was stirred at room temperature for 1 h. Afterwards, the slurry mixture was pumped into a vessel filled with water by using a syringe pump (inner diameter of a syringe tip is around 1 mm) at a flow rate of 0.2 mL min^{-1}. The solid spheres precipitated immediately. They were kept in water overnight and subsequently activated by heating in an vacuum oven at 350 ˚C (heating rate of 1 ˚C min^{-1}) under a nitrogen flow (100 mL min^{-1}) for 8 h.

Sphere stability test

To check the stability of the spheres in different solvents, the spheres were placed in a flask filled with a solvent under vigorous stirring (1000 rpm) at temperatures between 60 and 100 ˚C. The spheres were called stable if they did not undergo any decomposition and preserved their structure.

Ir@meso-CTF catalyst synthesis

A mixture of meso-CTF polymer (480 mg) and $[Cp^*Ir(Cl)_2]_2$ (40 mg) was placed in a Schlenk flask in a glovebox. Outside of the glovebox, degassed water (40 mL) was added with a syringe to the flask under a continuous Ar flow. The mixture was stirred overnight and filtered. The powder was further washed with a mixture of triflic acid (HOTf) (300 mg) and a 1:1 (volume) DMF/water mixture (50 mL) to remove the chloride ions. Finally, the powder was stirred in water at 50 ˚C for another 12 h, before being filtered and dried under vacuum at 50 ˚C.

Ir@CTF spheres catalyst synthesis

Sphere-shaped iridium catalyst Ir@CTF spheres were prepared by following the same iridium loading procedure as for Ir@meso-CTF, but with altered amounts: for the coordination of 480 mg of the CTF spheres, 145 mg of $[Cp^*Ir(Cl)_2]_2$ was used to achieve 2 wt% loading. The amounts of 14.5/7/3 mg were used for the coordination of 1/0.5/0.2 wt% respectively.

Carbon dioxide hydrogenation

Hydrogenation experiments were performed in a Parr 5000 Multi Reactor Stirrer System under pressure by using an equimolar mixture of gases H_2/CO_2 (batch conditions). The reaction vessels (autoclaves) had a volume of 45 mL and were stirred with suspended magnetic bars. Autoclaves were filled with 30 mL of water as solvent, $KHCO_3$, and Ir@CTF catalyst (40 mg). The gas mixture was then introduced in the autoclaves until 20 bar pressure was reached. The autoclaves were heated to the desired temperature with a heating rate of 2 ˚C min^{-1} and kept at this temperature for 2 h. Subsequently, the autoclaves were immediately depressurized, the gas mixture was replaced by flushing the system with He, and the vessels were cooled down to ambient temperature. Liquid samples were taken and analyzed by UPLC. The UPLC analysis was carried with a Shodex KC-811 column and a Rspak KC-G guard column with 0.1% H_3PO_4 in water as a mobile phase with a rate of 0.70 mL min^{-1} at 50 ˚C. The formic acid product was detected with a UV detector at a wavelength of 210 nm.

The recycling procedure was identical for both Ir@meso-CTF and Ir@CTF spheres. Spent catalyst was filtered from the reaction mixture, suspended in water at 50 ˚C overnight, and activated at 50 ˚C under vacuum for 12 h.

Carbon dioxide dehydrogenation

Formic acid reactant stock solutions were prepared by dilution of 13.00 mL of 88% formic acid with H_2O to 100 mL to yield solutions with a concentration of 3M. The pH is adjusted to 1.5 by addition of HBF_4 (aq) or NaOH (aq). Test reactions were carried out in a 100 mL round bottom flask equipped with septum caps. 200 mg Ir@spheres-CTF catalyst is dispersed in 30 mL of 3M aqueous formic acid solution. The reaction mixture is submerged in an oil bath and heated to desired temperature with continuous stirring. The reaction path was followed by 1H NMR experiments, and the collected gas phase was analysed by GC.

Characterization

Nitrogen adsorption measurements were performed by using a Tristar II3020 Micromeritics instrument employing N_2 gas (99.999 %). Argon adsorption was performed with a Micromeritics ASAP 2010 gas-adsorption analyzer (stainless-steel version) at -185.15 ˚C. For the DFT calculations, a Slit Pores N_2@77 on Carbon NLDFT model with a regularization factor

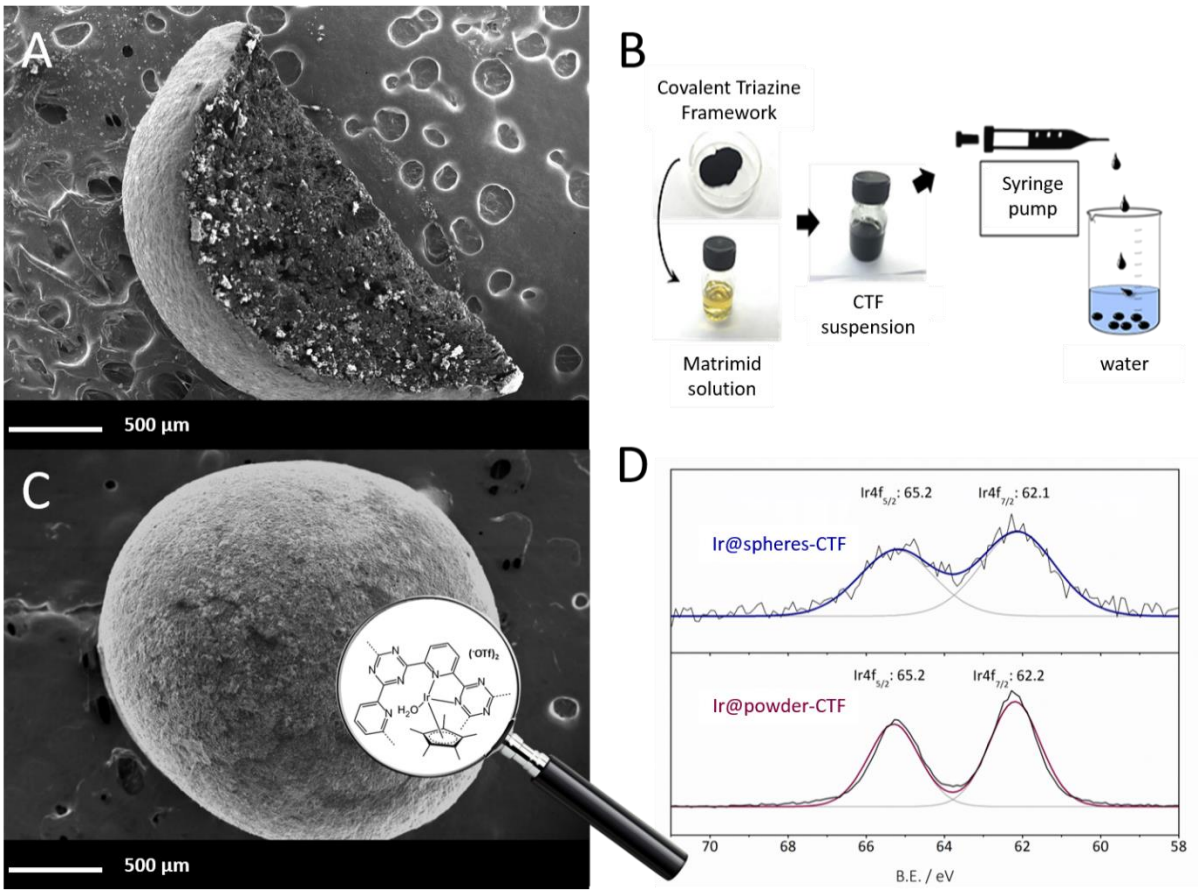

Figure 4.1. A) SEM of cut CTF sphere. B) Scheme of CTF sphere formation. C) SEM of CTF-based sphere with the molecular structure of the catalyst. D) XPS analysis of iridium in the powder and shaped Ir@CTF catalysts.

of 0.003160 was used. XPS measurements were performed by using a K-alpha Thermo Fisher Scientific spectrometer using a monochromatic Al$K\alpha$ X-ray source. The measurements were performed using a line scan of three points, each of which had a spot size of 300 mm at ambient temperature and chamber pressure of ~10^{-7} mbar. A flood gun is used for charge compensation. All the spectra measured were corrected by setting the reference binding energy of carbon (*1s*) at (285±0.025) eV. The electron energy analyser was operated with a pass energy of 50 eV, and each high-resolution spectrum was scanned 10 times. The spectra were analysed and processed using Thermo Avantage v5.52 software (Thermo Fisher Scientific). The peaks were fitted using a Lorentzian–Gaussian (L/G) ratio of 0.3. For elemental analysis, the samples were analyzed by Mikroanalytisches Laboratorium KOLBE, (Mulheim an der Ruhr, Germany). SEM images were recorded by using a JEOL JSM-6010 LA with a standard beam potential of 10 kV and an Everhart-Thornley detector. X-ray microanalysis (SEM/EDX)

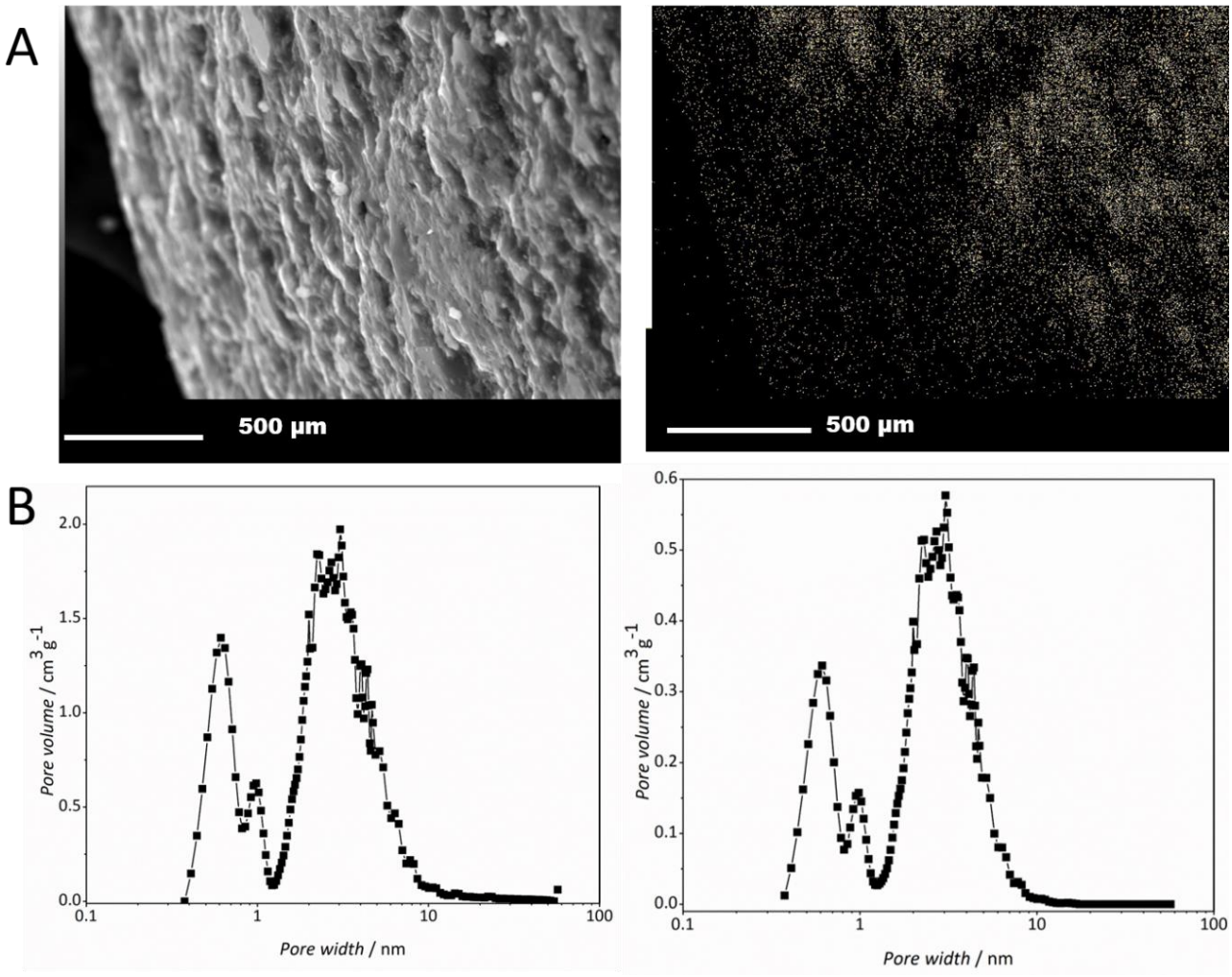

Figure 4.2. A) EDX analysis of Ir@spheres-CTF B) Pore size distribution of meso-CTF (*left*) and spheres- CTF (*right*)

confirmed the elemental composition in the sample by the scanning electron microscopy (SEM) coupled with a dispersive X-ray microanalysis system (EDX) with a silicon-drift detector.

4.3. RESULTS AND DISCUSSION

To shape the CTF-based catalysts whilst maintaining porosity, we used Matrimid 5218 as a binder, as it is highly stable, compatible with the CTF, inexpensive, and (in contrast to the CTF) highly soluble in most common organic solvents.[23,24] Additional experiments were performed by using polylactic acid as binder, but the resulting pellets collapsed upon mild temperature treatments (up to 160 ˚C). Homemade mesoporous copolymer meso-CTF was embedded within the Matrimid matrix to render shaped, hard-body spheres of CTF, of which the outer skin is denser than that of the inner part. The molecular catalyst, shown within the magnifier in Figure 4.1, was successfully obtained on spherical CTF by using the protocol

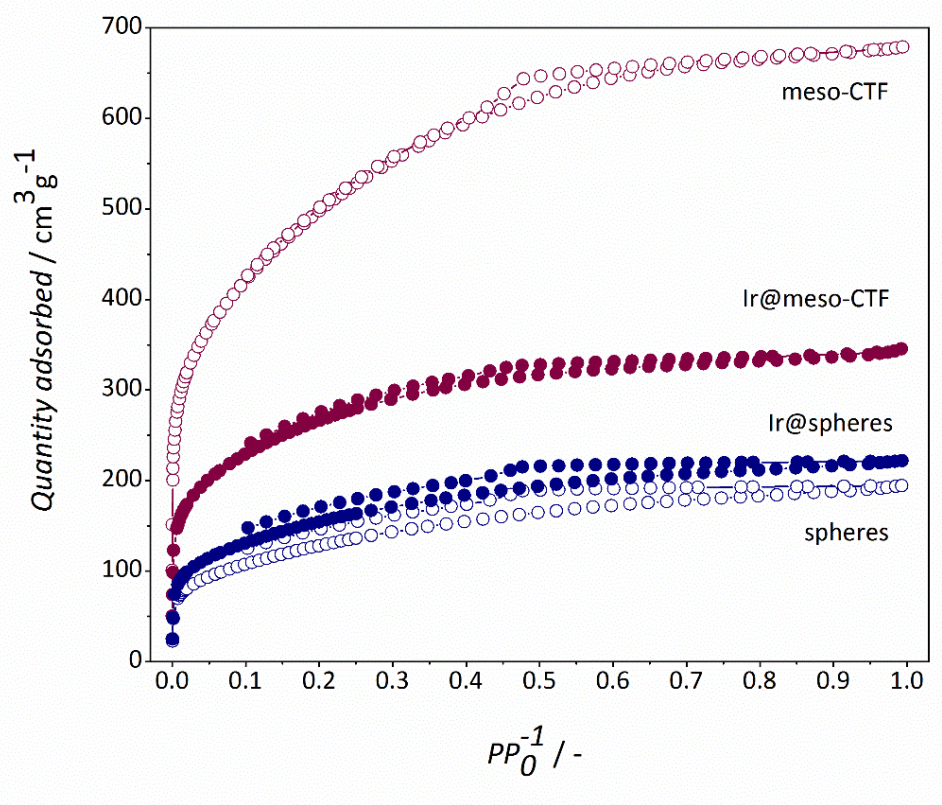

Figure 4.3. Nitrogen adsorption isotherms @ 77 K of meso-CTF (*open red*) (S_{BET}=1800 m^2g^{-1}), CTF-based spheres (*open blue*) (S_{BET}=465 m^2g^{-1}), Ir@meso-CTF catalysts with 2.4 wt% Ir (*solid red*) (S_{BET}=970 m^2g^{-1}), Ir@CTF spheres catalyst with 2 wt% Ir (*solid blue*) (S_{BET}=560 m^2g^{-1}).

reported earlier by our group.[10] Notably, SEM/EDX analysis of the Ir@CTF spheres composite shows that most of the iridium is located in the outer shell of the spheres, therefore providing good accessibility (Figure 4.2A).

Iridium's oxidation state of +3 was confirmed by X-ray photoelectron spectroscopy (XPS) analysis (Figure 4.1D). When iridium was coordinated to the meso-CTF powder prior to the shaping step, no porosity in the final composite material was preserved.

Tests for determining the chemical stability of the obtained spheres towards organic solvents were performed by leaving them overnight in acetonitrile or hexane at 60 ˚C under vigorous stirring (1000 rpm). Stability tests at different temperatures in water (up to 100 ˚C) showed that the composite material is highly stable in aqueous media.

The CTF powder within the spheres (which consisted of 60% CTF) preserves its mesoporosity and displays a Brunauer–Emmett–Teller (BET) area of 465 m^2g^{-1} (Table 4.1),

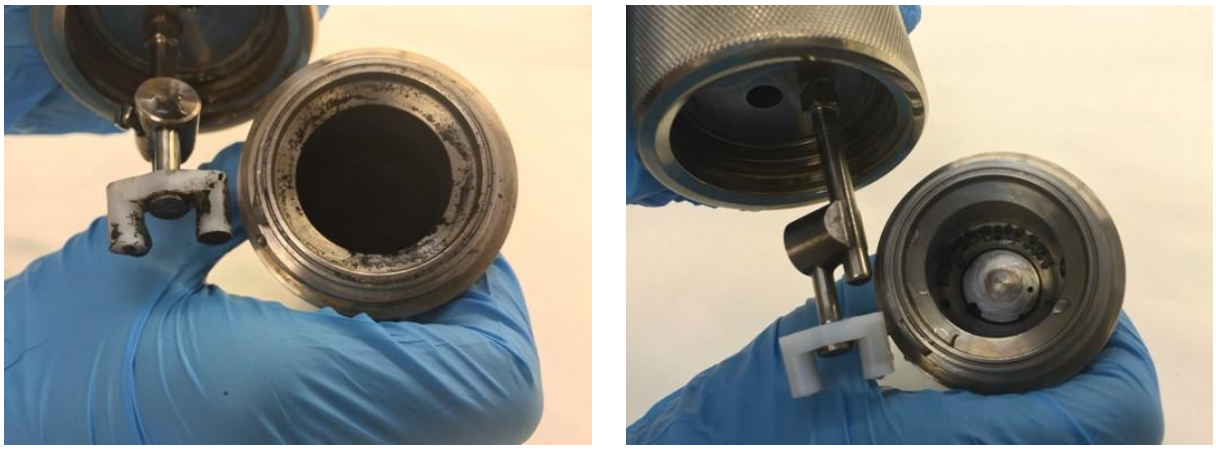

Figure 4.4. The autoclave open after the hydrogenation is complete using Ir@meso-CTF *(left)* and Ir@spheres-CTF *(right)* catalysts

meaning that roughly 43% of the original surface area of the CTF was preserved. It is important to note that the polymer binder does not contribute to this BET area.

Figure 4.2B shows a similar pore size distribution for both the shaped and unshaped catalysts along with a reduction in the total porosity upon shaping. These results indicate that part of the CTF porosity is used to host polymer chains: partial penetration of the CTF porosity by the polymer occurs, leading to totally blocked pores and polymer-free ones. In the latter, no pore size modification is observed.

The coordination of 2 wt% Ir on the powder-based CTF results in a decrease in the accessible surface area of the material (Figure 4.3). In contrast, the nitrogen uptake for Ir@CTF spheres is slightly higher than that for the original spheres. This could be rationalized by the fact that DMF was used during iridium coordination, resulting in the partial leaching of some binder without affecting the integrity of the spheres. Indeed, spheres that were treated overnight in acetonitrile, a highly polar nonprotic solvent like DMF, were seen to partially leach out binder, whilst the spheres after treatment in apolar hexane remained entirely intact. In addition to 2 wt% Ir@CTF, catalysts containing a lower amount of active phase were prepared. It must hereby be noted that “wt%” refers to the amount of Ir with respect to the entire sphere. This amounts to only 43% of the porosity available for the coordination of Ir. Using this definition, the samples are henceforth referred to as 1, 0.5, and 0.2 wt% and correspond to an Ir loading per accessible CTF of 2.3, 1.2, and 0.46 wt%, respectively (Table 4.2).

Table 4.1 Surface area of meso-CTF in forms of powder and spheres

Material	S_{BET}	S_{BET} after Ir coordination [m^2g^{-1}] [a]
meso-CTF	1800	970
Spheres-CTF	465	560

[a] Coordination of 2.4 wt% Ir to spheres-CTF and 2 wt% Ir to meso_CTF

Table 4.2 Loading of Ir for Ir@spheres-CTF catalysts

Entry	Total loading [wt%}	Effective loading [wt%] [a]
1	2	4.6
2	1	2.3
3	0.5	1.2
4	0.2	0.46

[a] Loading corresponding per accessible CTF amount, equal to total loading / 0.43

Tables 4.3 and 4.4 display the performance of the Ir@meso-CTF and Ir@CTF spheres catalysts in basic aqueous media. In contrast to the triphenylphosphine-based catalysts and most homogeneous catalysts in the literature, the herein reported Ir@meso-CTF does not require handling under an oxygen-free atmosphere during operation. Experiments with potassium bicarbonate as base showed a better performance than those with potassium hydroxide, suggesting that the hydrogenation mechanism proceeds via bicarbonates.[23]

All carbon dioxide hydrogenation experiments were performed in duplicate. Although both the shaped and the powder catalysts could be recycled, experiments with the powder catalyst resulted in a 25% deviation, as the sample tends to stick to the reactor walls (at all stirring rates).

In contrast, when Ir@CTF spheres are used, differences of less than 5% are found within the duplicate experimental range. In comparing the performance of the shaped and powder solids on an equal Ir wt% basis, an overall loss in catalytic activity of approximately 80% is observed in the case of the spheres (see Table 4.1 entries 10.1 and 10.2 vs. Table 4.2 entries 2.1–2.4). However, taking into consideration the amount of accessible CTF within the spheres, the activity loss for the samples with an effectively comparable Ir loading (Table 4.3 entries 10.1. and 10.2 vs. Table 4.4 entry 3) is approximately 40% of that of the CTF powder.

Table 4.3. Carbon Dioxide hydrogenation with Ir@meso-CTF catalyst. Iridium content is 2.4 wt%. [a]

Entry	Base	T [˚C]	*TON* [b,c]
1	None	90	-
2	KOH	50	29
3	KOH	70	66
4	KOH	90	83
5	$KHCO_3$ 1M	50	167
6	$KHCO_3$ 1M	70	194
7	$KHCO_3$ 1M	90	358
8	$KHCO_3$ 0.5M	50	155
9	$KHCO_3$ 0.5M	70	173
10.1	$KHCO_3$ 0.5M	90	302 (1st run)
10.2			330 (2nd run)

[a] Reactions were carried out at 20 bar with an equimolar H_2/CO_2 mixture and 50 mg catalyst. [b] *TON* obtained from UPLC analysis after 2h of reaction. [c] Presented as the average of two experiments with a reproducibility of ±25%.

Table 4.4. Carbon Dioxide hydrogenation with Ir@spheres-CTF catalyst.[a]

Entry	Ir loading [wt%]	T [˚C]	*TON* [b,c]
1	2	50	15
2.1[d]	2	90	54
2.2[d]	2	90	62
2.3[d]	2	90	57
2.4[d]	2	90	57
3	1	90	120
4	0.5	90	175
5	0.2	90	219

[a] Reactions were carried out at 20 bar with an equimolar H_2/CO_2 mixture using 0.5M $KHCO_3$ as a base and 50 mg catalyst. [b] *TON* obtained from UPLC analysis after 2h of reaction. [c]Presented as the average of two experiments with a reproducibility of ±5%. [d] Four consecutive catalytic runs with the recycled catalyst.

To explore whether this decrease in activity also occurs in the reverse reaction, namely the dehydrogenation of formic acid, we performed additional experiments using the shaped Ir@CTF spheres with 2 wt% Ir loading (corresponding to 4.6 wt% Ir of accessible CTF) in a 3M aqueous solution of formic acid at 80 ˚C. *TOFs* of 800 h^{-1} were obtained. Although this value is still far from the outstanding performance of the powder version (21300 h^{-1}, 2 wt% Ir),[10] it shows that the catalyst still outperforms systems based on nanoparticles[24–28] and has a similar activity to the Ru immobilized complex reported by Laurenczy.[29] The catalytic performance of Ir@CTF spheres in both the direct and reverse reactions demonstrate that active, stable, and readily shaped catalysts for reversible hydrogen storage can be manufactured by using the method here reported. Moreover, utilization of shaped particles carries the advantage of facile catalyst recycling and improved reproducibility.

4.4. CONCLUSIONS

Covalent Triazine Frameworks can be shaped into a spherical form without losing their properties. CTF spheres show high thermal stability, porosity, and the possibility of coordinating metal clusters. In contrast to the powder, the spheres-based catalyst is more easily handled, and fully recyclable without loss of material through at least four consecutive runs. A highly efficient organometallic complex such as IrCp* was immobilized through coordination within the CTF spheres to render a molecular yet heterogeneous, stable catalyst which is easy to handle and recycle in the carbon dioxide hydrogenation to formic acid. The development of methods for the facile shaping of new catalytic materials is of high interest to further demonstrate catalyst stability and recyclability, two key features for perspective applications.[30] We believe that the results reported here further highlight the promise that CTF-based materials hold for practical applications.

4.5. REFERENCES

[1] R. Palkovits, M. Antonietti, P. Kuhn, A. Thomas, F. Schüth, *Angew. Chemie Int. Ed.* **2009**, *48*, 6909–6912.

[2] Y. Zhao, K. X. Yao, B. Teng, T. Zhang, Y. Han, *Energy Environ. Sci.* **2013**, *6*, 3684–3692.

[3] F. Niu, L. Tao, Y. Deng, H. Gao, J. Liu, W. Song, *New J. Chem.* **2014**, *38*, 5695–5699.

[4] C. E. Chan-Thaw, A. Villa, L. Prati, A. Thomas, *Chem. – A Eur. J.* **2011**, *17*, 1052–1057.

[5] J. Bi, W. Fang, L. Li, J. Wang, S. Liang, Y. He, M. Liu, L. Wu, *Macromol. Rapid Commun.* **2015**, *36*, 1799–1805.

[6] J. Artz, S. Mallmann, R. Palkovits, *ChemSusChem* **2015**, *8*, 672–679.

[7] J. Roeser, K. Kailasam, A. Thomas, *ChemSusChem* **2012**, *5*, 1793–1799.

[8] P. Katekomol, J. Roeser, M. Bojdys, J. Weber, A. Thomas, *Chem. Mater.* **2013**, *25*, 1542–1548.

[9] P. Kuhn, M. Antonietti, A. Thomas, *Angew. Chemie Int. Ed.* **2008**, *47*, 3450–3453.

[10] A. V Bavykina, M. G. Goesten, F. Kapteijn, M. Makkee, J. Gascon, *ChemSusChem* **2015**, *8*, 809–812.

[11] Z. Xu, N. D. McNamara, G. T. Neumann, W. F. Schneider, J. C. Hicks, *ChemCatChem* **2013**, *5*, 1769–1771.

[12] C. Liu, J.-H. Xie, G.-L. Tian, W. Li, Q.-L. Zhou, *Chem. Sci.* **2015**, *6*, 2928–2931.

[13] J. F. Hull, Y. Himeda, W.-H. Wang, B. Hashiguchi, R. Periana, D. J. Szalda, J. T. Muckerman, E. Fujita, *Nat Chem* **2012**, *4*, 383–388.

[14] F. Zou, J. M. Cole, T. G. J. Jones, L. Jiang, *Appl. Organomet. Chem.* **2012**, *26*, 546–549.

[15] F. Gassner, W. Leitner, *J. Chem. Soc. Chem. Commun.* **1993**, 1465–1466.

[16] S. Moret, P. J. Dyson, G. Laurenczy, *Nat Commun* **2014**, *5*.

[17] C. Hao, S. Wang, M. Li, L. Kang, X. Ma, *Catal. Today* **2011**, *160*, 184–190.

[18] G. A. Filonenko, R. van Putten, E. N. Schulpen, E. J. M. Hensen, E. A. Pidko, *ChemCatChem* **2014**, *6*, 1526–1530.

[19] A. Boddien, F. Gärtner, C. Federsel, P. Sponholz, D. Mellmann, R. Jackstell, H. Junge, M. Beller, *Angew. Chemie Int. Ed.* **2011**, *50*, 6411–6414.

[20] A. Baiker, *Appl. Organomet. Chem.* **2000**, *14*, 751–762.

[21] Y. Zhang, J. Fei, Y. Yu, X. Zheng, *Catal. Commun.* **2004**, *5*, 643–646.

[22] K. Park, G. H. Gunasekar, N. Prakash, K.-D. Jung, S. Yoon, *ChemSusChem* **2015**, *8*, 3410–3413.

[23] J. Elek, L. Nádasdi, G. Papp, G. Laurenczy, F. Joó, *Appl. Catal. A Gen.* **2003**, *255*, 59–67.

[24] Y. Qin, Y. Liu, F. Liang, L. Wang, *ChemSusChem* **2015**, *8*, 260–263.

[25] Z.-L. Wang, J.-M. Yan, Y. Ping, H.-L. Wang, W.-T. Zheng, Q. Jiang, *Angew. Chemie Int. Ed.* **2013**, *52*, 4406–4409.

[26] J. H. Lee, J. Ryu, J. Y. Kim, S.-W. Nam, J. H. Han, T.-H. Lim, S. Gautam, K. H. Chae, C. W. Yoon, *J. Mater. Chem. A* **2014**, *2*, 9490–9495.

[27] Y.-Y. Cai, X.-H. Li, Y.-N. Zhang, X. Wei, K.-X. Wang, J.-S. Chen, *Angew. Chemie Int. Ed.* **2013**, *52*, 11822–11825.

[28] S. Zhang, Ö. Metin, D. Su, S. Sun, *Angew. Chemie Int. Ed.* **2013**, *52*, 3681–3684.

[29] W. Gan, P. J. Dyson, G. Laurenczy, *ChemCatChem* **2013**, *5*, 3124–3130.

[30] F. Akhtar, L. Andersson, S. Ogunwumi, N. Hedin, L. Bergström, *J. Eur. Ceram. Soc.* **2014**, *34*, 1643–1666.

CHAPTER FIVE

Monolith Supported Single Site Covalent Traiazine Framework Based Catalyst for Hydrogen Production from Formic Acid

Covalent Triazine Frameworks are a class of porous polymers made upon trimerisation of aromatic nitriles. Their application as catalyst support holds great promise owing to the *quasi*-bipyridine moieties within the framework. For practical application, a procedure for CTF coating on a cordierite monolith is given to improve catalyst utilisation to obtain a well-defined film on the surface of cordierite monoliths. Using a two-step *quasi*-Chemical Vapour Deposition, where the precursors for trimerisation are impregnated in the macropore space of the cordierite prior to synthesis *in vacuo* at high temperature, CTF films can be obtained. The CTF@monolith was prone to coordination with IrCp* complex, resulting in a stable and recyclable catalyst for hydrogen production from formic acid. Performance comparison of Ir@CTF@monolith and Ir@CTF@powder demonstrates the better mass-transport properties of the monolith supported catalyst.

This Chapter is based on the following publication:

A.V. Bavykina, A. Olivos Suarez, D. Osadchii, R. Valecha, M. Makkee, F. Kapteijn, J. Gascon, *in preparation*

5.1. INTRODUCTION

Covalent Triazine Frameworks (CTFs) are a class of porous polymers that are made upon trimerisation of aromatic nitriles.[1-2] Presently, CTFs are proposed for a wide range of applications. For instance, due to their high nitrogen content, their application in CO_2 capture and separation has been studied by several groups;[3-5] while their fully conjugated nature has been exploited in electro-[6-8] and photocatalysis.[9-10] Over and above, CTFs have been shown to bear excellent properties as supports for single site organometallic catalysts. This application holds a large promise owing to the free *quasi*-bipyridine moieties present within the framework, allowing coordination of a large array of organometallic complexes, as demonstrated over the last few years by several research groups.[11-15]

The high stability of CTFs is, to a large extent, related to the harsh conditions in which these materials are synthesised (excess of $ZnCl_2$ as a trimerisation catalyst, 500˚C synthesis temperature). Such extreme synthesis conditions usually lead to ill-defined CTF structure that consist of large agglomerates up to tens of microns (Figure 5.1). This structure is not ideal for application in catalysis in a stirred tank reactor: on the one hand, loss of material due to attrition of the agglomerates makes catalyst recycling cumbersome and on the other hand, large particles, even when resulting from the agglomeration of smaller units, may result in serious diffusion limitations and, therefore, poor catalyst utilisation. Moreover, the complex hydrodynamics of slurries in stirred tank reactors makes scale-up difficult, which can lead to problems like incomplete suspension of particles and non-uniform distribution of catalyst. In our recent work, we addressed the first issue by formulating CTF/polymer spherical composites. The obtained spheres showed high stability and recyclability during several catalytic runs.[12] However, CTF's porosity could not be completely preserved upon the sphere formulation. Moreover, the use of polymers as binders limits the scope of application of the resulting composites to reaction media in which the polymeric component would not dissolve.

In the present work, we demonstrate that both these issues can be addressed by CTF structuring using monoliths as supports. Due to the unusual synthesis conditions, we have developed a new manufacture protocol for the polymerisation of CTFs directly on the surface of cordierite monolith. This method, which can be described as a *quasi* Chemical Vapour Deposition, is a straightforward approach that results in very homogeneous and thin CTF

coatings. The resulting coatings are stable, easy to handle, and can be used in the same way as the parent material to coordinate metal complexes. Comparison between monolith and CTF powder performance upon incorporation of an IrCP* catalyst demonstrates the enhanced catalytic performance of the monolithic supported catalyst, attributed to the better mass transport properties of the thin layers coated on the monolith channels.

5.2. EXPERIMENTAL

Materials

$[IrCp^*Cl_2]_2$ was purchased from Strem Chemicals. All other chemicals were obtained from Sigma Aldrich and used without further purification.

Characterisation

XPS measurements were performed by using a K-alpha Thermo Fisher Scientific spectrometer using a monochromatic Al$K\alpha$ X-ray source. The measurements were performed using a line scan of three points, each of which had a spot size of 300 mm at ambient temperature and chamber pressure of ≈ 10^{-7} mbar. A flood gun is used for charge compensation. All the spectra measured were corrected by setting the reference binding energy of carbon (*1s*) at (285±0.025) eV. The electron energy analyser was operated with a pass energy of 50 eV and each high-resolution spectrum was scanned 10 times. The spectra were analysed and processed using Thermo Avantage v5.52 software (Thermo Fisher Scientific). The peaks were fitted using a Lorentzian–Gaussian (L/G) ratio of 0.3. Nitrogen (99.999 %) adsorption measurements were done at -196 ˚C using a Tristar II 3020 from Micromeritics. Samples degassing was done at 150 ˚C.

Scanning electron microscopy (SEM) images were recorded using a JEOL JSM-6010LA with a standard beam potential of 10 kV and an Everhart-Thornley detector. X-ray microanalysis (SEM/EDX) confirmed the elemental composition of the samples by the scanning electron microscopy (SEM) coupled with a dispersive X-ray microanalysis system (EDX) with a Silicon-drift detector.

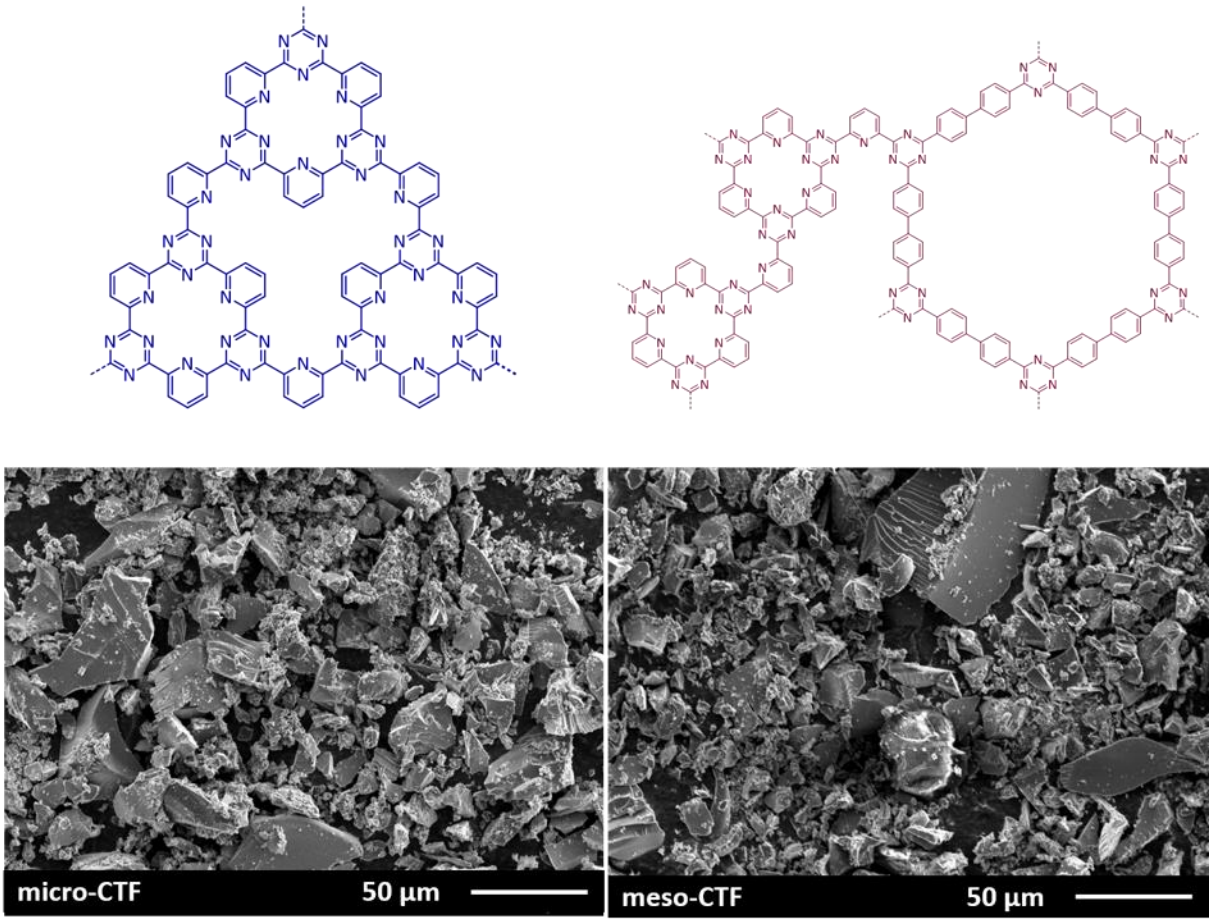

Figure 5.1. ***top:*** **Structures of micro-CTF (*left*) and meso-CTF (*right*); *bottom*: SEM micrograph of CTF powders (after crushing and given washing procedure).**

Thermogravimetric analysis (TGA) was performed on a Mettler Toledo TGA/SDTA851e equipment, where 11-20 mg of samples was screened for the change in mass while heated from 30 ˚C to 1000 ˚C with a heating rate of 2 ˚C min^{-1} under air flow.

Synthesis of micro-CTF

The synthesis was performed as described elsewhere[16] and Chapter 6 of this thesis. In short: a glass ampoule was charged with 2,6-pyridinedicarbonitrile (0.124 g, 0.96 mmol) and anhydrous $ZnCl_2$ (0.664 g, 4.8 mmol) in a glovebox. The ampoule was flame sealed and the mixture was heated at 500°C for 48 h and then cooled to room temperature. The product was crushed in a mortar and washed in the same methodology as the coated monolith (*vide infra*).

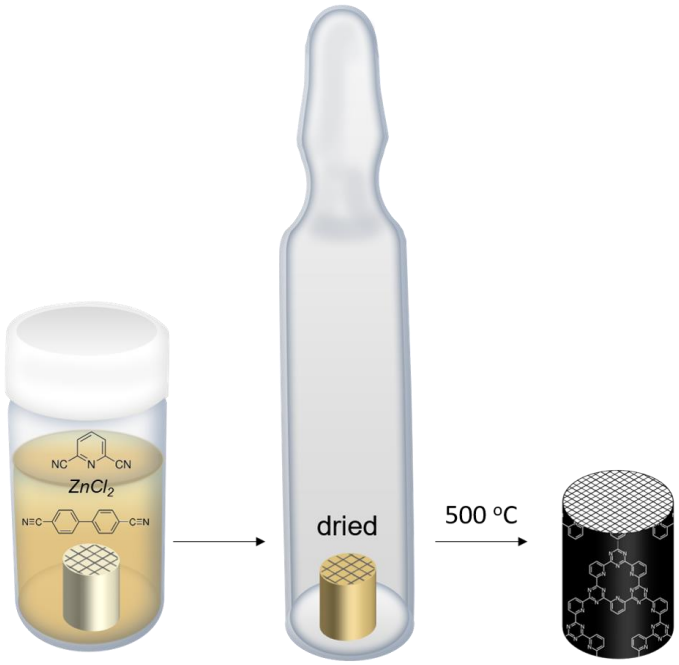

Figure 5.2. Representation of the coating protocol.

Synthesis of meso-CTF

The synthesis was performed as described elsewhere[11-12, 16] and Chapters 3, 4, and 6 of this thesis. The synthesis procedure is identical to the one of micro-CTF with a different ampoule loading: In short: 2,6-pyridinedicarbonitrile (0.041 g, 320 µmol), 4,4'-biphenyldicarbonitrile (0.131 g, 640 µmol), and anhydrous $ZnCl_2$ (0.664 g, 4.8 mmol).

Coating of monolith with Covalent Triazine Framework

The monolith pieces were cut down to a suitable size (around 1 cm long and 0.5 and 0.5 cm height and width, respectively). In order to prepare micro-CTF coated monolith, the monolith cut was dipped in a solution of 0.6 g 2,6-bipyridinedicarbonitrile and 1.7 g anhydrous zinc chloride in 5 mL acetone. For the preparation of the meso-CTF coated monolith, a cordierite monolith piece was dipped in a solution of 0.6 g 2,6-bipyridinedicarbonitrile, 1.9 g 4,4-biphenyldicarbonitrile and 1.7 g anhydrous zinc chloride in 5 ml acetone. In both cases the monolith was stirred overnight in the solution at room temperature. Following this step, the acetone wet (impregnated) support was dried at 60 ˚C overnight. Next, the monolith was placed in a glass ampoule under vacuum and this was flame sealed and subjected into an oven to the following temperature program: heating rate 60°C h^{-1} - 500°C for 10 h – cooling rate 10°C h^{-1}. The coated monolith was then washed with 50% HCl overnight at 100°C. Following

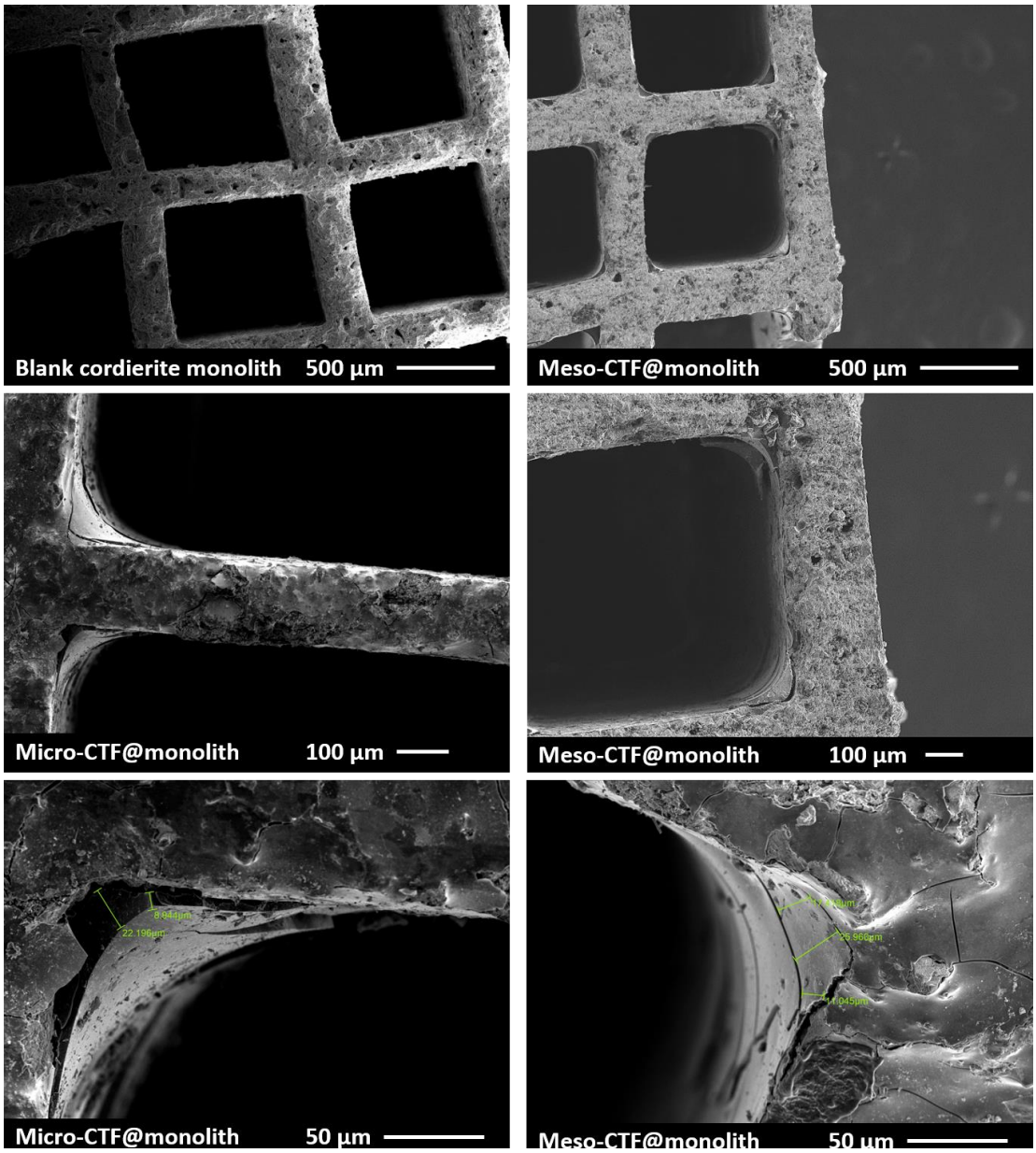

Figure 5.3. SEM micrographs of CTF@monolith

this, it was subsequently washed with 50% NH_4OH at 50°C overnight, with water overnight at 100°C, and finally with tetrahydrofuran (THF) at 50°C overnight. The washed monolith was vacuum dried at 180 ˚C. This washing procedure was optimised in a previous work to remove as much Zn from the material as possible.[16]

Coordination of iridium complex

Firstly, a solution of 0.0083 g $[IrCp^*Cl_2]_2$ in 60 mL H_2O was prepared. Next, the CTF-coated monolith was stirred overnight in this solution at room temperature. Following this, the Ir exchanged monolith was washed in a mixture of 30 mL water, 30 mL DMF and 0.283 g

trifluoromethanesulfonic acid (HOTf) at a temperature of 50 ˚C overnight in order to remove the Cl^- ions, and exchange the Cl^- ions by the weakly coordinated OTf^-. Subsequently, the monolith was washed with 50 ml water at 50 ˚C overnight. Finally, the Ir coated monolith was vacuum dried at 60 ˚C overnight.[11] Coordination of Ir to the powder was performed as described in Chapters 3 and 4 with an altered Ir loading (1 mg $[IrCl_2Cp^*]_2$ and 100 mg micro- or meso-CTF powder).

Catalyst testing

The Ir@CTF@monolith catalysts with 0.045 mg of Ir (0.23 mmol) were tested in a monolith stirrer reactor configuration.[17-19] To this end, the structured support was attached to a mechanical stirrer and placed in a 50 mL aqueous solution of 3 M formic acid (0.15 mol). The vessel containing the reaction mixture was submerged in an oil bath and heated to the desired temperature of 80°C under continuous stirring. The reaction was carried out for 24 h. For recycling the catalyst, the coated monolith was washed with water at 50 ˚C and dried in vacuum at 60˚C overnight. For the analysis of unreacted formic acid, ^1H NMR spectra were recorded in a Bruker Avance-400 NMR spectrometer, using 5 mm sample tubes, with 128 scans per sample. An inert internal standard, dimethyl sulfone, was used. The samples were taken after 10 min, 40 min, 90 min, 5h, 18 h, and 24 h after the beginning of the reaction (the catalyst was introduced to the reaction mixture when 80 ˚C were reached).

The Ir@CTF powder with 0.065 mg of Ir (0.34 mmol) was tested as described elsewhere (Chapters 3 and 4).[11-12]

The presented turnover frequency (*TOF*) after 10 minutes of reaction were calculated according to the following equation:

$$TOF = \frac{n_{formic\ acid\ converted}(\text{mol})}{n_{Ir}(\text{mol}) * time\,(\text{h})}$$

5.3. RESULTS AND DISCUSSION

In previous work, when comparing the catalytic performance of our spherical particulate Ir@CTF catalyst for the dehydrogenation of formic acid, we observed a lower catalytic activity per Ir site (*TOF*) than for the homogeneous catalyst counterpart (Chapter 4). Similar observations have been made for other CTF supported catalysts[13] and are usually attributed to diffusion limitations derived from heterogenization. It is indeed easy to envisage that active site accessibility will be better for a dissolved homogeneous catalyst than for a porous solid. In order to unravel differences in catalytic performance and to further improve Ir utilisation, in this study catalyst accessibility and mass transport have been modified at two different length scales: on the one hand CTFs with different pore architectures were synthesised: the one denoted as micro-CTF contains only micro-pores, while meso-CTF contains both micro- and meso-pores in a range from 1.5 to 10 nm (Chapter 4).[12] These materials differ in porosity and nitrogen content, while their chemical and thermal stability are the same. On the other hand, the performance of thin CTF coatings supported on a highly open substrate (a monolith) is compared with that of the bulk material (powder).

Monolithic structures are widely used in off-gas treatment, *e.g.* automotive exhaust gas purification[20] and de-NOx-ing of power plant stack gases[21]. Monoliths are also considered as attractive catalyst support alternatives compared to conventional carriers in other heterogeneous catalysis applications, including liquid-phase catalysis.[18, 22-23] Monoliths feature a high void fraction and large geometric surface area, which results in a large contact area between the catalyst and reactants and low-pressure drop under flow conditions.[22] Cordierite ($2MgO{\cdot}2Al_2O_3{\cdot}5SiO_2$) belongs to the group of alumino-silicates with a macro-porous wall structure.[24]

This macro-porous space may create an obstacle for applying a thin uniform layer of the catalyst, since diffusion can lead to a deposition of ineffective active phase within the macro-pores[25]. In this work, this property was partially turned to our advantage, the cordierite porosity was found to be crucial. Although the wall of the monoliths shows clearly a thin layer, the corner of the channel demonstrates higher deposition levels due to capillary forces in the drying after the acetone impregnation/exchange procedure into the monolith.

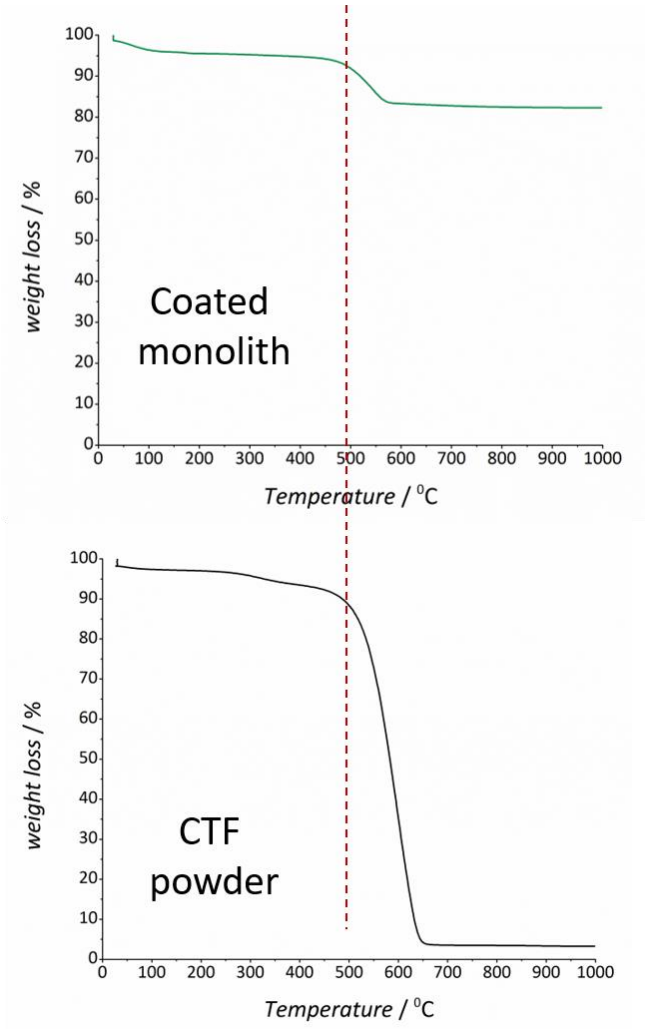

Figure 5.4. TGA analysis of CTF powder and CTF@monolith

CTFs are typically synthesised in molten $ZnCl_2$, which serves both as a solvent and trimerisation catalyst. The synthesis occurs at elevated temperatures, at which the CTFs' precursors, except $ZnCl_2$, become volatile. Figure 5.2 summarises the synthesis protocol followed for the preparation of the supported CTFs: the cordierite monolith was impregnated with CTF precursors by filling the macro-porosity using a low boiling point solvent (acetone). After acetone evaporation, the loaded monolith was placed in an ampoule and the trimerisation procedure was performed. Since the monolith was homogeneously coated with zinc chloride, trimerization of the evaporated monomers takes place selectively on the surface of the support. The obtained films are in this way strongly attached to the cordierite surface (see Figure 5.3) and display an excellent mechanically robustness while manipulating the catalyst. Additional experiments using γ-Al_2O_3 were not successful because of dissolution of the monolith during the HCl post-treatment step to remove $ZnCl_2$. Other tests using a copper plate as a dense support for CTF film was also performed. However, although a coating could be

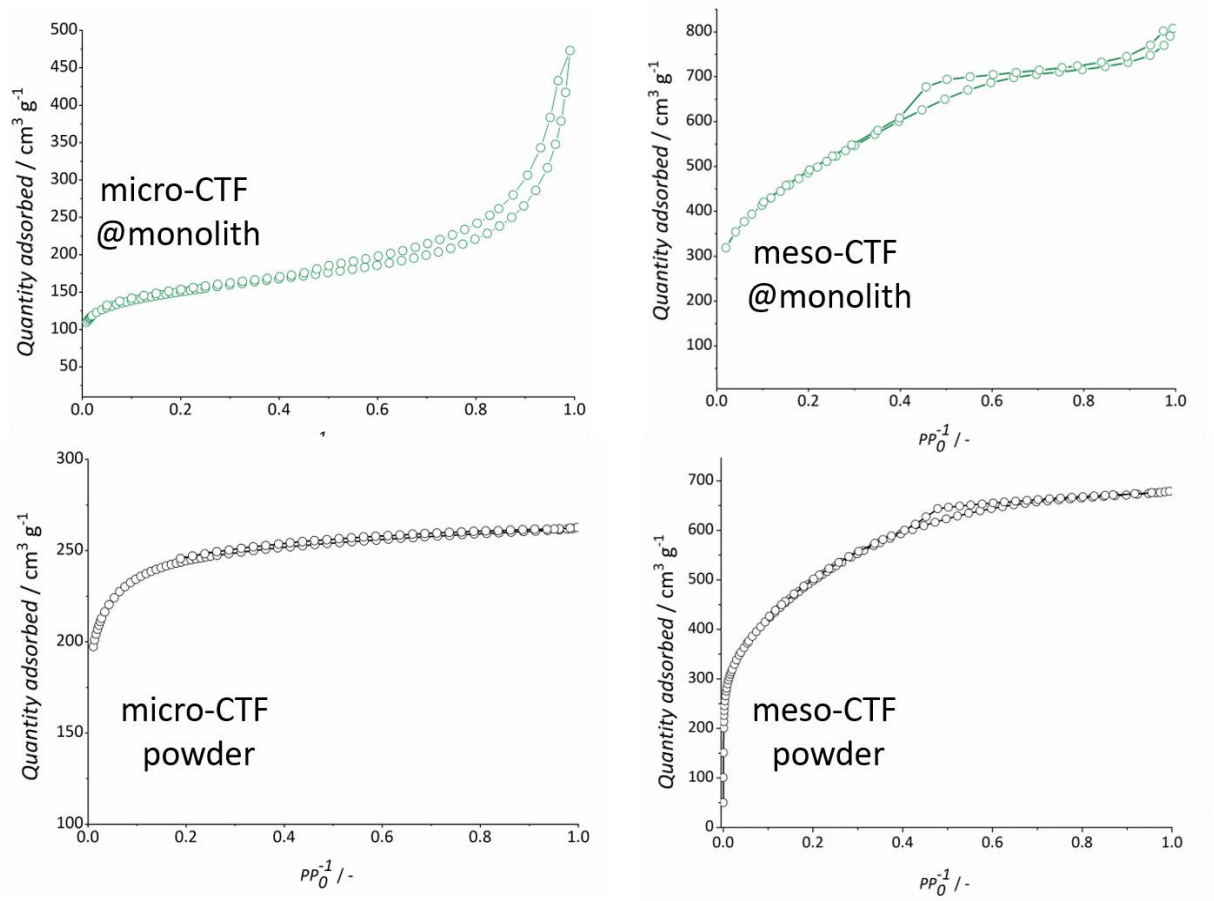

Figure 5.5. Nitrogen adsorption isotherms on powder CTF and CTF@monolith

obtained, it was not mechanically rigid and was easily removed from the surface while handling the material. Therefore, we can conclude that the porosity of the selected cordierite monolithic support indeed plays a very important role.

The CTF coating within the channel of the monolith is protected from external mechanical forces.

Since the proof of the pudding is in the eating, to demonstrate that the coatings observed in figure 5.3 are indeed the envisaged CTF, different characterisation techniques were applied. Thermo-gravimetric analysis in air (Figure 5.4) indicates a clear weight loss in the CTF@monolith sample at a temperature similar to that of the decomposition/oxidation of the CTF powder – ca. 500˚C. From this analysis, a CTF coating of about 20 wt.% could be calculated for the CTF@cordierite material. Having this in mind, N_2 adsorption isotherms using the whole CTF@monolith piece were performed (nitrogen adsorption of bare cordierite monolith was found to be negligible). The obtained values were normalised to the amount of

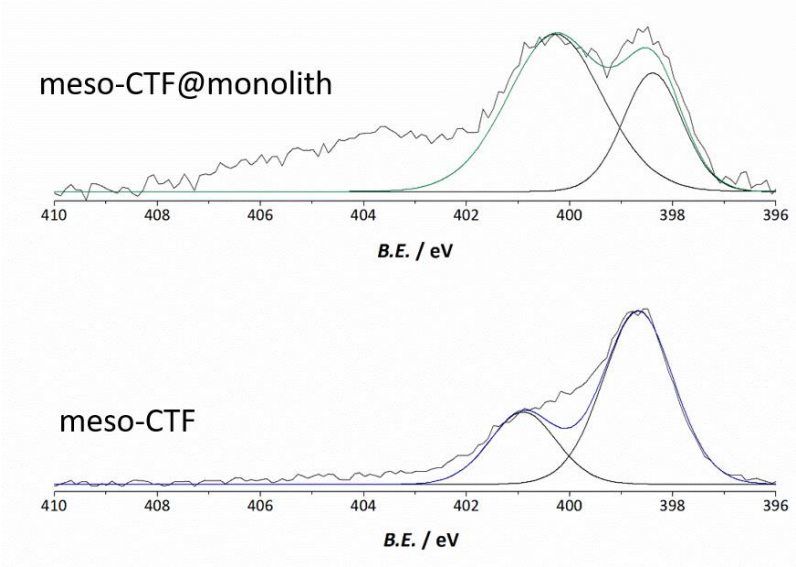

Figure 5.6. XPS analysis of nitrogen in meso-CTF and meso-CTF@monolith

Table 5.1 *TOF*s of the hydrogen production from formic acid [a]

Entry	Sample	*TOF* [h^{-1}] [b]
1	Ir@micro-CTF@monolith[c]	156 300
2	Ir@meso-CTF@monolith[c]	207 200
3	Ir@micro-CTF[d]	73 800
4	Ir@meso-CTF[d]	105 100

[a] 50 ml 3M aqueous formic acid solution; [b] calculated from ^{1}H NMR analysis of formic acid; [c] 0.045mg Ir (0.23 µmol); [d] 0.065mg Ir (0.34 µmol).

CTF within CTF@monolith (Figure 5.5). The amount of CTF within CTF@monolith is not high, therefore, the isotherms of pure micro-CTF and micro-CTF@monolith do not match completely. In contrast, in the case of meso-CTF@monolith, isotherms for the powder and the monolith are fairly identical.

The nature of nitrogen species was found to be identical in CTF and CTF@monolith by XPS analysis. N*1s* lines of CTF samples consist of two peaks centred at 398 eV and 401 eV. The peak with lower binding energy of 398 eV corresponds to pyridinic N species of the framework.

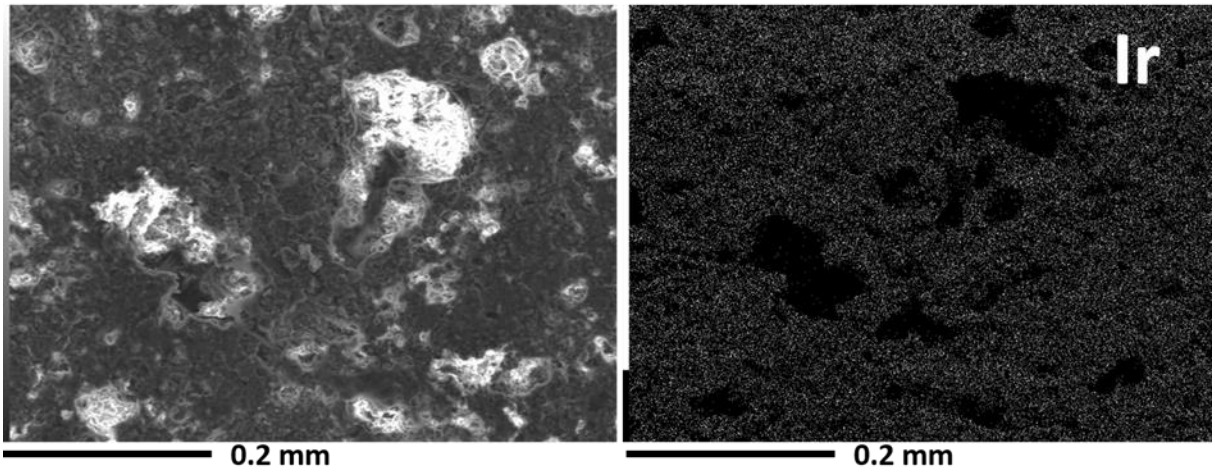

Figure 5.7. EDX analysis of Ir on the outside surface of Ir@CTF@monolith.

The peak at higher binding energy corresponds to partial framework decomposition due to high temperature treatment (Figure 5.6).[5, 26]

The results described above give a strong indication that the coating on the monolith has the same nature as CTF powder. Therefore, the iridium catalyst active in hydrogen production from formic acid was anchored to this coating in a similar fashion as it was done to the powder or spheres (Chapters 3 and 4). Iridium was successfully coordinated, as confirmed by EDX analysis (Figure 5.7). The obtained catalyst is denoted as Ir@CTF@monolith.

The performance of both micro- and meso-CTF@monoliths was tested in formic acid dehydrogenation and compared with that of powder samples with the same metal loading. All experiments were performed at exactly the same conditions – 3M aqueous formic acid solution, 80˚C and, an important aspect when comparing catalytsts' performance, the rate of rotation was constant and did not differ between the experiments. The results are presented in Table 5.1. During recycling, the catalyst was stored under ambient conditions, no precautions or a pre-treatment was required.

Going from entry 1 to 2 and from 3 to 4, it is clear that the porosity has an influence on catalyst performance. Comparison between the fully microporous version of the catalyst and its micro-mesoporous analogue shows an improvement in catalytic activity of circa 30 %, while in both cases, anchoring as a coating onto a monolith renders improvements in activity of almost a 100 %. These results demonstrate that CTF based catalysts can indeed be further

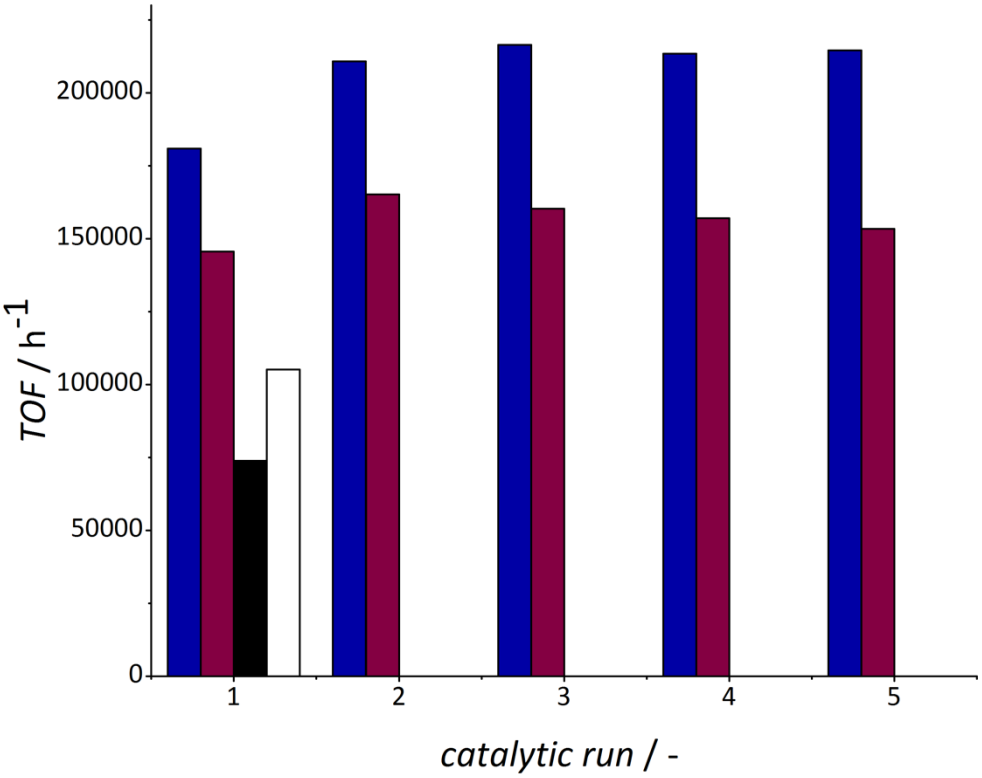

Figure 5.8. *TOF*s of Ir catalyst for several catalytic runs: Ir@micro-CTF@monolith (*red*); Ir@meso-CTF@monolith (*blue*); Ir@micro-CTF (*black*); Ir@meso-CTF (*white*).

improved by engineering these solids at different length-scales and by utilising more appropriate reactor configurations for slurry operations. We attribute the observed differences to both the shorter diffusion path-length in the monoliths (circa 5 times shorter, when comparing figures 5.1 (crushed powder) and 5.3. (coating on the monolith)) and to the improved mass transfer from the liquid by the flow rate that can be realised through the monolith when attached to the stirrer. Having in mind that the coating thickness for micro- and meso-CTF@monolith is smaller than the particle size of the powder catalysts (compare Figure 5.1 and 5.3) and the high dispersion of Ir on the surface, evidenced by the EDX analyses (Figure 5.7), we can conclude that diffusion limitations were reduced by creating a shorter diffusion length, resulting in higher *TOF*s.

Another clear advantage of catalyst anchoring is that recycling and stability testing becomes straightforward. Figure 5.8 shows the observed performance for both monoliths over 5 consecutive catalytic runs. In both cases the first run has a slightly lower activity than that of the following ones. We attribute this improvement in activity to the occurrence of ligand exchange: most probably, the weakly coordinating triflate anion is replaced by formates

in the first catalytic cycle. This was confirmed by EDX analysis, where fluorine is homogeneously distributed in the fresh catalyst and not detectable any more after several uses. Last but not least, it is worth highlighting, that the *TOF*s obtained for the monolithic systems are the highest among those reported in the literature for heterogeneous systems for this reaction.[14, 27-32]

5.4. CONCLUSIONS

By applying a new synthetic protocol, CTF homogeneous and stable films could be successfully deposited as a washcoat on the surface of cordierite monoliths. Extensive characterisation demonstrates that the resulting coatings have similar properties to those of the material in powder form. After coordination of an iridium complex, the obtained catalyst Ir@CTF@monolith was employed in the reaction of hydrogen production from formic acid. The obtained *TOF* is > 200.000 h^{-1} in case of Ir@meso-CTF@monolith. The catalyst is stable under ambient air and no pre-treatment was required prior to utilisation. These results demonstrate that CTF based catalysts can be further engineered by optimization at different length-scales (micro-, meso-, and macro-level) and alleviating internal and external mass transport limitations.[33] By utilising more appropriate reactor configurations for slurry operations, catalyst utilisation can be maximised.

5.5. REFERENCES

[1] P. Kuhn, M. Antonietti, A. Thomas, *Angewandte Chemie International Edition* **2008**, *47*, 3450-3453.

[2] P. Kuhn, A. Thomas, M. Antonietti, *Macromolecules* **2009**, *42*, 319-326.

[3] S. Hug, L. Stegbauer, H. Oh, M. Hirscher, B. V. Lotsch, *Chemistry of Materials* **2015**, *27*, 8001-8010.

[4] L. Tao, F. Niu, C. Wang, J. Liu, T. Wang, Q. Wang, *Journal of Materials Chemistry A* **2016**, *4*, 11812-11820.

[5] K. Wang, H. Huang, D. Liu, C. Wang, J. Li, C. Zhong, *Environmental Science & Technology* **2016**, *50*, 4869-4876.

[6] K. Iwase, T. Yoshioka, S. Nakanishi, K. Hashimoto, K. Kamiya, *Angewandte Chemie International Edition* **2015**, *54*, 11068-11072.

[7] K. Kamiya, R. Kamai, K. Hashimoto, S. Nakanishi, *Nature Communications* **2014**, *5*, 5040.

[8] T. Yoshioka, K. Iwase, S. Nakanishi, K. Hashimoto, K. Kamiya, *The Journal of Physical Chemistry C* **2016**, *120*, 15729-15734.

[9] J. Bi, W. Fang, L. Li, J. Wang, S. Liang, Y. He, M. Liu, L. Wu, *Macromolecular Rapid Communications* **2015**, *36*, 1799-1805.

[10] X. Jiang, P. Wang, J. Zhao, *Journal of Materials Chemistry A* **2015**, *3*, 7750-7758.

[11] A. V. Bavykina, M. G. Goesten, F. Kapteijn, M. Makkee, J. Gascon, *ChemSusChem* **2015**, *8*, 809-812.

[12] A. V. Bavykina, E. Rozhko, M. G. Goesten, T. Wezendonk, B. Seoane, F. Kapteijn, M. Makkee, J. Gascon, *ChemCatChem* **2016**, *8*, 2217-2221.

[13] R. Palkovits, M. Antonietti, P. Kuhn, A. Thomas, F. Schüth, *Angewandte Chemie International Edition* **2009**, *48*, 6909-6912.

[14] P. J. C. Hausoul, C. Broicher, R. Vegliante, C. Göb, R. Palkovits, *Angewandte Chemie International Edition* **2016**, *55*, 5597-5601.

[15] M. Pilaski, J. Artz, H.-U. Islam, A. M. Beale, R. Palkovits, *Microporous and Mesoporous Materials* **2016**, *227*, 219-227.

[16] E. Rozhko, A. V. Bavykina, D. Osadchii, M. Makkee, J. Gascon, *Journal of Catalysis* **2017**.

[17] I. Hoek, T. A. Nijhuis, A. I. Stankiewicz, J. A. Moulijn, *Chemical Engineering Science* **2004**, *59*, 4975-4981.

[18] T. A. Nijhuis, A. E. W. Beers, T. Vergunst, I. Hoek, F. Kapteijn, J. A. Moulijn, *Catalysis Reviews* **2001**, *43*, 345-380.

[19] E. V. Ramos-Fernandez, M. Garcia-Domingos, J. Juan-Alcañiz, J. Gascon, F. Kapteijn, *Applied Catalysis A: General* **2011**, *391*, 261-267.

[20] A. Cybulski, J. A. Moulijn, *Structured catalysts and reactors*, 2nd ed. ed., Taylor & Francis, Boca Raton :, **2006**.

[21] I. Nova, A. Beretta, G. Groppi, L. Lietti, E. Tronconi, P. Forzatti.

[22] T. Vergunst, M. J. G. Linders, F. Kapteijn, J. A. Moulijn, *Catalysis Reviews* **2001**, *43*, 291-314.

[23] A. F. Pérez-Cadenas, F. Kapteijn, J. A. Moulijn, *Applied Catalysis A: General* **2007**, *319*, 267-271.

[24] E. D. Banús, V. G. Milt, E. E. Miró, M. A. Ulla, *Applied Catalysis B: Environmental* **2013**, *132–133*, 479-486.

[25] E. Crezee, P. J. Kooyman, J. Kiersch, W. G. Sloof, G. Mul, F. Kapteijn, J. A. Moulijn, *Catalysis Letters* **2003**, *90*, 181-186.

[26] K. Artyushkova, B. Kiefer, B. Halevi, A. Knop-Gericke, R. Schlogl, P. Atanassov, *Chemical Communications* **2013**, *49*, 2539-2541.

[27] S. Zhang, Ö. Metin, D. Su, S. Sun, *Angewandte Chemie International Edition* **2013**, *52*, 3681-3684.

[28] Y.-Y. Cai, X.-H. Li, Y.-N. Zhang, X. Wei, K.-X. Wang, J.-S. Chen, *Angewandte Chemie International Edition* **2013**, *52*, 11822-11825.

[29] J. H. Lee, J. Ryu, J. Y. Kim, S.-W. Nam, J. H. Han, T.-H. Lim, S. Gautam, K. H. Chae, C. W. Yoon, *Journal of Materials Chemistry A* **2014**, *2*, 9490-9495.

[30] Z.-L. Wang, J.-M. Yan, Y. Ping, H.-L. Wang, W.-T. Zheng, Q. Jiang, *Angewandte Chemie International Edition* **2013**, *52*, 4406-4409.

[31] K. Koh, M. Jeon, D. M. Chevrier, P. Zhang, C. W. Yoon, T. Asefa, *Applied Catalysis B: Environmental*.

[32] W. Zhang, H. Huang, F. Li, K. Deng, X. Wang, *Journal of Materials Chemistry A* **2014**, *2*, 19084-19094.

[33] F. Kapteijn, J. J. Heiszwolf, T. A. Nijhuis, J. A. Moulijn, *Cattech* **1999**, *3*, 24-41.

CHAPTER SIX

Porous Organic Frameworks as Supports for a Molecular Ni based Ethylene Oligomerization Catalyst for the Synthesis of Olefins

The use of two different classes of Porous Organic Frameworks (covalent triazine and imine linked frameworks) as supports for molecular Ni^{2+} catalysts is presented. For POFs, a large concentration of N heteroatoms, either in the form of quasi bipyridine or as diiminopyridine moieties, allows for the coordination of $NiBr_2$ to the scaffold of the porous polymers. When applied as catalysts in the oligomerization of ethylene under mild reaction conditions (15 bar, 50 ˚C), these new catalysts display an activity comparable to that of their homogeneous counterpart and a fivefold higher selectivity to C6+ olefins. Accumulation of long chain hydrocarbons within the porosity of the POFs leads to reversible deactivation. Full activity and selectivity of the best catalysts can be recovered upon washing with dichlorobenzene.

This Chapter is based on the following publication:

E. Rozhko, A.V. Bavykina, D. Osadchii, M. Makkee, J. Gascon, *Journal of Catalysis, accepted*

6.1. INTRODUCTION

α-Olefins in the C_4–C_{20} range are of the utmost importance as they are valuable and versatile feedstocks and building blocks for a variety of products that people consume on a daily basis, i.e. detergents, plasticizers, polymers, *etc*. Currently oligomerization of ethylene is the prevalent method for the synthesis of these olefins.[2]

Existing commercial processes utilise homogeneous catalysts. The two-step Ziegler stoichiometric process (INEOS), the one-step Ziegler process (Chevron-Phillips (CP) Chemicals) and the Shell higher olefins process (SHOP) are among the most widely applied industrial production methods together with the Idemitsu and SABIC processes. The two-step and the one-step Ziegler processes use triethylaluminium as a catalyst and SHOP is catalysed by nickel complexes, while Idemitsu and SABIC processes use a combination of Zr and alkylaluminium.[4]

At the end of 1990s new efficient homogeneous catalysts were discovered and subsequently extensively studied. These are diimine and iminopyridine complexes of nickel, cobalt or iron in combination with alkylaluminium.[5-16] Though homogeneous catalysts in general show better performance, the use of a heterogeneous catalysts would be desired from a practical point of view, as it would ease catalyst handling and recycling and may result in enhanced selectivities to specially interesting products such as C_8 olefins. In this spirit, quite some research on heterogeneous catalysts has been performed in the past few decades, among which nickel-exchanged zeolites[18-27], Ni-MCM and Ni-SBA catalysts[28-36], supported $NiSO_4$[37-44], supported NiO[45-51] and nickel-exchanged silica-alumina[52-56]. The most active Ni-exchanged zeolite[22] and silica-alumina catalysts[53] show the formation of mainly C_4-C_8 olefins, with high selectivity to butenes (circa 70%). Selectivity to higher olefins can be enhanced by using bigger pore materials such as Ni-MCM catalysts[31-32]. In all these cases, the formation of a minor amount of C_{10+} olefins was also detected (<10%). Supported $NiSO_4$ catalyses ethylene dimerization with selectivity to butenes of 100%.[41, 44] In case of supported NiO, at low temperatures (20 ˚C) the only products are butenes, but when high temperatures (150-200 ˚C) and high pressures are used, selectivity to butenes decreases to 10-13%, while, particularly, the formation of C_{6+} is enhanced.

From a design point of view, the immobilization of well optimized homogenous catalysts offers a number of advantages such as better selectivity control and metal utilization. Several groups have followed this approach. In these works, diimine nickel complexes have

been anchored to MCM-41 and MFS[60] and to hybrid silica[62], iminopyridine metal complexes have been supported on carbon nanotubes[63-64] and diimine, iminopyridine, bis(imino)pyridine metal complexes have been immobilized into mica layered materials[65-69]. Catalysts supported on MCM-41, MFS and carbon nanotubes show a high activity in the polymerization of ethylene, whereas hybrid silica supported catalysts form butenes with 100 % selectivity. Another interesting and unique approach is reported by Malgas-Enus *et al.*, who used nickel metallodendrimers in a combination with alkylaluminium compound as catalyst,[70] reaching a maximum selectivity to butenes of 55%, with most of the other products being C_{22}-C_{60} oligomers.

Recently, molecular heterogeneous catalysts based on Ni^{II} complexes supported on MOF materials were developed.[1, 3, 17, 57-58, 71] Dinca *et al*. used a MOF support with a secondary building unit structurally homologous to a 3-mesitylpyrazolyl Ni homogeneous catalyst.[58] In most cases, these catalysts display high selectivities to butenes (range from 85 to 95%) along with the formation of polyethylene on the surface of the catalyst.[17]

The use of molecular catalysts requires the presence of a co-catalyst, alkylaluminium in most cases. According to the proposed reaction mechanisms[1, 17, 72-73] (Figure 6.1), reaction with alkylaluminium has been proposed to either promote proton abstraction to active metal-hydride species (**A**), or to generate mono (**B**) or dialkylated (**I**) metal adducts. In case of metal-hydride or monoalkylated metal species, the next step is the insertion of ethylene to form a dialkylated adduct (**I**). Then the formation of an alkyl-metal intermediate (**II**) takes place that leads to intermediate **IV** after releasing butene through *β*-hydride elimination. Further inclusion of additional ethylene molecules on complex (**II**) yields to the formation of higher olefins that are finally released via *β*-hydride elimination.

Considering the reaction mechanism (see figure 6.1) and the examples summarized above, prediction of the product spectrum of a given catalyst is not trivial, although, in general, it is proposed that stabilization of the first oligomerization product (**III**) at the surface of the catalyst is crucial in determining the “chain growth probability” of the process. In view of this, we speculate that hydrophobic supports with higher affinity for oligomerization products result in the production of a larger amount of longer olefins, while more hydrophilic supports mostly produce butenes.

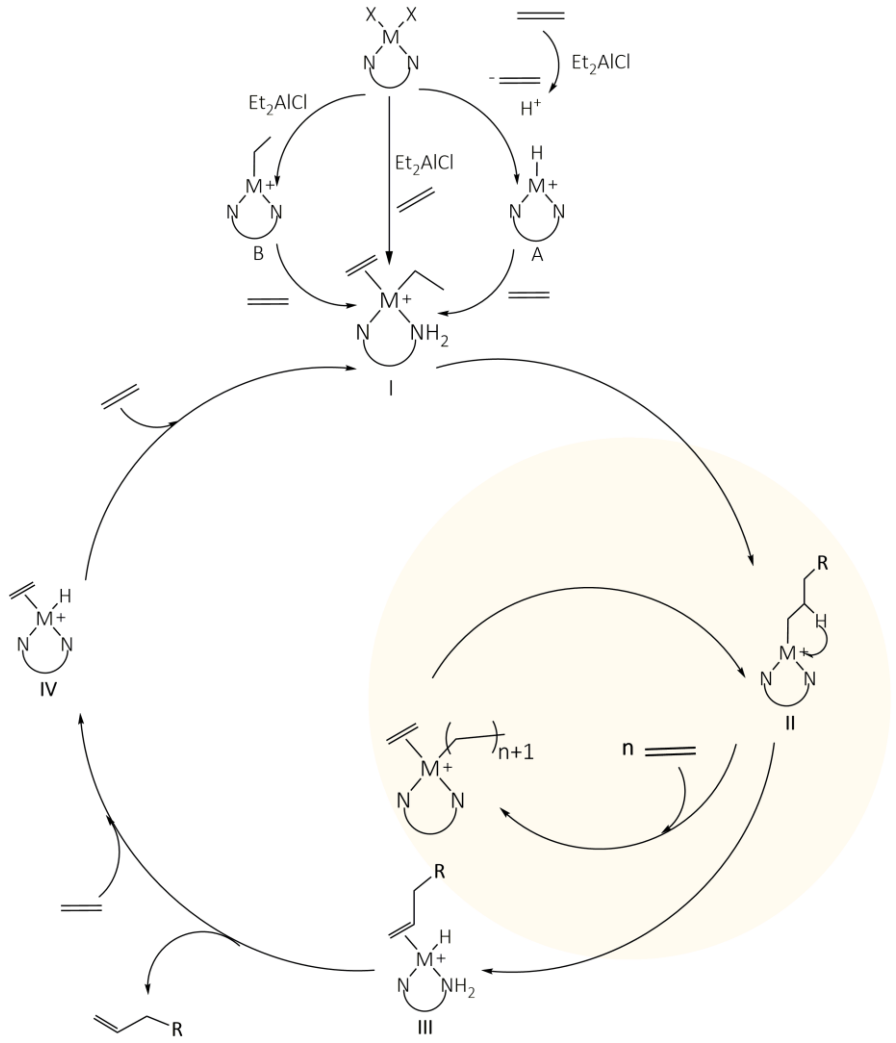

Figure 6.1. Proposed mechanism for ethylene oligomerization.

Herein we decided to explore the use of Porous Organic Frameworks (POFs), as potential supports for Ni ethylene oligomerization catalysts. POFs consist only of light elements (C, N and H) and display a high degree of tunability, both in terms of pore size and surface area. Two different families of POFs were studied: Covalent Triazine Frameworks (CTFs) with micro- and mesoporous structures, and a lamellar structured imine-linked polymer network (IL-PON). In both cases, a large concentration of N heteroatoms (either in the form of quasi bipyridine moieties in case of CTFs or in the form of diiminopyridine moieties in case of the IL-PON) within the porous structure of these materials allows for the direct coordination of Ni^{2+}. Our results demonstrate that both families of solids hold great promise for the selective formation of C_8 olefins and that deactivation of the catalysts due to the adsorption of C_8-C_{30} products can be easily mitigated by catalyst reactivation in dichlorobenzene.

6.2. EXPERIMENTAL

Materials

1,3,5-Tris(*4*-aminophenyl)benzene was purchased from TCI Europe N.V. and used as received. All other reagents and solvents were purchased from Sigma-Aldrich and used as received.

Synthesis of imine-linked porous organic network (IL-PON)

The following general procedure was followed to prepare the *IL-PON* support: 116 mg (0.858 mmol) *2,6*-pyridinedicarboxaldehyde were dissolved in 10 mL DMSO; 200 mg (0.569 mmol) *1,3,5*-tris(*4*-aminophenyl)benzene were dissolved in another 10 mL DMSO. Then, solutions were mixed in a round-bottom flask and 1 mL 99.8% acetic acid was added. Almost immediately there was a formation of the yellow polymer. Polymer was subsequently washed with methanol and THF and dried at 150^{o}C under vacuum giving 286 mg (yield based on the monomers ~90%) of a yellow powder.

Synthesis of mesoporous and microporous Covalent Triazine Framework (meso-CTF and micro-CTF)

To synthesise microCTF, a glass ampoule was charged with 2,6-pyridinedicarbonitrile (0.124 g, 0.96 mmol) and anhydrous $ZnCl_2$ (0.664 g, 4.8 mmol) in a glovebox. For the mesoCTF, the ampoule was charged with 2,6-pyridinedicarbonitrile (0.041 g, 320 µmol), 4,4'-biphenyldicarbonitrile (0.131 g, 640 µmol) and anhydrous $ZnCl_2$ (0.664 g, 4.8 mmol). The ampoule was flame sealed and the mixture was heated at 500°C for 48 h and then cooled to room temperature. The product was consecutively washed in 5M HCl at 100^{o}C, in NH_4OH at 60^{o}C, in H_2O at 100^{o}C and then in THF at 60^{o}C, each step overnight. The washing steps might seem excessive, but were, as we found, required to remove $ZnCl_2$. Finally, the powder was dried in vacuum at 180^{o}C overnight.

Coordination of DME·$NiBr_2$

A mixture of 0.1 g Nickel(II) bromide ethylene glycol dimethyl ether (DME*$NiBr_2$) and 15 mL THF was placed in a round-bottom flask and stirred for 5 minutes, then 0.2 g of a polymer was added. The mixture was stirred at 67^{o}C overnight and filtered. Afterwards, the powder was washed with 50 mL THF at 70^{o}C overnight to remove DME. The final product was filtered and dried under vacuum at 100^{o}C.

Characterization Techniques

Argon adsorption was performed on a Micromeritics ASAP 2010 gas adsorption analyser (stainless steel version) at -186 ºC. For the DFT calculations on the pore size distribution, the MicroActive v. 3.00 (Micromeritics) software package was used using a Argon on oxides at 87 K NLDFT (Non Local Density Functional Theory) model for CTF based samples, using a non-negative regularization method with a factor of 0.03160, Standard deviation of fit: 1.00 cm^3/g STP for micro-CTF, 0.56 cm^3/g STP for Ni@micro-CTF, 0.85 cm^3/g STP for meso-CTF and 0.59 cm^3/g STP for Ni@meso-CTF. Carbon slit pores NLDFT model was used for IL-PON based samples, using a non-negative regularization method with a factor of 0.20000, Standard deviation of fit: 3.35 cm^3/g STP for IL-PON, 1.24 cm^3/g STP for Ni@IL-PON.

XPS measurements were performed on a *K-alpha* Thermo Fisher Scientific spectrometer using a monochromatic Al *Kα* X-ray source. The measurements were performed at ambient temperature and chamber pressure of about 10^{-7} mbar. A flood gun was used for charge compensation. All the spectra measured were corrected by setting the reference binding energy of carbon (C1s) at 285.0 ± 0.025 eV. Spectra were analysed using the Thermo Avantage software package, background subtraction is done using the setting “SMART”. From the intensity ratios, the following selectivity factors were used – 3.726 for Zn, 4.044 for Ni and 0.477 for N.

For elemental analysis, the Ni@CTF samples were analyzed by Mikroanalytisches Laboratorium KOLBE, (Mülheim an der Ruhr, Germany), Ni@IL-PON samples were analyzed using PerkinElmer Optima 5300 (torch:4300) instrument, with ICP-OES 5300DV.

Scanning electron microscopy (SEM) images were recorded using a JEOL JSM-6010LA with a standard beam potential of 10 kV and an Everhart-Thornley detector. X-ray microanalysis (SEM/EDX) confirmed the elemental composition in the sample by the scanning electron microscopy (SEM) coupled with a dispersive X-ray microanalysis system (EDX) with a Silicon-drift detector.

Diffuse reflectance infrared Fourier transform spectroscopy (DRIFTS) was performed in a Bruker model IFS66 spectrometer equipped with a high temperature cell with CaF_2 windows and a 633 nm laser. The spectra were registered after accumulation of 128 scans and a resolution of 4 cm^{-1}. A 10 mL/min flow of helium was maintained during the measurements. Before collecting the spectra, the different samples were pre-treated in a helium flow at 393 K for 30 min. KBr was used for background.

Thermogravimetric analysis (TGA) was performed on a Mettler Toledo TGA/SDTA851e equipment, where samples of 0.011–0.02 g were screened for the change in mass while heated from 303 to 1273 K at a rate of 2 K min^{-1} under air flow.

The gas phase was analysed by a CompactGC4.0 from Interscience equipped with a FID detector and two consecutive columns: Rt-QBond, length 14 m, diameter 0.32 mm, and Rt-UBond, length 10 m, diameter 0.32 mm. Liquid phase was analysed by GC (Agilent 7890A) equipped with a FID detector and Durabond (DB-1) column, length 30 m, diameter 0.25 mm.

Transmission Electron Microscopy (TEM) analysis was performed in a JEOL JEM-1400-Plus microscope operated at 120 keV with LaB6 emission filament.

Ethylene oligomerization

Oligomerization experiments were performed in a Parr 5000 Multi Reactor Stirrer System under ethylene pressure (batch conditions). The six reaction vessels (autoclaves) have a volume of 45 mL each and were stirred at 1000 rpm with suspended magnetic bars. Autoclaves were filled inside the glovebox with 20 mL heptane as solvent, 1.2 mL 1M triethylaluminium solution in heptane as co-catalyst and 20 mg Ni@micro-CTF, Ni@meso-CTF or Ni@IL-PON as catalyst. Before starting the reaction the air in the gas lines was removed by consecutive pressurizing and depressurizing the system with He. Ethylene was then introduced in the autoclaves until a pressure of 15 bar was reached. The autoclaves were heated to the desired temperature with a heating rate of 2 °C min^{-1} and kept at this temperature for 2 hours. After the reaction, the gas mixture was collected with gas-bags and the liquid-phase was separated from the catalyst. In every case, the spent catalyst was filtered from the reaction mixture using a Nylon filter with 0.45 µm pore size, washed in heptane at 50 °C for 1 h and dried overnight. Afterwards, heptane and triethylaluminium were added to the catalyst and reaction repeated as described above.

A series of blank experiments were also carried out: (1) in the presence of only activator Et_3Al; (2) in the presence of only catalyst; (3) only using heptane, to estimate ethylene solubility under chosen conditions. From the blank experiment (3), the dimensionless Henry solubility was calculated: $H^{cc} = \frac{C_a}{C_g}$, where C_a is liquid-phase concentration and C_g is gas-phase concentration, At 20°C and 15 bar of initial pressure, a value of 0.66 was found for H^{cc}.

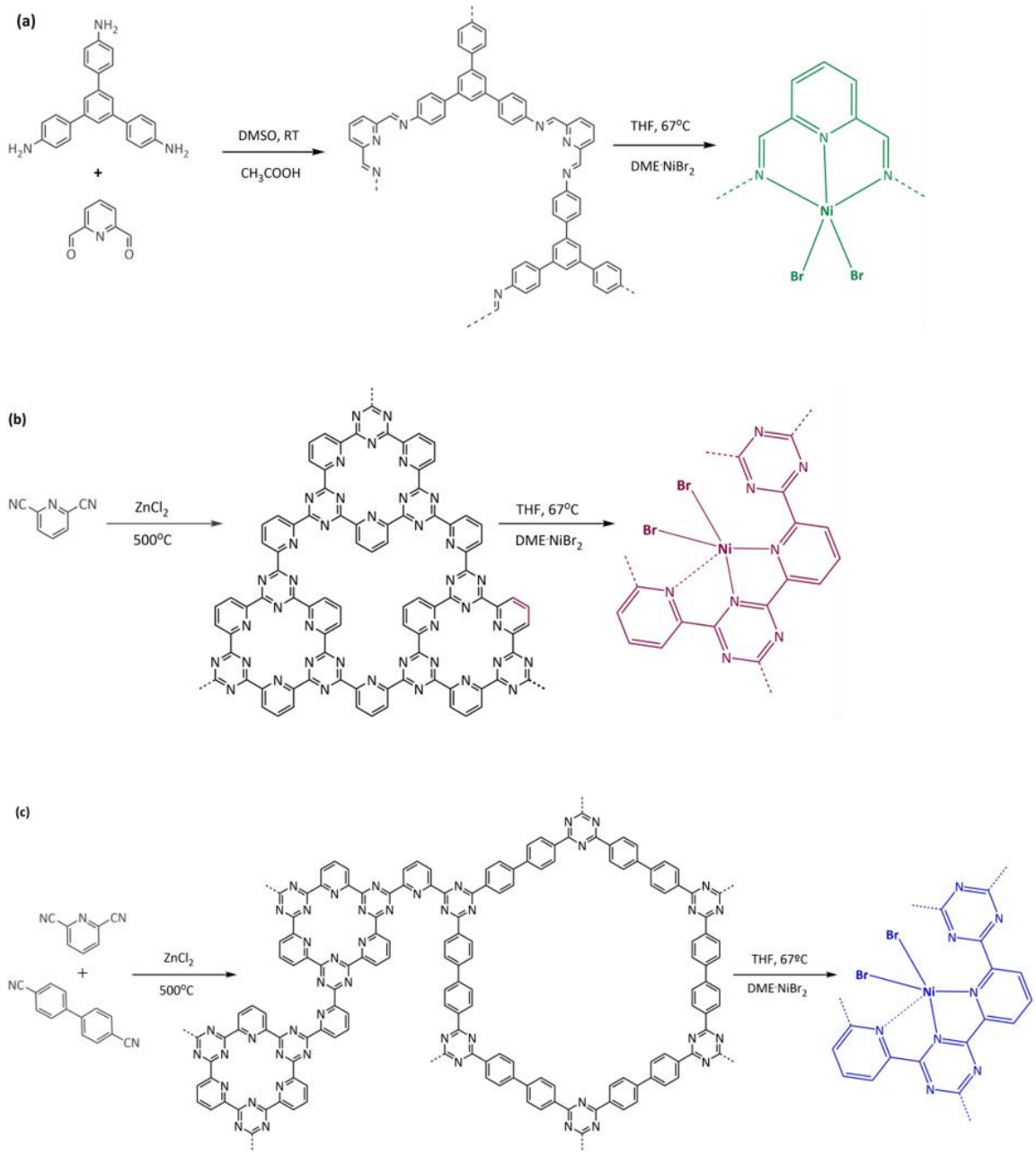

Figure 6.2. Synthesis of the IL-PON through polyimine condensation (a), micro-CTF (b) and meso-CTF (c) and expected coordination of Ni^{2+} to the nitrogen species in the frameworks.

The carbon based selectivity (*S*) and total number of turnovers (*TON*) were calculated according to the following equations:

$$S = \frac{n_{\text{product}}(\text{mol})}{\Sigma n_{\text{product}}(\text{mol})} \cdot 100\%$$

$$TON = \frac{\sum(n_{oligomers} * carbon\ number * 1/2)\ (\text{mol})}{n_{\text{Ni}}(\text{mol})}$$

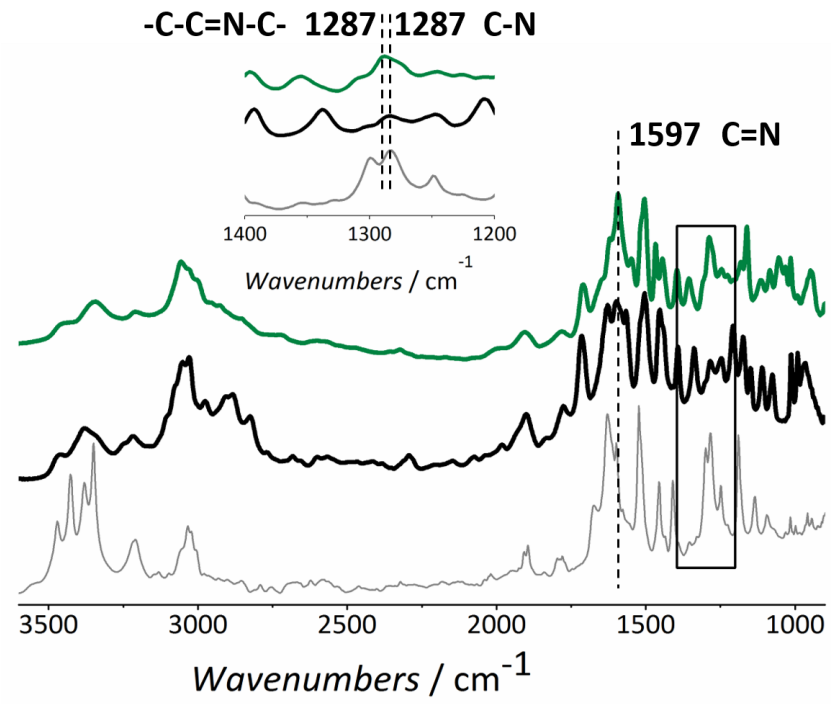

Figure 6.3. DRIFT spectrum of 1,3,5-tris(4-aminophenyl)benzene (*grey*), IL-PON (*black*) and Ni@IL-PON (*green*).

6.3. RESULTS AND DISCUSSION

With the aim of exploring the suitability of different highly stable POFs as supports for the immobilization of Ni, we selected two different types of solids: type one, the so called IL-PON is an diiminopyridine POF and was synthesized via the acid catalysed condensation of *2,6*-pyridinedicarboxaldehyde and *1,3,5*-tris(*4*-aminophenyl)benzene, as previously described by Zamora *et al.* [74] (Figure 6.2a). The second type of supports belongs to the family of Covalent Triazine Frameworks (CTF, see Figure 6.2b,c), a highly porous class of organic polymers synthesized through the high temperature polymerisation of nitrile containing aromatic building blocks. In order to tune the final porosity of the CTF, we synthesized a purely microporous material based on the polymerisation of *2,6*-pyridinedicarbonitrile (denoted as micro-CTF) and a micro-mesoporous solid obtained from the condensation of *2,6*-pyridinedicarbomitrile and *4,4'*-biphenyldicarbonitrile in a 1:2 ratio (denoted as meso-CTF). Synthesis methods previously reported by our group were followed for the preparation of the CTF supports [75].

DRIFTS confirmed the successful imine condensation during the synthesis of IL-PON (Figure 6.3). The spectrum of the polymer shows the presence of C=N (1597 cm^{-1}) and C-C=N-

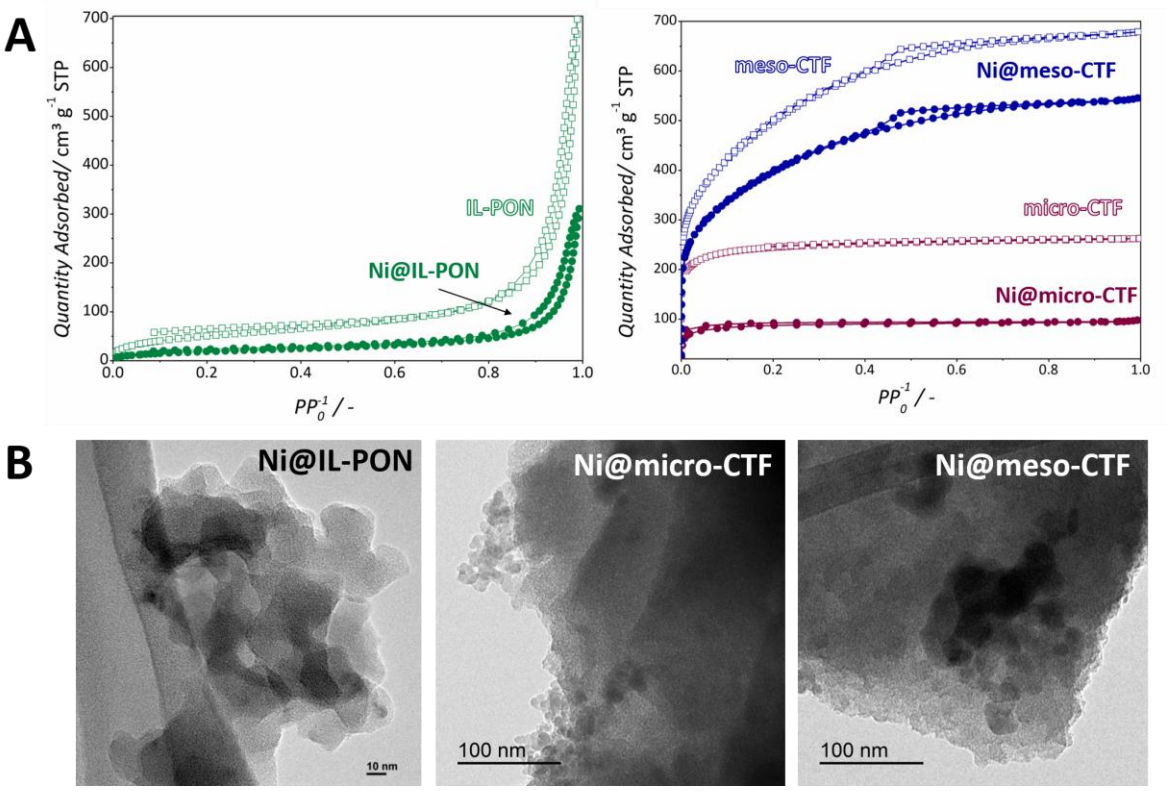

Figure 6.4. A) Argon adsorption isotherms at -186 ˚C for IL-PON support (*open symbols*) and Ni@IL-PON catalyst (*solid symbols*), micro-CTF support (*open red*), Ni@micro-CTF catalyst (*solid red*), meso-CTF support (*open blue*) and Ni@meso-CTF catalyst (*solid blue*). B) TEM images of Ni catalysts.

C (1287 cm^{-1}) moieties, while the C-N stretching mode from the *1,3,5*-tris(*4*-aminophenyl)benzene precursor (1279 cm^{-1}) is not present in the final solid, demonstrating the full polymerization of the monomers [74, 76].

The argon adsorption isotherm of IL-PON (Figure 6.4a) displays the typical "house of cards" shape with a low pore volume accompanied by a relatively larger uptake at moderate pressures. We attribute the three different regimes in the isotherm to adsorption in the pore mouth of the lamellar material (P/P_0<0.05), formation of several Ar layers on the surface of the lamellas (0.05<P/P_0<0.7) and condensation of Ar in the interlamellar space (0.7<P/P_0<0.98).[77]

In contrast, adsorption isotherms on both CTF materials (Figure 6.4b) show the fully microporous nature of micro-CTF and the micro-meso porous character of meso-CTF, in good agreement with our previous results [75, 78]. Table 6.1 summarizes the main textural properties of the different supports and catalysts.

Table 6.1 Textural properties of polymers and catalysts		
Sample name	S_{BET} [$m^{-2}g$]	V_p [$cm^{-3}g$]
IL-PON	106	0.87
Ni@IL-PON	86	0.34
Micro-CTF	930	0.54
Ni@micro-CTF	330	0.24
Meso-CTF	1803	1.15
Ni@meso-CTF	1439	0.63

CHN analysis performed on the three different supports revealed the following C:H:N ratios: IL-PON: 82.3: 5.5: 12.2; micro-CTF: 69.7: 3.0: 27.3; meso-CTF: 87.1: 2.0: 10.9. When compared to the expected values according to polymerization stoichiometry (81.2: 3.9: 14.9; 65.1: 2.3: 32.6; and 78.2: 3.5: 18.2), the obtained N content is circa 80% of the expected one for IL-PON and micro-CTF and 60% of the expected content for meso-CTF. While in case of IL-PON and micro-CTF this can be attributed to the presence of solvent occluded in the pores and/or to the high temperature used for the formation of the CTF (see XPS characterization, *vide infra*), in case of meso-CTF, this may be an indication of a slightly different polymerization ratio between the two monomers used.

Ni^{2+} was coordinated to the diiminopyridine and *quasi* bipyridine moieties of the support materials by excess impregnation of Nickel^{II} bromide ethylene glycol dimethyl ether ($DME{\cdot}NiBr_2$) under mild conditions. Upon a one-step impregnation, Ni loadings of 4.7, 2.8 and 2.8 wt % were obtained for Ni@IL-PON, Ni@micro-CTF and Ni@meso-CTF, respectively. These loadings correspond to molar N:Ni ratios of 10, 40 and 16, respectively, and demonstrate that in all cases not all potential coordination sites are occupied by Ni.

TEM micrographs of the different catalysts (Figure 6.4B) reveal the expected lamellar structure of IL-PON and a good dispersion of Ni (note that no metal nanoparticles could be observed in any of the samples). On the other hand, the three polymers seem to macroscopically result from the agglomeration of small (10-50 nm) primary particles.

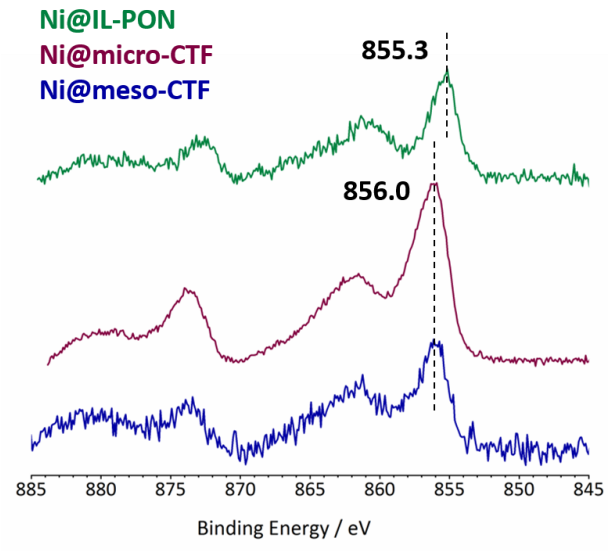

Figure 6.5. Ni*2p* XPS spectra of Ni@IL-PON, Ni@micro-CTF and Ni@meso-CTF catlysts.

Table 6.2 Relative content of Ni and Zn in different catalysts

Sample name	I_{Zn2p}/I_{N1s}	I_{Ni2p}/I_{N1s}
IL-PON	-	-
Ni@IL-PON	-	0.31
Micro-CTF	0.06	-
Ni@micro-CTF	0.06	0.54
Meso-CTF	0.15	-
Ni@meso-CTF	0.08	0.25

Coordination of Ni^{2+} leads to a decrease in surface area for all catalysts (see Figure 6.4 and Table 6.1), with a much bigger impact on micro-CTF, where a 65% of the available porosity is lost after incorporation of a 2.8 wt% of Ni. In contrast, only a loss of a 20 % is observed for the bigger pore CTF material upon introduction of a similar amount of Ni and for the IL-PON upon coordination of a 4.7 wt% of Ni. These results are in good agreement with the expected accessibility of each support: in case of micro-CTF, addition of the relatively bulky $NiBr_2$ moieties would produce the blockage of part of the porosity, while addition of mesopores already mitigates this effect in meso-CTF. In case of IL-PON, with most surface being available as external surface (lamellae), the effect on final textural properties is even smaller. The available external surface together with the fact that all N atoms from the framework can engage in coordination explain the higher metal loading achieved for IL-PON.

In order to study the coordination of Ni^{2+} to the frameworks, X-ray photoelectron spectroscopy (XPS) analysis (Figures 6.5 and 6.6) was performed before and after Ni^{2+} impregnation. Table 6.2 shows the relative surface content of N, Zn and Ni for all samples. The Ni:N ratio on the surface is much higher for Ni@micro-CTF than for Ni@IL-PON and Ni@meso-CTF. It indicates that micro-CTF is less accessible for Ni compared to IL-PON and meso-CTF, in good agreement with the data from adsorption measurements. While IL-PON has a lower BET area, the pore volume is higher, probably due to the space between lamellae, where Ni might

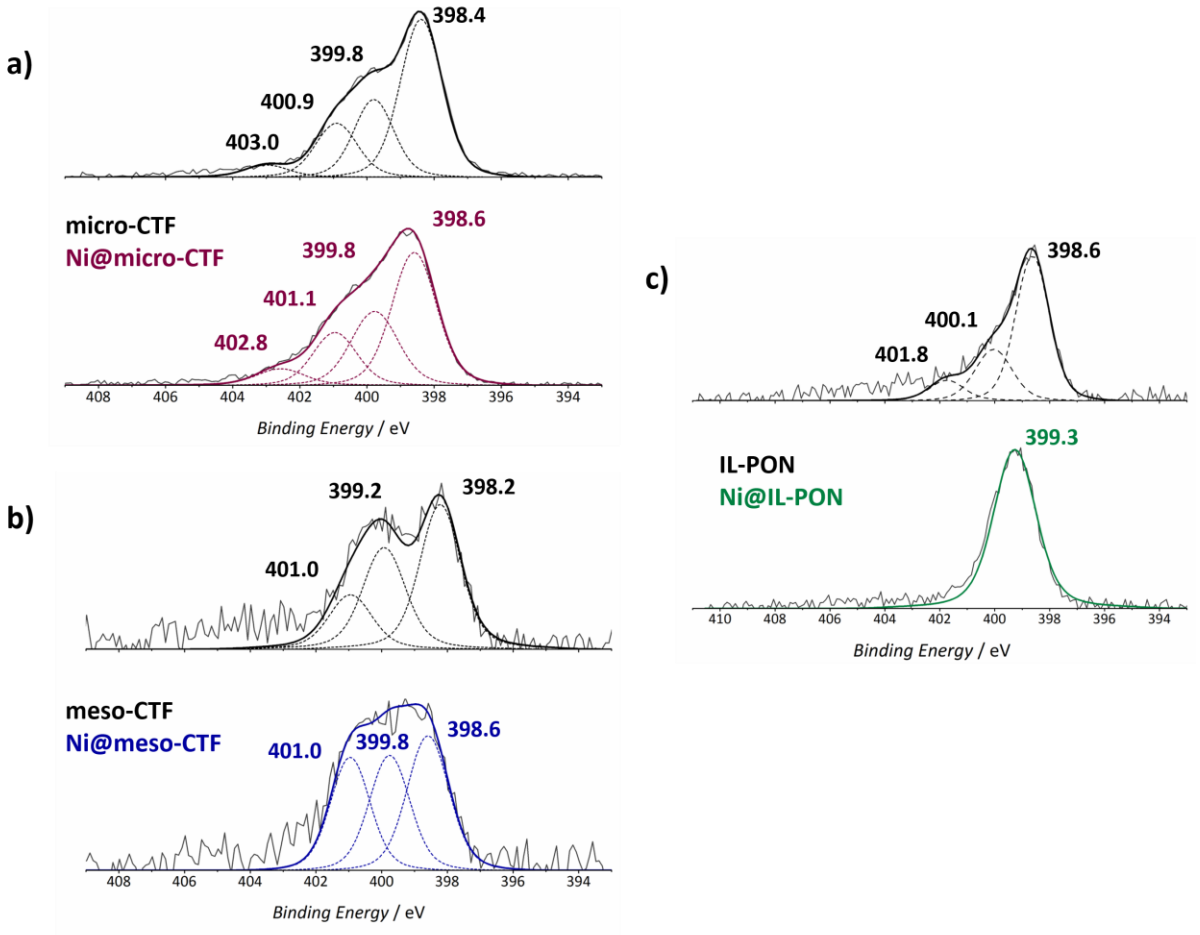

Figure 6.6. N*1s* XPS spectra of a) pristine micro-CTF and Ni@micro-CTF catalyst b) pristine meso-CTF and Ni@meso-CTF catalyst c) pristine IL-PON polymer and Ni@IL-PON catalyst.

be 'trapped' within the lamellae, therefore it is not detectable by a surface technique. With microCTF the whole particles are inaccessible and nickel is accumulated at the outside regions.

XPS shows the presence of residual Zn on the surface of CTF samples, coming from $ZnCl_2$ used as catalyst for CTF synthesis. Introduction of Ni leads to further decrease of the high Zn surface content of meso-CTF.

According to the synthesis procedure, Ni can be either chemically coordinated to N functional sites of the framework or remain adsorbed on the surface and in the pores as non-coordinated complexes or clusters. In order to reveal the chemical state of Ni in the catalysts, high resolution spectra of N*1s* and Ni*2p* line were analysed. Figure 6.5 shows Ni*2p* spectra for all samples after Ni introduction. All spectra represent the line shape typical for Ni^{2+} compounds, but the binding energies of the main Ni$2p_{3/2}$ peak are different: 855.3 eV for Ni@IL-PON and 856.1 eV for Ni@CTF samples. These binding energies definitely do not

correspond to Ni(II) oxide (NiO, main peak at 853.7 eV), but are in the range of typical values for most Ni-O and Ni-N complexes [79].

Figure 6.6c shows N*1s* line of IL-PON before and after introduction of Ni. The main peak of N*1s* line with binding energy of about 398.6 eV is clearly shifted to a higher binding energy (399.3 eV), indicating the donation of electron density from N atoms, something normally observed upon coordination of N-containing groups to metal ions [80]. Additional peaks of N*1s* line of IL-PON with higher binding energy (400.1 eV, 401.8 eV) disappear after Ni coordination, that let us attribute it to unreacted monomer removed during the process of Ni introduction and washing and N atoms of imine moieties which become XPS equal to pyridinic sites after metal coordination.

A similar, but less pronounced, behaviour is observed in case of micro-CTF and meso-CTF species (Figure 6.6). N*1s* lines of CTF samples consist of three peaks. First peak with binding energy of 398.2 eV in case of meso-CTF and 398.4 eV in case of micro-CTF corresponds to pyridinic N species of the framework. Peaks at higher binding energy (399.8 and 401 eV), corresponding to partial framework decomposition due to high temperature treatment (pyrrolic and quaternary N species, respectively) [80-81]. Introduction of Ni shifts the first peak to higher binding energy: this shift is very small in case of micro-CTF (0.2 eV) and more obvious in case of meso-CTF (0.4 eV). For both samples the binding energy of pyridinic N*1s* peak becomes equal to 398.6 eV after coordination of Ni. No shift is observed for peaks with binding energy of 399.8 and 401 eV, indicating preferential coordination of Ni to pyridinic N species within the CTF. However, the observed shifts are small compared to the one observed in case of IL-PON samples. This might indicate weaker coordination of the Ni^{2+} ions in case of CTFs.

A possible explanation for this effect could be attributed to the difference between N-containing coordination sites of CTFs and IL-PON. IL-PON contains pincer-like diimino-pyridinic groups in its structure that afford strong coordination of metal ions with its three nitrogen atoms. Though in the ideal case CTFs might expose up to six nitrogen atoms (Figure 6.2a, b) available for one Ni atom to coordinate, due to geometric constrains coordination of Ni to only two N atoms is much more likely.

The catalytic performance in ethylene oligomerization of the different POF based catalysts was studied in batch mode at 50^{o}C under initial ethylene pressure of 15 bar in heptane using 20 mg catalyst and Et_3Al as co-catalyst. When the pressure in the reactor

Table 6.3 Ethylene oligomerization catalysed by Ni containing catalysts[a]

Entry	Catalyst	Selectivity				*TON*[b,c]
		$C_{4=}$	$C_{6=}$	C_8	C_{10+}	
0[68]	(bpy)$NiBr_2$ (2.8µmol)	90	10		0	2240±100
1	Ni@IL-PON (16 µmol)	58	20	15	7	370±60
2	Ni@micro-CTF (9.6 µmol)	59	9	29	3	252±6
3	Ni@meso-CTF (9.6 µmol)	54	17	17	12	301±50
4	Ni@meso-CTF (9.6 µmol)[d]	68	15	10	7	269
5	Ni@IL-PON-RT (16 µmol)[e]	70	14	10	6	561±30

[a] Reaction was carried out in batch mode at 50 ˚C, at 15 bar initial ethylene pressure, heptane as solvent, 20 mg catalyst, 1.2 mmol Et_3Al as activator. [b] *TON* was calculated as mol of carbon converted/mol Ni, after 2 h reaction. The amounts of products formed were calculated from GC-FID analysis of the reaction mixture. This number does not include the possible formation of alkenes larger than C_{20}. [c] The value is given as average of two experiments. [d] 0.7 mmol Et_3Al (Al/Ni = 70), one run. [e] Experiments performed at 25 ˚C.

reached 15 bar, reactors were switched to a batch mode and stirring of the mixtures started. Due to the stirring, part of ethylene dissolves in heptane and pressure drops to about 8 bar. Reactor loading and all manipulations with reaction mixtures were carried out under inert atmosphere to avoid decomposition of Et_3Al.

Table 6.3 shows the total number of turnovers achieved by each catalyst based on the analysed amount of liquid and gaseous products along with the selectivity to C_4, C_6 and C_{6+} olefins. While blank experiments performed with only Et_3Al or POF catalyst did not result in any conversion of ethylene, the combination of the solid catalyst and the homogenous co-catalyst was active. The obtained total number of turnovers is lower than reported for the homogeneous counterpart ((bpy)$NiBr_2$) under similar reaction conditions and reaction time [17], but for every POF based catalyst at 50 ˚C, the selectivity to higher olefins is 5 times larger than that of the homogeneous counterpart and 3 times higher than for experiments performed with the Ni@IL-PON catalyst at room temperature.

Although small increases (*i.e.* 5 or 10 percentage points) in selectivity to higher olefins have been reported upon immobilization of similar homogeneous systems [82], the much larger ones found here are remarkable. When comparing the POF based catalysts with each other, in spite of the small differences found in number of turnovers, these results are in good agreement with the textural properties of the solids: on one hand, Ni@IL-PON, in spite of containing the highest amount of Ni, displays the highest activity per atom of metal, followed by the mesoporous material and with Ni@micro-CTF being the least active. These results suggest a link between active site accessibility and catalytic performance, with the small pore material most likely suffering from internal diffusion limitations and from the fact that not all Ni has been coordinated to the N moieties (*vide supra*). On the other hand, clear differences are found in terms of selectivities: while Ni@IL-PON displays a product distribution close to a classical ASF polymerization, with selectivity decreasing with the number of carbons in the olefin, the Ni@micro-CTF sample shows higher selectivities to $C_{8=}$ than to $C_{6=}$. A similar trend, although less prominent, is found for Ni@meso-CTF. We rationalize these results on the basis of re-adsorption of products due to a slower diffusion in the micropores of both CTFs, leading to further oligomerization. In this way, $C_{4=}$ formed in the external surface region of the particles would directly desorb, while those olefins formed inside the narrow micropores will suffer from subsequent reactions leading to higher hydrocarbons. This effect is less important in case of the micro-meso catalysts, where diffusion of products will be faster than in case of micro-CTF. When compared to the literature (see Table 6.4 and references [1, 3, 17, 57, 59, 61, 71]), the selectivity of the POF based catalysts to medium chain olefins is higher than those reported for other systems based either on MOFs or silica based supports. With this comparison, one should keep in mind that experiments here reported were performed at slightly higher temperatures (50 *vs.* 20-25 °C) than in most of the references listed in Table 6.3. We intentionally chose a slightly higher temperature than that commonly used in order to have a better control over reaction conditions.

It is indeed well known that the rate of the β-H elimination displays the lowest activation energy and may become the rate limiting step at higher temperatures (see Figure 6.1), leading to higher selectivities to C_{6+} olefins and to lower overall reaction rates. [83] However, even for those cases where similar reaction temperatures were used (Table 6.4 entries 9, 10 and 12) the selectivity shown by the POF based catalysts to longer hydrocarbons

Table 6.4 Comparison of reported catalytic activity of heterogeneous catalysts for ethylene oligomerization.

Entry	Catalyst	*T* [°C]	*P* [bar]	Al/Ni	Ni [wt%]	S_{C4} [%]	S_{C6+} [%]	Reference
1	Ni@IL-PON	50	15	70	4.7	58	42	This study
2	Ni@micro-CTF	50	15	100	2.84	59	41	This study
3	Ni@meso-CTF	50	15	100	2.83	54	46	This study
4	Ni@meso-CTF	50	15	70	2.83	68	32	This study
5	Ni@IL-PON-RT	25	15	100	4.7	70	30	This study
6	Ni@MIL101	25	30	70	2	95	5	[1]
7	Ni@MOF	5	15	70	27.7	89.1	10.9	[3]
8	NU-1000-bpy-$NiCl_2$[a]	21	15	70	2.7	93	7	[17]
9	Ni@MixMOF	40	20	100	1.17	92.7	7.3	[57]
10	Ni-MFU	50	15	100	10	85.2	14.8	[58]
11	Ni(N,N)/MCM-41	25	12	5	3.5	84	5.8	[59]
12	Ni(P,P)@silica	60	10	250	n.a.	54	45	[61]

[a] Pressure was kept constant at 15 bar during the reaction.

is striking. In the same line, experiments performed with the Ni@IL-PON at room temperature (Table 6.4, entry 5) display at least a three-fold increase in selectivity to C_{6+} compared to other systems. Only in case of the wide pore silica Ni phosphine immobilized catalyst in entry 12, similarly low selectivities to $C_{4=}$ have been reported, even when these expensive P containing ligands are known to promote the formation of longer hydrocarbons [82].

The results presented so far demonstrate that the chosen POFs display catalytic performances in terms of activity not far from their homogenous counterparts and selectivities to more interesting olefins (C_{8+}) higher than for most homo- and heterogeneous catalysts reported to date based on Ni-pyridine systems. We attribute this change in selectivity to the higher affinity of the fully organic POF supports for the reaction products, that may lead

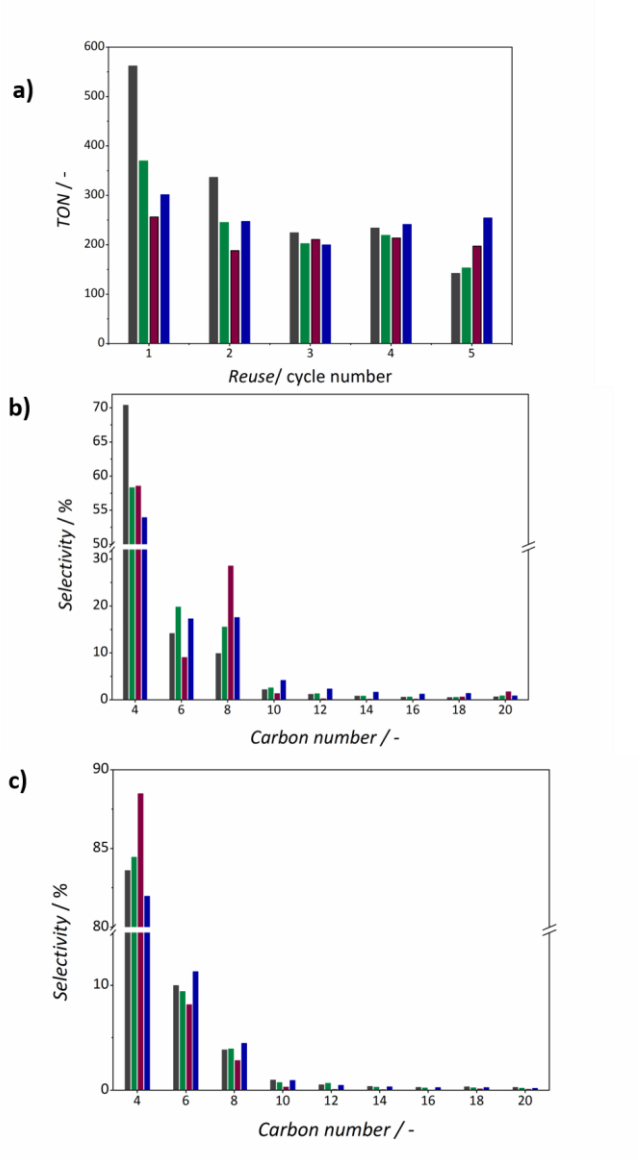

Figure 6.7. (a) Catalytic activity in ethylene oligomerization vs. number of cycles and change of selectivity vs. cycle for Ni@IL-PON (experiments performed at room temperature) (*grey*), Ni@IL-PON at 50 ˚C (*green*), Ni@micro-CTF (*red*) and Ni@meso-CTF (*blue*): (b) 1st cycle, (c) 5th cycle. Reaction conditions: 20 mL heptane solvent, 1.2 mL 1M triethylaluminium solution in heptane as co-catalyst and 20 mg catalyst. *T* = 50 ˚C; reaction time = 2 h; P_0 = 15 bar; autoclave volume = 45 mL.

to a higher surface concentration of olefins and therefore to higher chances for multiple oligomerization reactions. In order to further explore the stability of these new systems, they were re-used in consecutive catalytic runs.

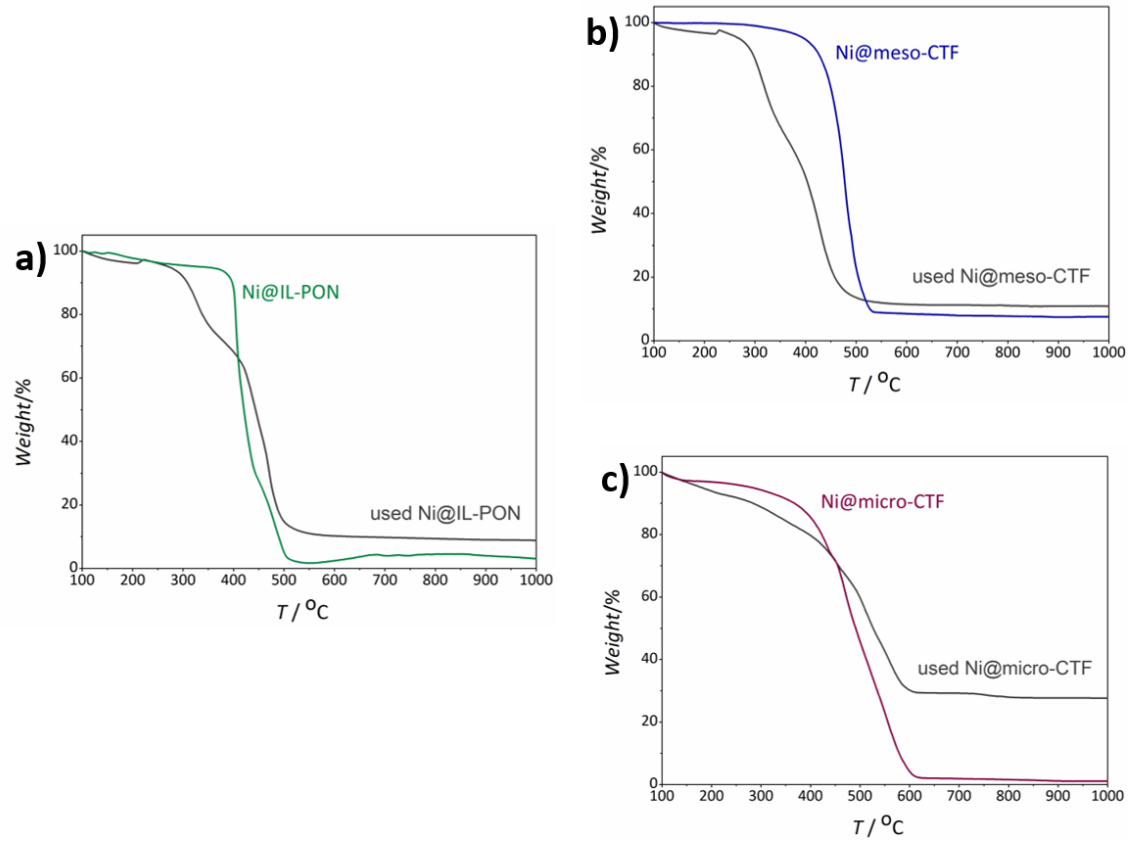

Figure 6.8. TGA analysis in air of fresh and spent catalysts after one reaction cycle. Heating rate = 2 ˚C min^{-1}

Figure 6.7 shows the changes observed in activity and selectivity over 5 consecutive runs for all catalysts. Going from the first to fifth cycle the selectivitites to butenes rises and reaches values over 80%, while the formation of $C_{8=+}$ oligomers becomes negligible for all samples. Surprisingly, both in terms of activity and selectivity, the microporous CTF catalyst is the one that shows the smallest decline. A decrease in selectivity to longer hydrocarbons along with a clear drop in catalytic activity after the first reaction cycle can be rationalized on the basis of pore blocking by either the co-catalyst or by the retention of oligomers in the porosity of the material. In order to quantify the effect of both options, we performed a thermogravimetric analysis of the spent catalysts after one reaction cycle. TGA analysis in air of spent catalysts (Figure 6.8) confirms the presence of an additional inorganic residue (attributed to a mixture of Al_2O_3 and NiO upon calcination) and the presence of carbon deposits that are combusted at circa 300 ˚C, prior to the decomposition of the organic frameworks. These carbon deposits are attributed to reaction products and ethyl groups from Et_3Al and made a proper quantification of the amount of high olefins adsorbed in the catalysts not possible.

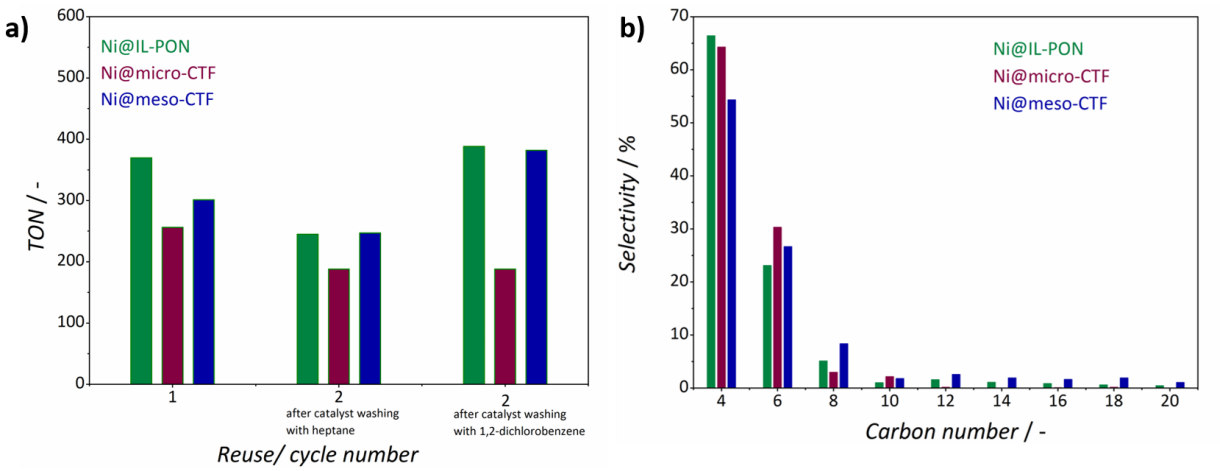

Figure 6.9. a) Effect of catalyst reactivation conditions on catalytic activity expressed as number of turnovers (*TON*) after 2 h reaction. b) Olefin selectivity after catalyst re-activation with 1,2-dichlorobenzene. Reaction conditions: 20 mL heptane solvent, 1.2 mL 1M triethylaluminium in heptane as co-catalyst and 20 mg catalyst. *T* = 50 ˚C; reaction time = 2 h; P_0 = 15 bar; autoclave volume = 45 mL.

From Figure 6.8, it is clear that the mesoporous CTF and IL-PON contain a bigger amount of adsorbed olefins. Hence, the lower decrease in performance and selectivity of the micro-CTF can be explained by the lower formation of long hydrocarbons within the porosity of the material, most likely due to the fact that most reaction takes place at the surface of the catalyst's particles. On the other hand, although Ni@meso-CTF seems to accumulate a minor amount of Al species, no clear correlation between this accumulation and the observed deactivation can be drawn at this point.

Having in mind that the observed deactivation is mostly due to the formation of long chain olefins insoluble in heptane, we performed additional experiments by recycling the catalysts with an intermediate washing step using dichlorobenzene instead of heptane. The choice of the solvent was based on the much higher solubility of long chain olefins on the aromatic solvent. When using this procedure (Figure 6.9), both mesoporous POF based catalysts (IL-PON and meso-CTF) fully recover their initial activity, while the smaller pore Ni@micro-CTF still presents a drop in activity similar to that shown after washing with heptane. Further, Ni@IL-PON and Ni@micro-CTF display a slightly higher selectivity to C_4 olefins, while Ni@meso-CTF exhibits a similar product distribution as during the first cycle. GC analysis of the *1,2*-dichlorobenzene used in the washing step demonstrated the presence of olefins up to C_{30} for all three catalysts. These results support the hypothesis that the main

reason for deactivation is strong adsorption of long chain olefins in the porosity of the different catalystsCurrent efforts are focused on the inclusion of an activator function within these scaffolds with the objective of developing a truly heterogeneous catalyst that does not require the use of alkylaluminium in solution.

6.4. CONCLUSIONS

In summary, we have explored the use of two different classes of covalent organic frameworks (covalent triazine and imine linked frameworks) as supports for molecular Ni^{2+} catalysts. A thorough XPS analysis of these materials demonstrates that the large concentration of N heteroatoms, either in the form of *quasi* bipyridine moieties or as diiminopyridine moieties, allows for the coordination of $NiBr_2$ to the scaffold of the porous polymers. Electronic effects of coordination seem to be stronger in case of the IL-PON. This fact together with the sheet like morphology of this material render catalysts with a higher concentration of Ni and activities per atom of Ni, higher than those found for the CTF based materials. Textural properties of the support have been shown to play a key role in product distribution, with meso-CTF and IL-PON displaying a higher selectivity to long chain olefins and a stronger deactivation due to the accumulation of long olefins on the catalyst under reaction conditions. Full performance of the mesoporous catalysts can be recovered upon thorough washing with dichlorobenzene.

Our results demonstrate that porous aromatic frameworks hold great promise as catalyst supports: the outstanding stability and rich design tunability of these materials, along with the possibility of including additional nitrogen atoms for the coordination of metals and their intrinsic hydrophobic nature render POFs as ideal supports for the heterogenization of molecular complexes.

6.5. REFERENCES

[1] J. Canivet, S. Aguado, Y. Schuurman, D. Farrusseng, *Journal of the American Chemical Society* **2013**, *135*, 4195-4198.

[2] A. Finiels, F. Fajula, V. Hulea, *Catalysis Science & Technology* **2014**, *4*, 2412-2426.

[3] K. Kyogoku, C. Yamada, Y. Suzuki, S. Nishiyama, K. Fukumoto, H. Yamamoto, S. Indo, M. Sano, T. Miyake, *Journal of the Japan Petroleum Institute* **2010**, *53*, 308-312.

[4] G. R. Lappin, L. H. Nemec, J. D. Sauer, J. D. Wagner, in *Kirk-Othmer Encyclopedia of Chemical Technology*, John Wiley & Sons, Inc., **2000**.

[5] C. Bianchini, G. Giambastiani, L. Luconi, A. Meli, *Coordination Chemistry Reviews* **2010**, *254*, 431-455.

[6] C. Bianchini, G. Giambastiani, I. G. Rios, G. Mantovani, A. Meli, A. M. Segarra, *Coordination Chemistry Reviews* **2006**, *250*, 1391-1418.

[7] A. Boudier, P.-A. R. Breuil, L. Magna, H. Olivier-Bourbigou, P. Braunstein, *Journal of Organometallic Chemistry* **2012**, *718*, 31-37.

[8] C. Carlini, M. Marchionna, A. M. Raspolli Galletti, G. Sbrana, *Applied Catalysis A: General* **2001**, *206*, 1-12.

[9] W. Keim, R. P. Schulz, *Journal of Molecular Catalysis* **1994**, *92*, 21-33.

[10] C. M. Killian, L. K. Johnson, M. Brookhart, *Organometallics* **1997**, *16*, 2005-2007.

[11] C. Obuah, B. Omondi, K. Nozaki, J. Darkwa, *Journal of Molecular Catalysis A: Chemical* **2014**, *382*, 31-40.

[12] B. L. Small, M. Brookhart, *Journal of the American Chemical Society* **1998**, *120*, 7143-7144.

[13] S. A. Svejda, M. Brookhart, *Organometallics* **1999**, *18*, 65-74.

[14] A. H. D. P. S. Ulbrich, R. R. Campedelli, J. L. S. Milani, J. H. Z. d. Santos, O. d. L. Casagrande Jr, *Applied Catalysis A: General* **2013**, *453*, 280-286.

[15] L. Wang, W.-H. Sun, L. Han, Z. Li, Y. Hu, C. He, C. Yan, *Journal of Organometallic Chemistry* **2002**, *650*, 59-64.

[16] W. Zhang, W.-H. Sun, C. Redshaw, *Dalton Transactions* **2013**, *42*, 8988-8997.

[17] S. T. Madrahimov, J. R. Gallagher, G. Zhang, Z. Meinhart, S. J. Garibay, M. Delferro, J. T. Miller, O. K. Farha, J. T. Hupp, S. T. Nguyen, *ACS Catalysis* **2015**, *5*, 6713-6718.

[18] D. Barthomeuf, R. Beaumont, *Journal of Catalysis* **1973**, *30*, 288-297.

[19] L. Bonneviot, D. Olivier, M. Che, *Journal of Molecular Catalysis* **1983**, *21*, 415-430.

[20] I. V. Elev, B. N. Shelimov, V. B. Kazansky, *Journal of Catalysis* **1984**, *89*, 470-477.

[21] J. Heveling, A. van der Beek, M. de Pender, *Applied Catalysis* **1988**, *42*, 325-336.

[22] M. Lallemand, A. Finiels, F. Fajula, V. Hulea, *Applied Catalysis A: General* **2006**, *301*, 196-201.

[23] A. Martínez, M. A. Arribas, P. Concepción, S. Moussa, *Applied Catalysis A: General* **2013**, *467*, 509-518.

[24] F. T. T. Ng, D. C. Creaser, in *Studies in Surface Science and Catalysis, Vol. Volume 73* (Eds.: J. S. Kevin, C. S. Emerson), Elsevier, **1992**, pp. 123-131.

[25] F. T. T. Ng, D. C. Creaser, *Applied Catalysis A: General* **1994**, *119*, 327-339.

[26] J. R. Sohn, J. H. Park, *Applied Catalysis A: General* **2001**, *218*, 229-234.

[27] T. Yashima, Y. Ushida, M. Ebisawa, N. Hara, *Journal of Catalysis* **1975**, *36*, 320-326.

[28] M. O. de Souza, L. R. Rodrigues, H. O. Pastore, J. A. C. Ruiz, L. Gengembre, R. M. Gauvin, R. F. de Souza, *Microporous and Mesoporous Materials* **2006**, *96*, 109-114.

[29] M. Hartmann, A. Pöppl, L. Kevan, in *Studies in Surface Science and Catalysis, Vol. Volume 101* (Eds.: W. N. D. E. I. Joe W. Hightower, T. B. Alexis), Elsevier, **1996**, pp. 801-809.

[30] V. Hulea, F. Fajula, *Journal of Catalysis* **2004**, *225*, 213-222.

[31] A. Lacarriere, J. Robin, D. Świerczyński, A. Finiels, F. Fajula, F. Luck, V. Hulea, *ChemSusChem* **2012**, *5*, 1787-1792.

[32] M. Lallemand, A. Finiels, F. Fajula, V. Hulea, in *Studies in Surface Science and Catalysis, Vol. Volume 170* (Eds.: Z. G. J. C. Ruren Xu, Y. Wenfu), Elsevier, **2007**, pp. 1863-1869.

[33] M. Lallemand, A. Finiels, F. Fajula, V. Hulea, *Chemical Engineering Journal* **2011**, *172*, 1078-1082.

[34] M. Lallemand, O. A. Rusu, E. Dumitriu, A. Finiels, F. Fajula, V. Hulea, in *Studies in Surface Science and Catalysis, Vol. Volume 174, Part B* (Eds.: P. M. Antoine Gédéon, B. Florence), Elsevier, **2008**, pp. 1139-1142.

[35] M. Lallemand, O. A. Rusu, E. Dumitriu, A. Finiels, F. Fajula, V. Hulea, *Applied Catalysis A: General* **2008**, *338*, 37-43.

[36] S. Lin, L. Shi, H. Zhang, N. Zhang, X. Yi, A. Zheng, X. Li, *Microporous and Mesoporous Materials* **2014**, *184*, 151-161.

[37] T. Cai, *Catalysis Today* **1999**, *51*, 153-160.

[38] T. Cai, D. Cao, Z. Song, L. Li, *Applied Catalysis A: General* **1993**, *95*, L1-L7.

[39] W. Hua, Y. Xia, Y. Yue, Z. Gao, *Journal of Catalysis* **2000**, *196*, 104-114.

[40] C. Sohn J. R.; Park W, *Nickel sulfate supported on γ-Al[2]O[3] for ethylene dimerization, Vol. 133*, Elsevier, Amsterdam, PAYS-BAS, **1998**.

[41] J. R. Sohn, E. S. Cho, *Applied Catalysis A: General* **2005**, *282*, 147-154.

[42] J. R. Sohn, S. H. Lee, *Applied Catalysis A: General* **2007**, *321*, 27-34.

[43] J. R. Sohn, W. C. Park, *Applied Catalysis A: General* **2003**, *239*, 269-278.

[44] J. R. Sohn, W. C. Park, H. W. Kim, *Journal of Catalysis* **2002**, *209*, 69-74.

[45] J. P. Hogan, R. L. Banks, W. C. Lanning, A. Clark, *Industrial & Engineering Chemistry* **1955**, *47*, 752-757.

[46] A. V. Lavrenov, E. A. Buluchevskii, M. A. Moiseenko, V. A. Drozdov, A. B. Arbuzov, T. I. Gulyaeva, V. A. Likholobov, V. K. Duplyakin, *Kinetics and Catalysis* **2010**, *51*, 404-409.

[47] J. R. Sohn, H. J. Kim, *Journal of Catalysis* **1986**, *101*, 428-433.

[48] J. R. Sohn, H. W. Kim, M. Y. Park, E. H. Park, J. T. Kim, S. E. Park, *Applied Catalysis A: General* **1995**, *128*, 127-141.

[49] J. R. Sohn, S. H. Kwon, D. C. Shin, *Applied Catalysis A: General* **2007**, *317*, 216-225.

[50] J. R. Sohn, S. Y. Lee, *Applied Catalysis A: General* **1997**, *164*, 127-140.

[51] J. R. Sohn, D. C. Shin, *Journal of Catalysis* **1996**, *160*, 314-316.

[52] R. L. Espinoza, C. P. Nicolaides, C. J. Korf, R. Snel, *Applied Catalysis* **1987**, *31*, 259-266.

[53] R. L. Espinoza, R. Snel, C. J. Korf, C. P. Nicolaides, *Applied Catalysis* **1987**, *29*, 295-303.

[54] J. Heveling, C. P. Nicolaides, *Catalysis Letters* **2006**, *107*, 117-121.

[55] J. Heveling, C. P. Nicolaides, M. S. Scurrell, *Applied Catalysis A: General* **1998**, *173*, 1-9.

[56] M. D. Heydenrych, C. P. Nicolaides, M. S. Scurrell, *Journal of Catalysis* **2001**, *197*, 49-57.

[57] B. Liu, S. Jie, Z. Bu, B.-G. Li, *RSC Advances* **2014**, *4*, 62343-62346.

[58] E. D. Metzger, C. K. Brozek, R. J. Comito, M. Dincă, *ACS Central Science* **2016**, *2*, 148-153.

[59] E. Angelescu, M. Che, M. Andruh, R. Zăvoianu, G. Costentin, C. Miricã, O. Dumitru Pavel, *Journal of Molecular Catalysis A: Chemical* **2004**, *219*, 13-19.

[60] Z. Ye, H. Alsyouri, S. Zhu, Y. S. Lin, *Polymer* **2003**, *44*, 969-980.

[61] D. Schaarschmidt, J. Kühnert, S. Tripke, H. G. Alt, C. Görl, T. Rüffer, P. Ecorchard, B. Walfort, H. Lang, *Journal of Organometallic Chemistry* **2010**, *695*, 1541-1549.

[62] E. Rossetto, M. Caovilla, D. Thiele, R. F. de Souza, K. Bernardo-Gusmão, *Applied Catalysis A: General* **2013**, *454*, 152-159.

[63] S. M. Alshehri, T. Ahamad, A. Aldalbahi, N. Alhokbany, *Advances in Polymer Technology* **2016**, *35*, n/a-n/a.

[64] L. Zhang, E. Castillejos, P. Serp, W.-H. Sun, J. Durand, *Catalysis Today* **2014**, *235*, 33-40.

[65] H. Kurokawa, M. Matsuda, K. Fujii, Y. Ishihama, T. Sakuragi, M.-a. Ohshima, H. Miura, *Chemistry Letters* **2007**, *36*, 1004-1005.

[66] K. Fujii, Y. Ishihama, T. Sakuragi, M.-a. Ohshima, H. Kurokawa, H. Miura, *Catalysis Communications* **2008**, *10*, 183-186.

[67] T. Kondo, K. Yamamoto, T. Sakuragi, H. Kurokawa, H. Miura, *Chemistry Letters* **2012**, *41*, 461-463.

[68] H. Kurokawa, K. Miura, K. Yamamoto, T. Sakuragi, T. Sugiyama, M.-a. Ohshima, H. Miura, *Catalysts* **2013**, *3*.

[69] H. Kurokawa, M. Hayasaka, K. Yamamoto, T. Sakuragi, M.-a. Ohshima, H. Miura, *Catalysis Communications* **2014**, *47*, 13-17.

[70] R. Malgas-Enus, S. F. Mapolie, *Inorganica Chimica Acta* **2014**, *409, Part A*, 96-105.

[71] S. Liu, Y. Zhang, Q. Huo, S. He, Y. Han, *Journal of Spectroscopy* **2015**, *2015*, 7.

[72] F. Speiser, P. Braunstein, L. Saussine, *Accounts of Chemical Research* **2005**, *38*, 784-793.

[73] Z. Boudene, A. Boudier, P.-A. R. Breuil, H. Olivier-Bourbigou, P. Raybaud, H. Toulhoat, T. de Bruin, *Journal of Catalysis* **2014**, *317*, 153-157.

[74] A. de la Peña Ruigómez, D. Rodríguez-San-Miguel, K. C. Stylianou, M. Cavallini, D. Gentili, F. Liscio, S. Milita, O. M. Roscioni , M. L. Ruiz-González, C. Carbonell, D. Maspoch, R. Mas-Ballesté, J. L. Segura, F. Zamora, *Chemistry – A European Journal* **2015**, *21*, 10666-10670.

[75] A. V. Bavykina, M. G. Goesten, F. Kapteijn, M. Makkee, J. Gascon, *ChemSusChem* **2015**, *8*, 809-812.

[76] F. J. Uribe-Romo, J. R. Hunt, H. Furukawa, C. Klöck, M. O'Keeffe, O. M. Yaghi, *Journal of the American Chemical Society* **2009**, *131*, 4570-4571.

[77] M. F. de Lange, L.-C. Lin, J. Gascon, T. J. H. Vlugt, F. Kapteijn, *Langmuir* **2016**.

[78] A. V. Bavykina, E. Rozhko, M. G. Goesten, T. Wezendonk, B. Seoane, F. Kapteijn, M. Makkee, J. Gascon, *ChemCatChem* **2016**, *8*, 2217-2221.

[79] J. Matienzo, L. I. Yin, S. O. Grim, W. E. Swartz, *Inorganic Chemistry* **1973**, *12*, 2762-2769.

[80] K. Artyushkova, B. Kiefer, B. Halevi, A. Knop-Gericke, R. Schlogl, P. Atanassov, *Chemical Communications* **2013**, *49*, 2539-2541.

[81] M. Soorholtz, L. C. Jones, D. Samuelis, C. Weidenthaler, R. J. White, M.-M. Titirici, D. A. Cullen, T. Zimmermann, M. Antonietti, J. Maier, R. Palkovits, B. F. Chmelka, F. Schüth, *ACS Catalysis* **2016**, *6*, 2332-2340.

[82] G. A. Nesterov, V. A. Zakharov, G. Fink, W. Fenzl, *Journal of Molecular Catalysis* **1991**, *69*, 129-136.

[83] R. Gao, M. Zhang, T. Liang, F. Wang, W.-H. Sun, *Organometallics* **2008**, *27*, 5641-5648.

SUMMARY AND OUTLOOK

This thesis focuses on the development of functional Porous Organic Frameworks (POFs) for various catalytic applications. POF supported molecular catalysts allow to combine the advantages of both homogeneous and heterogeneous catalysts, offering excellent prospects in the quest to heterogenize homogeneous catalysts. The framework tunability of POFs can be used to obtain an optimal catalytic performance, while the fully heterogeneous character of the POFs allow easy handling and recycling. In some cases, they may even directly participate in the catalytic cycle by activating substrates.

Chapter 1 introduces the reader into the subject of the thesis, giving general information of different types of POFs, their classification, nomenclature and synthesis, together with a comprehensive overview of the state-of-the-art in POF-based catalysts. The POFs classification is based on their crystallinity and other properties, e.g. porosity, level of crosslinking and other. The review on current progress in developing POFs based catalysts is split in two subparts depending on the approach employed for a catalyst synthesis: "bottom-up" one, where catalytically active molecular site is already present in a building block, or a post-synthetic approach, where a metal complex is immobilised on a framework comparable to a pendant to a necklace.

Chapter 2 describes the synthesis and characterisation of two new POF based acid catalysts. Porous aromatic frameworks were synthesized through the Pd^{II}-catalyzed Suzuki–Miyaura coupling of commercially available building blocks – benzene-1,4-diboronic acid and 1,3,5-tris(4-bromophenyl)benzene or tris(4-bromophenyl)amine to obtain catalysts **1** and **2,** respectively. Although the resulting polymers are not crystalline, they are highly stable and chemically tunable. The frameworks were used as supports for acidic functionalities. The sulfonation procedure led to swelling – a significant increase in porosity, so the initially microporous materials showed a 250% increase in specific surface area. Compared to state-of-the-art Amberlyst-15, sulfo-**1** displayed a higher activity per sulfonic acid moiety in a simple esterification reaction. Catalyst sulfo-**2** showed a slightly lower activity, which was attributed to the interplay between diffusion and polarity. Both polymers showed a higher stability than Amberlyst-15: the commercial catalyst can be only used at temperatures below 120 ˚C, the sulfonic acid groups in the sulfonated PAFs do not decompose up to ~240 ˚C.

In Chapter 3, a heterogeneous molecular catalyst for formic acid dehydrogenation based on $Ir^{III}Cp^*$ attached to a Covalent Triazine Framework is presented. A mesoporous CTF was employed as catalyst support. The obtained CTF based molecular heterogeneous catalyst has an outstanding performance in hydrogen production from formic acid, achieving *TOFs* as high as 27000 h^{-1} in the case of the catalyst with Ir loading of 0.2 wt.%. A very important aspect that has to be underlined is that the system did not require a use of additional base, usually necessary for formic acid activation – the first step of the catalytic cycle. The framework possesses pyridine building blocks, and pyridine itself is known to be able to activate formic acid. Therefore, CTF itself works as a non-innocent ligand, providing the basicity needed for the first catalytic step.

Chapter 4 describes an engineering approach to formulate the mesoporous CTF based catalyst into a spherical-composite *via* phase-inversion. Covalent Triazine Frameworks were shaped into spherical particles without losing their properties – high thermal stability, porosity, and the possibility of coordinating organometallic moieties. $Ir^{III}Cp^*$ was immobilized through coordination within the CTF spheres to render a molecular yet heterogeneous, stable catalyst which is easy to handle and to recycle in the carbon dioxide hydrogenation to formic acid. EDX analysis indicated that most of the Ir was located on the surface of the sphere, that was found to be denser than the inner part. The performance of sphere-based catalyst in carbon dioxide hydrogenation was found to be lower than the powder version, which is attributed to the lower porosity of the obtained composite. However, the spheres-based catalyst outperforms the sticky powdery system in handling and recyclability, without loss of material through consecutive runs.

Chapter 5 deals further with the formulation engineering of this catalyst, describing a new methodology to manufacture CTF films. Such coatings were successfully deposited on the surface of cordierite monoliths, resulting in a homogeneous stable film on the interior walls of the monolith channels. The obtained material was proven to have the same nature as CTF in the form of powder. Two CTFs with different types of porosity (micro- and mesoporous) were explored. After the coordination of iridium complex, the obtained catalyst Ir@CTF@monolith was employed in the reaction of hydrogen production from formic acid. The obtained *TOF*s are as high as 207 200 h^{-1}, demonstrating a much better catalyst utilization through engineering at different length scales, resulting in improved internal and external

mass transport. During recycling all Ir@CTF catalysts were filtered and stored under ambient conditions, no extra precaution or pre-treatment was required.

Chapter 6 reports on a range of new Ni based catalysts supported on CTF and IL-PON solids for the oligomerization of ethylene to long chain olefins. In this work, the influence of the support on reaction selectivity is extensively discussed. Textural properties of the support are shown to play a key role in product distribution, with meso-CTF and IL-PON displaying a higher selectivity to long chain olefins and a stronger deactivation due to the accumulation of organics on the catalyst under reaction conditions.

Overall, the results presented in this thesis demonstrate that POFs hold great promise as catalyst supports. POFs fulfil most of the requirements one aims for when developing a catalyst; they possess a high specific surface area, a tunable pore size and have adjustable skeletons. POFs hold outstanding stability and rich design tunability – by simple variation of building units, framework's properties can be adjusted to the desired ones. Last but not least, different molecular complexes can be anchored to POF scaffolds, opening the door to the rational design of a wide range of heterogeneous molecular catalysts.

It has to be noted, that POFs' synthesis is not undemanding. Sealing glass ampoules for CTFs, noble metal catalyst for PAFs obtained *via* Suzuki-Miyaura approach, generally high temperatures and extensive multistep washing are accompanying every synthesis. Synthesis optimisation has never stopped in this field, and still more attention has to be paid to it.

While classical adsorption techniques have proven their importance, in future, the development of new catalytic system should go hand by hand with the application of advanced characterization techniques. As highlighted along this Thesis, POFs characterisation is very often not straightforward. For instance, the amorphous nature of many POFs along with their usually black colour due to conjugation make the use of classical characterization techniques such as X-ray diffraction or infra-red spectroscopies extremely challenging. Hence, other methods have to be applied, and Solid State NMR, SAXS and PDF seem most promising tools. These three techniques, without requiring crystallinity, provide valuable information at different length-scales, from the atomic to the meso-level. NMR is one of the most powerful techniques for studying structural properties for both ordered and disordered materials. For instance, multidimensional NMR can provide the information about atoms connectivity within a framework, which can help to solve some obscurities. On top of that, solid-state NMR

spectroscopy can deliver information about guest molecules located within pores as well as to gain the insight into the immobilization of a catalyst on the surface of a framework. SAXS is a technique currently gaining more and more attention in the field of porous solids. With SAXS it is possible to measure the closed and molecular sized pores, which cannot be detected by sorption techniques. Finally, the pair distribution function (PDF) can be used to study the local structure of liquids, glasses and disordered crystalline materials, delivering both chemical and spatial information.

Engineering of a catalyst is an important aspect elaborated in this Thesis. Catalyst shaping is often discarded in academic research, while aiming for an economically viable process strong attention should be paid to it instead. In this Thesis, it was shown how shaping affects the performance – activity and recycling. A composite material, described in the Chapter 4, solves a problem of powder handling, while a price was paid in terms of obtained *TON*s. The monolith based catalyst (Chapter 5) showed the highest *TOF*s for hydrogen production from formic acid, showing the importance of improving the accessibility of catalytically active sites for substrates. As one would expect, the improved mass transfer to a thin accessible film of CTF based catalyst results in outperforming its powder counterpart. Here more research has to be done in optimising a coating. (*Quasi*-) Chemical Vapour Deposition may open a door to obtaining sustainable CTF based heterogeneous catalysts.

POFs, being in general more stable than the majority of Metal Organic Frameworks and more tunable than zeolites, are a very stable and attractive platform for developing new functional solids. The field is currently growing and it is easy to foresee a rapid further development in the coming decade.

SAMENVATTING EN VOORUITZICHTEN

Dit proefschrift richt zich op de ontwikkeling van Porous Organic Frameworks (POFs) voor de toepassing als katalysator in verschillende chemische reacties. Moleculaire katalysatoren op basis van POFs combineren de voordelen van heterogene en homogene katalysatoren. Deze combinatie biedt ongekende mogelijkheden voor de verankering van homogene katalysatoren. De structuur van POFs biedt chemische veelzijdigheid om katalytische eigenschappen te variëren, terwijl het heterogene karakter van de POFs gebruik en hergebruik vergemakkelijkt. In bepaalde gevallen kan de POF zelfs reactanten activeren.

Het onderwerp en de context van het proefschrit worden in hoofdstuk 1 uiteengezet. Hier worden de verschillende POF-types met hun klassificatie, nomenclatuur en synthese besproken. Ook worden de laatste ontwikkelingen van deze materialen als katalysator kort doorgenomen. De klassificatie van POFs is gebaseerd op de kristalliniteit en andere fysische eigenschappen, zoals porositeit, netwerk, enz. De POF-katalysatoren worden verdeeld in twee onderdelen, die afhangen van de manier waarop zij zijn gesynthetiseerd: enerzijds bestaat er een “bottom-up” benadering, waarin katalytisch-moleculaire eigenschappen vooraf worden aangebracht in de (moleculaire) bouwstenen van de POF, anderzijds kan men kiezen voor post-synthetische modificatie, waarin katalytische complexen in een vooraf gesynthetiseerde POF worden verankerd.

Hoofdstuk 2 beschrijft de synthese en karakterisering van twee nieuwe POF- vastzure-katalysatoren. Het betreft twee materialen die via Pd^{II}-gekatalyseerde Suzuki-Miyaura koppeling uit commercieel verkrijgbare bouwstenen worden gemaakt. Deze bouwstenen zijn enerzijds 1-4-diboorzuur benzeen, en anderzijds hetzij 1,3,5-tris(4-bromophenyl)benzeen hetzij tris(4-bromophenyl)amine. Deze twee materialen worden als **1** of **2** aangeduid. Alhoewel deze POFs niet kristallijn zijn, zijn ze zeer stabiel en chemisch te functionaliseren. De structuren worden vervolgens gebruikt om middels sulfonering zuur-katalytische eigenschappen aan te brengen. De sulfoneringsprocedure leidt tot zwelling van de materialen, hetgeen de porositeit significant verhoogt; een toename van 250%. Vergeleken met de commerciële katalysator “Amberlyst-15”, doet **sulfo**-**1** (de gesulfoneerde versie van **1**) het beter in de verestering. **Sulfo-2** is ietwat minder actief, wat aan een wisselwerking van diffusie en polariteit toegeschreven kan worden. Beide polymeren blijven katalytisch stabiel

tot temperaturen van 240 ˚C en zijn daarmee stabieler dan Amberlyst-15 (maximale werktemperatuur tot 120 ˚C).

In hoofdstuk 3 wordt een heterogene, moleculaire katalysator beschreven, die gebaseerd is op $Ir^{III}Cp^*$, gecomplexeeerd aan een mesoporeuze Covalent Triazine Framework (CTF). Deze katalysator is actief in de dehydrogenering van mierenzuur. De katalytische prestatie van deze Ir-CTF-katalysator, met 0.2 gewichtsprocent aan iridium (Ir), in de productie van waterstof en kooldioxide uit mierenzuur is fenomenaal met zijn 27000 moleculaire omzettingen per uur per katalytisch complex. Een zeer belangrijk aspect dat benadrukt moet worden, is dat dit katalytische systeem geen base nodig heeft. Normaal gesproken wordt voor deze reactie een sterke base toegevoegd om de eerste stap te initiëren – in de omzetting van mierenzuur. De reden dat geen base nodig is heeft te maken met het feit dat het CTF rooster zelf deze basische een rol in de katalytische cyclus voor zijn rekening neemt; deze CTF structuur bevat pyridine-eenheden met de gewenste basische eigenschap.

Hoofdstuk 4 behandelt een opschalingsmethode om de mesoporeuze CTF-katalysator uit hoofdstuk 3 in een bolvormige composiet om te zetten door middel van een fase-inversie methode.. Deze omzetting naar bolletjes ging niet ten koste van de nuttige eigenschappen van de CTF - hoge stabiliteit, porositeit, en de mogelijkheid om organometaalverbindingen te coördineren. $Ir^{III}Cp^*$ werd vervolgens aan de CTF bolletjes gecomplexeerd. Dit levert een stabiele, katalysator die gemakkelijk afgescheiden en hergebruikt kan worden in de hydrogenering van koolstofdioxide naar mierenzuur. EDX analyse liet echter zien dat het merendeel van het iridium zich op het buitenoppervlak van deze bolletjes bevindt. De activiteit van deze bolvormige katalysator in de hydrogenering van koolstofdioxide, was lager dan die van van het uitgangs-CTF poeder. Dit wordt aan de lagere porositeit van het composietmateriaal toegeschreven. De bolvormige katalysator is echter een stuk beter hanteerbaar en makkelijker in hergebruik. Er is geen verlies aan materiaal in tegenstelling tot het gebruik van het plakkerige CTF poeder.

Hoofdstuk 5 gaat een stap verder met het vormgeven van dezelfde CTF-katalysator. Een nieuwe methodologie wordt geïntroduceerd waarmee een dunne filmlaag van dit polymeer geproduceerd kan worden op het oppervlak van cordieriet monolieten. Deze laag heeft dezelfde moleculaire structuur als het originele CTF poeder, echter met een veel betere toegankelijkheid van de katalytisch actieve plaatsen. Twee verschillende CTF materialen met verschillende porositeit (micro- en mesoporositeit) zijn onderzocht. Na de coördinatie van

$Ir^{III}Cp^*$, werd het systeem getest in de productie van waterstof uit mierenzuur. De katalytische omzetting, per uur en per katalytische plaats, bedraagt ruim 207200. Dit laat zien dat deze katalysatorfilm een stuk beter werkt dan de composietbolletjes beschreven in hoofdstuk 4 door het optimaliseren van de verschillende lengteschalen, resulterend in een verbeterd in- en uitwendig massatransport. Deze katalysator heeft verder als sterk voordeel dat er geen speciale omstandigheden voor opslag en gebruik nodig zijn.

In hoofdstuk 6 wordt een serie nieuwe, op nikkel gebaseerde katalysatoren geïntroduceerd, met CTF en IL-PON als dragermaterialen. Deze vaste katalysatoren zijn gebruikt voor de oligomerisatie van etheen naar lange olefineketens. Het hoofdstuk behandelt specifiek de invloed van de structuur op de katalytische selectiviteit in de reactie. De structuureigenschappen spelen een sleutelrol in de uiteindelijke productdistributie. Katalysatoren gebaseerd op meso-poreus CTF en IL-PON gaven de hoogste selectiviteiten , maar deze materialen deactiveerden ook het snelst door de ophoping van organische verbindingen op de katalysator gedurende de reactie.

Concluderend kan gesteld worden dat POFs zoals beschreven in dit proefschrift veelbelovende materialen voor katalysetoepassingen zijn. POFs bezitten veel van de eigenschappen die men van een katalysator wenst: een hoge porositeit met aanpasbare poriegroottes en een hiërarchische structuur. Verder zijn POFs zeer stabiel en bieden mogelijkheden tot design door het variëren van de bouwstenen. Tenslotte kunnen POF-structuren verschillende moleculaire complexen binden, wat de mogelijkheid biedt om nieuwe heterogene moleculaire katalysatoren te ontwerpen.

De synthese van POFs is niet triviaal. Het afsluiten van glazen ampullen voor CTF's, het gebruik van katalysatoren gebaseerd op edelmetalen voor PAFs via de Suzuki-Miyaura methode, de over het algemeen hoge temperaturen, en een uitgebreide purificatieprocedure begeleiden elke synthese. Optimalisatie van syntheseroutes betreft een veld in ontwikkeling, en een veld wat nog zeker meer aandacht verdient.

Klassieke adsorptietechnieken hebben hun waarde als textuurkarakteriseringsmethode bewezen, maar de ontwikkeling van nieuwe katalytische systemen zal in de toekomst hand in hand moeten gaan met nieuwe karakteriseringstechnieken. Karakteriseren van POFs is niet eenvoudig. Het amorfe karakter van veel POFs, alsmede het feit dat ze zwart zijn, bemoeilijkt toepassing van klassieke karakteriseringatietechnieken, zoals röntgendiffractie of infraroodspectroscopie. Daarom

zullen andere methodes goed van pas komen, zoals vaste-stof NMR, SAXS en PDF. Deze technieken vereisen niet dat het materiaal kristallijn is, en leveren informatie over de structuur op verschillende lengteschalen – van atomair tot mesoscopisch. NMR is een van de meest krachtige technieken in het bestuderen van zowel moleculair geordende als ongeordende materialen. Multidimensionele NMR, bijvoorbeeld, kan informatie bieden over de locale ordening rond atomen binnen een structuur. Bovendien kan vaste-stof NMR informatie bieden over gastmoleculen die binnen de poriën aanwezig zijn, en inzicht bieden in het complexeringsproces bij het aanbrengen van katalysator op het oppervlak. Verder is SAXS een techniek die momenteel toenemende aandacht krijgt op het gebied van poreuze materialen. Het is met SAXS mogelijk gesloten poriën en zeer kleine poriën van moleculaire dimensies te analyseren, iets wat niet mogelijk is met adsorptie technieken. Tenslotte moet PDF vermeld worden, wat gebruikt kan worden om de locale structuur van vloeistoffen, glasachtige en ongeordende structuren te beschrijven, waaruit zowel chemische als ruimtelijke informatie verkregen kan worden..

Het ontwerp van een katalysator is, zoals omschreven in dit proefschrift, een essentieel aspect in de ontwikkeling, Het naar de hand zetten van de morfologie van een katalysator wordt weinig onderzocht, terwijl dit cruciaal is in het ontwikkelen van een economisch rendabel proces. Dit proefschrift laat zien hoe de morfologie een belangrijke rol speelt in de activiteit en bruikbaarheid van katalysatoren. Een composiet, zoals omschreven in hoofdstuk 4, lost het probleem op wat een poedervorming materiaal met zich meebrengt, alhoewel deels ten koste van totale activiteit. Echter, de katalysator aangebracht als een dunne laag op de wanden van een monolietstructuur (hoofdstuk 5) liet uiteindelijk de hoogste activiteit in waterstofproductie zien. Dit laat zien hoe belangrijk de toegankelijkheid van actieve plaatsen is. Zoals te verwachten, is het massatransport naar en in een dunne laag een stuk beter dan een poeder van samengeklonterde agglomeraten. In dit verband is er nog veel werk te doen. (Quasi) Chemical Vapour Deposition zou een nieuwe mogelijkheid kunnen bieden in de ontwikkeling van duurzame heterogene katalysatoren gebaseerd op CTF's.

POF's zijn in het algemeen stabieler dan het merendeel van de Metal-Organic Frameworks, en veelzijdiger te functionaliseren dan zeolieten. Daarmee zijn POF's een aantrekkelijk platform voor het ontwikkelen van nieuwe functionele materialen. Op het moment van schrijven is het veld van deze POF's groeiende, en naar verwachting zal er in het komende decennium een indrukwekkende ontwikkeling plaatsvinden.

ACKNOWLEDGEMENTS

All in all, here I am – writing the final, acknowledging text of this book. Though you expect it, I won't say it was "tough and long way". I enjoyed it. It was a beautiful, fascinating part of my life. Doing a PhD includes not only research. It is a lot about self-development. I came to the group like a frightened Bambi, but became wiser, calmer and assertive. May be. But these truly amazing transformation of me happened because of the people I met through these four years.

Freek, thank you so much for letting me being a part of this. Part of the group, of catalysis engineering, of the Pore meetings, of those scientific discussions we had. Your penetrating look and the wise smile have challenged me a lot throughout my PhD, and this was a significant part of my scientific development.

Michiel, thank you for your support, for the discussions we had. Thank you for being not fully convinced all the time, it gave me motivation to go deeper in my research.

Jorge, thank you isn't enough for all of your support and understanding. Working under your encouraging and inspiring supervision was a greatly valued experience for me. I have learnt a lot from you.

Canan, Dima and Francesc, my dear officemates, thank you for our nice time in the 0.420 office, where we were sharing sweets, happiness and frustrations. The girls from the official Catalysis Crochet Club are also gratefully acknowledged for a very efficient mental and physical therapy. Edu, your part of the group teambuilding cannot be overestimated, thank you for keeping our Friday Drinks tradition alive. Alyona, never imagined 11 years ago, when we just met for the first time, that we will have a paper together under TU Delft affiliation! Alla, thank you for being you, I am so happy to find such a friend. Irina! Hashtag #instagram, #onlineshopping and #lets_finally_mix_zeolites_and_ctf. Thank you for being my pillow for four years. Alexey, I will always remember our discussions about literature, movies and very "deep philosophical matters". My "new building" officemates, it was a pleasure to share that cosy openspace with you; Adrian, finally soon you can take over my chair. Ina, I hope once we will run 10 more kilometres together. Robert, thank you for tolerating my humour, good luck with that nasty black powder. I would like to thank people with whom I collaborated on scientific papers – Agi, Alma, Beba, Dima, Elena, Martijn, Tim, I enjoyed that experience. I would also like to thank my students Ivo, Jasper, Zixian, Haiyue and Rahul. It was a pleasure to be your supervisor. Dear Els and Caroline, I am very grateful for your help with all these bureaucratical issues. Bart, Harrie, Willy and Kevin, thank you for making the labwork easier for us. And warm hugs to every person in the CE group.

My parents and sister, thank you for supporting me with my decisions. We are not used to express emotions like this, so two lines of text here is enough.

And the biggest heartiest thank you goes to you, Maarten. This all would never happen without your faith and support. Because of you, science for me does not stop at the moment I leave the lab, it continues during an evening, dinner and a dream or nightmare. But it is because of you I developed such a passion towards it and I feel like continue doing it. And I can't lose this opportunity to tease you here with "there is chemistry between us".

Nastya.

LIST OF PUBLICATIONS

1. M.G. Goesten, A. Sceszeny, M. De Lange, **A.V. Bavykina**, K.B.S. Sankar-Gupta, F. Kapteijn and J. Gascon.
   Sulfonation of two new ultrastable porous aromatic polymers: high catalytic activities and remarkable sorption properties.
   ChemCatChem 8 (2016) 961-967

2. **A.V. Bavykina**, M.G. Goesten, M. Makkee, F. Kapteijn and J. Gascon
   Efficient production of hydrogen from formic acid using Covalent Triazine Framework supported molecular catalyst.
   ChemSusChem 8 (2015) 809-812

3. **A.V. Bavykina**, E. Rozhko, M.G. Goesten, T. Wezendonk, B. Seoane, F. Kapteijn, M. Makkee and J. Gascon.
   Shaping Covalent Triazine Framework for the Hydrogenation of Carbon Dioxide to Formic Acid
   ChemCatChem 13 (2016) 2217-2221 *Cover Picture*

4. E. Rozhko, **A.V. Bavykina**, D. Osadchii, M. Makkee, and J. Gascon
   Covalent organic frameworks as supports for a molecular Ni based ethylene oligomerization catalyst for the synthesis of long chain olefins.
   Journal of Catalysis 345 (2017) 270-280

5. M.G. Goesten, M.F de Lange, A. I. Olivos-Suarez, **A.V. Bavykina**, P. Serra-Crespo, C. Krywka, F.M. Bickelhaupt, F. Kapteijn and J. Gascon.
   Evidence for a chemical clock in oscillatory formation of UiO-66.
   Nature Communications 7 (2016) 1-8

6. S.M.J. Rogge, **A. Bavykina**, J. Hajek, H. Garcia, A. Olivos, A. Sepúlveda-Escribano, A. Vimont, G. Clet, P. Bazin, F. Kapteijn, M. Daturi, E. V. Ramos-Fernandez, F.X. Llabrés i Xamena, V. Van Speybroeck, and J. Gascon.
   Metal-organic and covalent organic frameworks as single-site catalysts
   Chemical Society Reviews, accepted

7. X. Sun, A. Olivos, L. Oar Arteta, E. Rozhko, D. Osadchii, **A. Bavykina**, F. Kapteijn, and J. Gascon.
   Metal-Organic-Framework Mediated Cobalt/N-Doped Carbon Hybrids as Efficient and Chemoselective Catalysts for the Hydrogenation of Nitroarenes.
   ChemCatChem, accepted

8. **A.V. Bavykina**, A. Olivos, D. Osadchii, R. Valecha, R. Franz, M. Makkee, F. Kapteijn, and J. Gascon.
   A facile method for the preparation of Covalent Triazine Framework Based Monoliths – applications in C_1 catalysis
   submitted

9. A. Álvarez, A. Bansode, A. Urakawa, **A. V. Bavykina**, T. Wezendonk, M. Makkee, J. Gascon, and Freek Kapteijn.
Strategies for the design of heterogeneous catalysts for the direct hydrogenation of carbon dioxide to formate/formic acid, methanol and dimethyl ether.
Chemical Reviews, submitted

10. **A.V. Bavykina**, H. -H. Mautscke, M. Makkee, F. Kapteijn, J. Gascon, and F. X. Llabrés i Xamena.
Base Free Transfer Hydrogenation using a Covalent Triazine Framework Based Catalyst.
in preparation

11. D. Osadchii, **A.V. Bavykina**, A. Olivos, and J. Gascon
Revisiting Nitrogen Sites in Covalent Triazine Frameworks with XPS
in preparation

ORAL PRESENTATIONS AT CONFERENCES

1. *Porous Polymers as Heterogeneous Catalysts*
Dutch Zeolite Association (DZA), Ghent, Belgium, October 2014

2. *Reversible hydrogen storage using CO_2 and a heterogeneous iridium catalyst*
NCCC-XVI, Noordwijkerhout, The Netherlands, March 2015

3. *Hydrogen storage using carbon dioxide and a molecular heterogeneous iridium catalyst*
EuroMOF 2015, Potsdam, Germany, November 2015

4. *Hydrogen storage using CO_2 and a molecular heterogeneous iridium catalyst*
NCCC-XVII, Noordwijkerhout, The Netherlands, March 2016

5. *Covalent Triazine Frameworks as Platform for Heterogeneous Molecular Catalyst Development – From Powders to Shaped Spheres*
MOF2016, Long Beach, USA, September 2016

6. *Single Site Covalent Triazine Framework Based Monoliths for C1 Catalysis*
NCCC-XVIII, Noordwijkerhout, The Netherlands, March 2017

ABOUT THE AUTHOR

Anastasiya V. Bavykina was born on June 3, 1988 in Berdsk (Novosibirsk region, USSR). After she graduated from a lyceum in her hometown in 2005, she studied chemistry at Novosibirsk State University, Natural Sciences department. She conducted her graduation research at Boreskov Institute of Catalysis on the topic of enantiomers separation with capillary and multicapillary GC columns; graduated in 2010. The same year she received an Erasmus Mundus scholarship and obtained a joint Master degree from University of Barcelona and Gdansk University of Technology within “Erasmus Mundus Master in Quality in Analytical Laboratories” program in 2012.

In 2013 she joined the Catalysis Engineering group of Delft University of Technology and started her PhD research, presented in this book, under the supervision of Prof. Kapteijn, Prof. Makkee and Prof. Gascon.